Democratic and Popular Republic of Algeria
Ministry of Higher Education and Scientific Research

University of Echahid Hamma Lakhdar El-Oued
FACULTY OF SCIENCES
DEPARTEMENT OF PHYSICS

THESE

Presented to obtain the degree of

SCIENCE DOCTORAT

Option: Physics of Materials

THEME

Synthesis and characterization of ZnO nanostructures and ZnO/$Ni_{1-x}Cu_xO$ heterostructures Application to photovoltaics

Presented by:

Mrs. Hanane Guezzoun

Publicly defended on: 12/12/2024

In front of the Jury committee composed of:

Mr.	Beggas Azzeddine	Professor	University of El-Oued	President
Mr.	Said BENRAMACHE	Professor	University of Biskra	Supervisor
Mr.	Boubaker BENHAOUA	Professor	University of El-Oued	Co-Supervisor
Mr.	Lakel Abdelghani	MCA	University of Biskra	Examiner
Mr.	Belhamra Nadjat	MCA	University of Biskra	Examiner
Mr.	Rahal Achour	MCA	University of El-Oued	Examiner

2024-2025

Dedications

Not all words can express the gratitude, love, respect, and appreciation, it is simply that: I dedicate this doctoral thesis to:

To the spirit of my dear father, Abderrazak: No dedication can express the love, esteem, dedication, and respect I have always had for you. Nothing in the word is worth the day and night efforts you have made for my education and well-being. This work is the fruit of the sacrifices you have made for my education and training over the years.

To my loving mother, Yamina: You represent for me the source of tenderness and an example of dedication that has never ceased to encourage me. You have done more than a mother can do to guide her children on the right path in their studies.

To my beloved husband, Samir: You sacrifices, moral support, and material support have allowed me to succeed in my studies. This work is a testament to my gratitude and sincere and faithful love.

To my children, Tasnim and Anis, I love you immensely. To my dear brothers: Abdelmalek, Abdelmadjid, Abdelkader and Belguasem.

To my sisters: Karima and Maroi.

To all those whom I love, near and far. To all those who supported me.

Acknowledgements

First and for most, I would like to thank ALLAH for his helping me in making this quest of knowledge possible.

Apart from the efforts of me, the success of this work depends on the encouragement and support of many others. I take this opportunity to express my gratitude to people who help to complete this project successfully.

Initially, I would like to acknowledge my heartfelt gratitude to my supervising guide, Professor **Boubaker BENHAOUA** and Professor **Said BENRAMACHE** his willingness to motivate me contributed tremendously to my research work. Without his insightful guidance and persistent help, this thesis would never have been accomplished. I am thankful for his guidance, enthusiastic encouragement, valuable suggestions and useful critiques he gave me during the course of this research work.

I express my sincere gratitude and appreciation to my reading committee members, Professor **Azzeddine BEGGAS** of El-Oued University, Professor **Achour RAHAL** of El-Oued University, Professor **Nadjette BELHAMRA** of Biskra University, and Professor **Abdelghani LAKEL** of Biskra University for their precious time to read my thesis and for ac-accepting to judge it.

Finally, I express my sincere thanks to all my, family, friends, colleagues, and to everyone who helped me to accomplish this research work.

Table of Contents

Liste of figures :

List of tables

General Introduction

Transparent electronics is showing as one of the most advantageous technologies for future electronic products, away from the traditional silicon technology. The fact that circuits founded on conventional semiconductors as silicon and conductors as copper can be turned transparent by using different materials, the so-called transparent conducting oxides TCOs. TCOs are dominated by combinations of indium (In_2O_3), zinc (ZnO) and tin oxide (SnO_2), and to a lesser-extent gallium (Ga_2O_3) and cadmium oxide (CdO) [1-4], with indium-tin oxide (ITO) prevalent. TCOs are applied as thin-films and have been made by spray-pyrolysis, sputtering, CVD, PVD, PLD, ALD and chemical solution deposition [1-7]. Recent years, research in TCOs thin films has assumed great popularity due to good stability, and important optical and electrical properties.

During the past few years, zinc oxide (ZnO) is extremely an attractive material due to its good optical and electrical properties coupled with the low cost, non-toxicity and abundance in nature. ZnO is one of the most important binaries II–VI semiconductor compounds which is an n-type semiconductor and an important optoelectronic device material, for use in the violet and blue regions because of its direct wide band gap energy (3.37 eV) and large exciton binding energy (60 meV) at room temperature [8]. Other favorable properties include high electrochemical and good thermal stability. ZnO thin films are promising candidates for applications in short-wavelength light-emitting devices, lasers, field emission devices, solar cells, gas sensors, surface acoustic wave and transparent contacts.

On the other hand, recently, a great interest has been devoted to thin films of p-type metaloxide due to their important applications such as optoelectronic devices, gas sensors devices, and electrochemical capacitors etc. However, not much study has been achieved on p-type metal oxide with wide band gap energy. Among these p type semiconductors, Nickel oxide (NiO) is one of the most attractive semiconductors which has a cubic structure and exhibits a wide band- gap ranging from 3.4 eV to 4.0 eV [9] depending on the crystallinity and preparation methods. Furthermore, it has excellent chemical stability as well as good optical, electrical and magnetic properties [10]. All these excellent properties make NiO in the basis for enormous range of applications. Such as super capacitor, electrochromic devices, photo-catalytic [11]. It is an anti- ferromagnetic semiconductor oxide. NiO can be prepared in the form of conducting thin films byvarious techniques that involve electron beam evaporation, magnetron sputtering, chemical deposition [12-15], and sol–gel and spray pyrolysis technique (SPT).

The metal oxides ZnO and NiO are mainly used for their simplicity, their small dimensions, their good performance and their low price. It remains to develop them by the so-called "pyrolysis spray" method. To overcome this problem, deposition of semiconductor thin films or metal oxide such as NiO. doped Copper to increase the electrical conductivity, power and transmission of these films becomes a necessity.

As objectives of this thesis, synthesis ZnO and NiO thin films and heterojunctions (n-p)

from the both concerning materials, on glass substrates will be taken in consideration. spray pyrolysis method was preferred to prepare our thin films because it is simple and low cost. To achieve this study some of structural, optical and electrical properties of these films for use it in photovoltaic performance. At first step, we will prepare series of pure ZnO thin films taken in account investigation of both the effect of precursor solution concentration and substrate temperature on the structural and optical properties. Then codoped Al and Na NiO thin films series preparation will be done. Study of Al concentration effect on structural, optical and electrical properties will be undertaken. Later heterojunction ZnO/$Ni_{(1-x)}$ CuxO thin films will be prepared by deposition of nickel oxide NiO doped copper Cu onto the above synthesized ZnO. A study of both the effect of copper concentration and substrate temperature of deposited NiO onto pure synthesized ZnO will be investigated.

To sum up the aim of our work is:

- ✓ The development of ZnO thin films, NiO thin films and heterojunction (n-p) ZnO/Ni1-xCuxO deposited by spray pyrolysis technique on glass substrates.
- ✓ Optimizing the quality of ZnO, NiO and $Ni_{(1-x)}$ CuxO thin films by studying the influence of operating conditions (substrate temperature, molarity and dopant level) on the physical properties of alternated thin films.
- ✓ Improving the quality of these films by studying the influence of dopant on the structural, optical and electrical properties of the product in order to obtain transparent and conductive films.

In this thesis, we will carry out the following characterizations:

- ✓ The physical properties of these films will study according of: X-rays diffraction and FTIR techniques, in order to deduce the evolution of their microstructure.
- ✓ The electrical characterization wills determine by four-point method and that is by determination of electrical conductivity (sheet resistance Rsh) and the study of the transport mechanism in the films.
- ✓ The optical properties will study using transmission in UV-visible spectroscopy technique, with a view to know the transparency of the prepared samples and to determine the values of gap energy Eg and Urbach energy Eu. More details about the characterization techniques will take place in the chapter characterization.

This thesis consists of five chapters organized as follows:

The first chapter is entitled "Literature Review on TCOs, ZnO and NiO. At first part, we will exhibit bibliographic search on transparent and conductive oxides and their importance in several fields, then we will present zinc oxide ZnO and nickel oxide NiO which are the focus of this research. Also, we will mention their (structural, chemical, optical, and electrical) properties.

Then we will cite some of ZnO and NiO thin films applications. In the end of this context, we will talk about the different deposition methods of ZnO and NiO thin films.

In the second chapter, a detailed explanation of the used method (spray pyrolysis) by simple instruments will take place, and then we will describe all the different stages, from the preparation of the solutions to get the thin films. Then we will talk about the techniques available to study the prepared samples, which are X-rays diffraction, Fourier transform infrared spectroscopy, UV-visible, and the 4-point method respectively.

In the third chapter, which is entitled: Study of ZnO thin films we will present the results. obtained for the study of zinc oxide samples and then we will interpret them?

While the fourth chapter entitled: Study of NiO thin films codoped Na and Al results and discussion we will explain the effect of aluminum Al and sodium Na as codopant on the (structural, optical and electrical) properties of NiO thin films.

In the fifth chapter, we will present the results obtained of the heterojunction (n-p) ZnO/Ni(1-x) Cux.

Finely a conclusion about this work will be given which summaries the principal results and the over view.

References :

[1] M. Obaida, A.M. Fathi, I. Moussa et al. Characterization and electrochromic properties of NiO thin films prepared using a green aqueous solution by pulsed spray pyrolysis technique. Journal of Materials Research 37 (2022)2282–2292.

[2] S. Benramache, B. Benhaoua, H. Guezzoun, Study the Effect of Cu Doping on Optical and Structural Properties of NiO Thin Films, Annals of West University of Timisoara-Physics 62 (2020) 15-22.

[3] I. Loyola Poul Raj, S. Valanarasu, R.S. Rimal Isaac, M. Ramudu, the role of silver doping in tuning the optical absorption, energy gap, photoluminescence properties of NiO thin films for UV photosensor applications, Optik 254 (2022) 168634.

[4] M. Terlemezoglu, O. Surucu, M. Isik, N. M. Gasanly, M. Parla, Temperature- dependent optical characteristics of sputtered NiO thin films Vol.:(0123456789)1 3Applied Physics A (2022) 128:50.

[5] I.L.P. Raj, S. Valanarasu, A. Asuntha et al. Development of a highly sensitive UV sensor using Al, Ga, and In-doped NiO thin films via nebulizer spray pyrolysis method for photodetector applications. J Mater Sci: Mater Electron 33, 11753–11767 (2022).

[6] S.C. Bulakhe, R.J. Deokate, Electrochemically prepared Fe: NiO thin film catalysis for oxygen evolution reaction. J Mater Sci: Mater Electron 33, 18180–18186 (2022).

[7] K. Haunsbhavi, D. Alagarasan, N.J. Shivaramu et al. Nanostructured NiO Thin Film for Ammonia Sensing at Elevated Temperatures. J. Electron. Mater. 51, 6356–6368 (2022).

[8] C Zaouche, A Gahtar, S Benramache, Y Derouiche, M Kharroubi, A Belbel, C Maghni, L Dahbi, The determination of urbach energy and optical gap energy by many methods for Zn doped NiO

thin films fabricant semiconductor by spray pyrolysis, Digest Journal of Nanomaterials & Biostructures (DJNB) 17 (2022).

[9] K.S. Usha, R. Sivakumar &, C. Sanjeeviraja, Preparation of pure NiO thin film by radio frequency magnetron sputtering technique and investigation on its properties. J Mater Sci: Mater Electron 33, 16136–16143 (2022).

[10] N.R. Aswathy, J. Varghese &, R. Vinod Kumar, Photocatalytic degradation of malachite green using vanadium pentoxide-doped NiO thin film by sol–gel spin coating. Eur. Phys. J. Plus 137, 1344 (2022).

[11] G. Vijaya Prasath, K.S. Usha, M. Karuppaiah et al. Fabrication of heterostructure NiO/ZnO thin film for pseudocapacitor application. J Sol-Gel Sci Technol 104, 198–210 (2022).

[12] M.H. Mohsin, M.J. Haider, Z.Y.A. Al-Shibaany et al. Synthesis of NiO/Si Using Sol-Gel as a Photosensor. Silicon 14, 1349–1355 (2022).

[13] S. Benramache, Y. Aoun, S. Lakel, H. Mourghade, R. Gacem, B Benhaoua, Effect of Annealing Temperature on Structural, Journal of Nano- and Electronic Physics 10 No 6, 06032 (2018).

[14] M. Aftab, M.Z. Butt, D. Ali, F. Bashir, T.M. Khan, Optical and electrical properties of NiO and Cu- doped NiO thin films synthesized by spray pyrolysis, Optical Materials 119 (2021) 111369

I.1 Introduction:

This chapter is divided into two part: The first part deals with a bibliographical research on conductive transparent oxides (TCOs); In particular those of zinc oxide and nickel oxide, and theirs general properties such as crystallographic structures and electronic structures of bands, as well as theirs optical and electrical properties, while in the second part a discussion of the various methods of ZnO and NiO thin films deposition, focusing on providing a detailed explanation of spray pyrolysis method.

I.2 Historical review of TCOs:

Metal oxides are a chemical family of primary importance both in terms of the quantity of compounds, it is well known by the abundance of these compounds in nature. In particular an interest is given to this family because of their interesting physical properties that conjugate electrical conduction and optical transparency in the visible spectral domain. These oxides are called; transparent conductive oxides TCOs [1]. The discovery of the TCOs turns back to the beginning of the twentieth century, in 1907 when Badeker noted that after exposure to air a film of cadmium oxide becomes while maintaining its conductive appearance. Since this report a number of transparent conductive oxides appeared in particular including, SnO2 on 1931[6], ZnO on 1971[4], and NiO 1993 [2].

One of the most coveted semiconductors by researchers is zinc oxide ZnO, which is a wide band gap semiconductor (Eg=3.37 eV at room temperature) with n type conductivity. In addition, ZnO has the largest exciton bonding energy (E =60 meV) more than the ZnS (20 meV) and GaN (21 meV) [3]. For these reasons ZnO applications range from optoelectronics (solar cells, lasers, and photodiodes) up to chemical and biological sensors or electro-acoustic transducers [4].

The other most known semiconductor is nickel oxide NiO. It is one of the most popular electrochromic materials due to its excellent chemical stability, magnetic and optical properties. NiO is an important p-type semiconductor with a wide forbidden band range from 3.6 to 4.0 eV [1]. NiO films are making good films for optoelectronic applications such as LEDs and Laser [5].

I.3 Properties of TCOs:

I.3.1 Optical properties of TCOs:

I.3.1 a Transmittance:

Transmission is the most important optical property that determines the quality of a TCOs. It consists of an optical window that covers a large part of the visible spectrum. By definition, the optical transmission is defined as the ratio between the intensity of the incident light and the intensity of the transmitted light through the considered material. The transmittance of TCOs varies according to the used method for their deposition. Table I.1 give the transmittance of some conductive oxides deposited by

spray pyrolysis technique.

Table I.1: Transmittance of some TCOs deposited by SPT

TCO	T (%)
ZnO	between 70 to 80 [4]
NiO	60 to 85 [5]
SnO_2	92 [6]
CdO	nearly 70 [7]
TiO_2	70-90 [8]

I.3.1 b The band gap:

TCOs have a wide gap that varies between 3.01 eV [12] and 4.6 eV see Table I.2 [5], the width of the forbidden band varies according to the used method for its deposition.

Table I.2: Gap energy of some TCOs

TCO	Gap (eV)
ZnO	about 3.37 [4]
NiO	3.6–4.0 [5]
SnO_2	3.7 [6]
CdO	2.20 [8]
TiO_2	≈ 3.5 [9]

I.3.2 Electrical properties:

The electrical properties of TCOs films have been studied widely for over 20 years as a result of their extensive applications in optoelectronic devices, these electrical properties are described by those of wide-gap semiconductors [6].

a) <u>The conductivity σ:</u>

The physics of large gap semiconductors describes the electrical properties of TCO such as the conductivity σ. The latter is expressed as ($\Omega^{-1}.cm^{-1}$) which is the product of the density of charge carrier's η_v (cm^{-3}) by the mobility μ of these charges ($cm^2.V^{-1}.s^{-1}$) and the elementary electric charge of the electron q. The resistivity ρ, defined as the inverse of the conductivity σ, is expressed in (Ω.cm).

$$\sigma = q.\eta_v \mu = \frac{1}{\rho}.\mu = \frac{1}{\rho} \qquad (I.1)$$

b) <u>The surface resistance R_{sh}:</u>

An important electrical property of the surface in the TCO is the surface resistance R_S which known as the resistance square, defined as the ratio of the resistivity to the thickness t of the layer according to the relationship.

$$R_{sh} = \frac{\rho}{t} = \frac{1}{t.\sigma} \quad \ldots\ldots\ldots\ldots\ldots\ldots\ldots\ldots \quad (I.2)$$

where R_S: surface resistance (Ω), ρ: resistivity (Ω.cm), t: thickness of the layer (cm), and σ: conductivity $(\Omega.cm)^{-1}$.

I.4 Principal factors to TCO Choice:

The choice of TCOs depends on a few parameters such as: thermal, chemical and mechanical stability, stress, toxicity, low cost of preparation and the figure of merit Q, the later can be defined as the ratio between electrical conductivity σ and the optical absorption coefficient in the visible α. Q is given with equation (I.4).

$$Q = \frac{\sigma}{\alpha} = -\{R_{sq} \ln(T + R)\}^{-1} = \frac{T_{moy}^{10}}{R_S} \qquad (I.3)$$

σ (Ω^{-1} cm^{-1}): the conductivity

α (cm^{-1}): the absorption coefficient

R_s (Ω cm^{-2}): the square resistance

T (%): the total transmission

R (%): the total reflection

Using the equation (I.4) one can compare several TCOs; If the TCO absorption is too high so its conductivity is too low. In other hand the best TCO will have high conductivity and low visible absorption and a large quality factor between 0-7 (10^{-3}) [2]. For solar cells application it is interesting to evaluate this factor, high transparency and feeble sheet resistance are necessary for this purpose.

I.5 Presentation of our choice TCOs:

In this part, we try to explain in detail by bibliographical research, the materials utilized in this work; Zinc oxide (ZnO) and nickel oxide (NiO) which make it possible to use in various applications.

I.5.1 Presentation of zinc oxide ZnO:

Zinc oxide ZnO is a semiconductor material of the II-VII family having an excitonique emission around 375 nm, stable at ambient temperature. Among the forbidden broadband materials that can emit light in the visible (blue-violet) and near ultraviolet [10]. ZnO exists in itsnatural state in the form of a red-orange mineral called zincite, this color is due to the presence of(Fe^{+2}, Mn^{+2}) impurities forming deep levels in the semiconductor.

Experiment on ZnO has a significant peak in the 1960s; the main applications of zinc oxide have been in the fields of the chemical and pharmaceutical industry. Currently numerous optoelectronic researches lead to a great interest for this material because of its properties are multiple: high thermal conductivity and heat capacity, average dielectric constant, high resistivity, low water absorption. It is important to note that in its pigment form it diffuses and strongly absorbs ultraviolet radiation. It is an attractive and promising material for many applications in surface acoustic wave devices [13], transparent electrode [14], blue and ultraviolet (UV) light emitters

[12], solar cell windows [15], gas sensors [16], photovoltaic apparatus [17], and ultraviolet laser chamber temperature [17].

I.5.2 Physicochemical properties of ZnO

a. <u>Structural property:</u>

As it was mentioned earlier, zinc oxide is known as zincite in its natural state, crystallizes according to the compact hexagonal structure of the wurtzite type [18]. It consists of layers of zinc atoms alternating with layers of oxygen atoms as represented in Fig. I.1. Lattices parametersare as follow:

$a = b = 3{,}249 A^{\circ}$ $c = 5.207 A^{\circ}$

The zinc and oxygen atoms are located in the special Wyckoff positions 2b of the P63mc space group [19].

Zn: 0, 0, 0; 1/3, 2/3, 1/2

O: 0, 0, μ; 1/3, 2/3, μ+1/2 with μ = 0,375

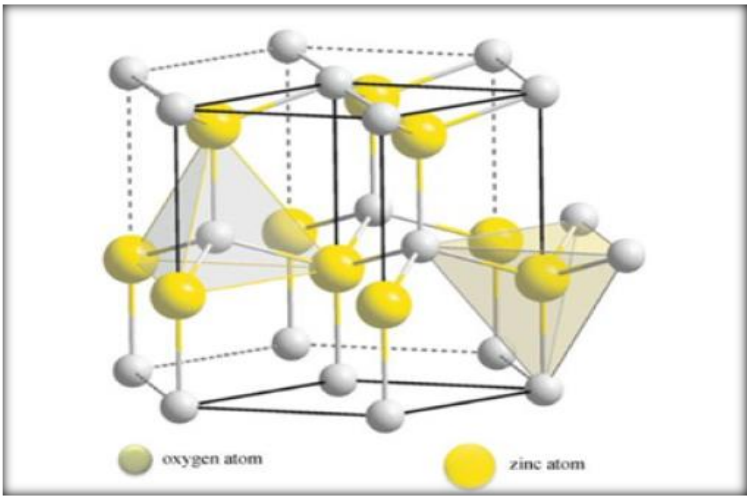

Figure I.1: Hexagonal wurtzite structure of zinc oxide (ZnO) [18]

From the ionic radiation values of the cation and anion, shown in Tab I.3, it can be seen that the structure is relatively open. Each zinc atom is surrounded by four oxygen atoms located at the vertices of a tetrahedron (see Fig I.1). In fact, the zinc atom is not exactly in the center of the tetrahedron but is displaced by 0.11 Å in a direction parallel to the c axis. Indeed, the atoms of zinc and oxygen occupy only 40% of the volume of the crystal, leaving empty spaces of radius 0.95 Å. It is possible that, under certain conditions, excess zinc atoms may become lodged in these spaces that is to say in the interstitial position [20], the same phenomena happen with the dopant. This characteristic makes it possible to explain certain particular properties of the oxide, related to semiconductivity, photoconductivity, luminescence phenomena and magnetic properties, as well as the catalytic and chemical properties of the solid.

Table I.3: Atomic and ionic rays of zinc and oxygen atoms in ZnO

Covalent bond	Neutral Zn: 1.31Å	Neutral O: 0,66Å
Ionic bond	Zn^{2+}: 0.70Å	O^{2-}: 1.32Å (Pauling) [21]
	Zn^{2+}: 0.78Å	O^{2-}: 1,24Å (Goldsmith) [22]
	Zn^{2+}: 0.60Å	O^{2-}: 1,38 Å (Shannon) [23]

b. Electronic band structure :

It is recalled that the electronic band structures of oxygen and zinc are:

O: $1s^2\ 2s^2\ 2p^4$

Zn: $1s^2\ 2s\ ^2 2p^6\ 3s^2\ 3p^6\ 3d^{10}\ 4s^2$

The 2p states of oxygen form the valence band and the 4s states of zinc constitute the conduction zone of the ZnO semiconductor. The existence of an empty band of states between 0 and 3.27 eV, this band is the forbidden band or "gap" of the material. The Fermi levels of an ideal single crystal are located in the center of this band. These two characteristics confer ZnO its semiconductor character at large gap, since it does not drive the current but the energy barrier to make it conductive, although important, is not enough to make it an insulator. The point Γ or k=0 corresponds to an absolute minimum of energy of the conduction band and an absolute maximum of energy of the valence band, which makes ZnO a direct gap semiconductor (See Fig. I.2).

As well known, the valence band has an energy lower than that of the gap. Indeed, the promotion of an electron of the valence band to the conduction band leave behind it a positive charge. This positive sign charge is called a hole. The electron promoted in the driving band and the hole present in the valence band is then linked by a Colombian interaction within the crystalline structure.

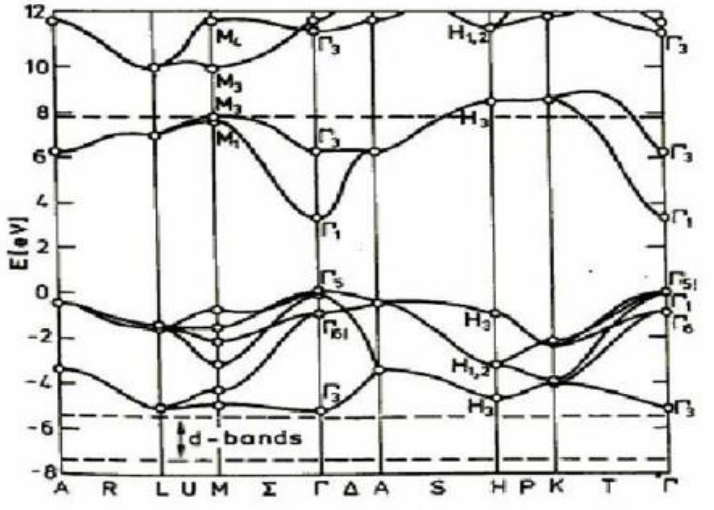

Figure I.2: Measured band structure for zinc oxide in wurtzite symmetry [24]

c. Electrical properties:

Zinc oxide is a AII BIV group semiconductor with a wide band gap of about 3.37 eV. This band gap value varies depending on the method of preparation and the doping rate. The Hall electron mobility corresponding to 300 K for a low conductivity type n is μ 200 $cm^2.V^{-1}.S^{-1}$ [25].

The following table summarizes some electrical properties of ZnO [26].

Table I.4: shows some electrical properties of ZnO.

Nature of the forbidden band	Direct
Forbidden band width at 300°K	3.27± 0.02
Conductivity type	N
Effective mass of electrons	$0.28m_0$
Effective mass of holes	$0.6m_0$
State density s in BC	$3.71*10^{18}$ Cm^{-3}
State density in BV	$1.16*10^{19}$ Cm^{-3}
Maximum resistivity	10^{-6} Ω.cm
Minimum resistivity	10^{-1}Ω.cm

d. Optical and luminescence properties:

Table I.5: shows some optical properties of ZnO [27].

Dielectric constant	$\varepsilon_{//}$=8.7, ε =7.8
Absorption coefficient	$\alpha= 10^{-4}$ cm^{-1}
Refractive index at 560 nm	n=1.8-1.9
Refractive index at 590 nm	n=2.013 - 2.029
Width of the excitonique band	60 MeV
Transmittance	>90%

ZnO is a transparent material whose refractive index in the massive form is equal ≈ 2 but in the form of a thin film, its refractive index and absorption coefficient are varied depending on the condition of deposition. ZnO belongs to the family of transparent semiconductor oxides and has a strong absorption and diffusion of ultraviolet rays [27]. Under the action of a high-energy light beam (E > 3.4 eV), the zinc oxide emits photons. This phenomenon corresponds to the luminescence according to the conditions of further elaboration and processing. The different bands of photoluminescent light have been observed and they range from close UV (λ=350 nm) to a visible green radiation of wavelength close to (λ =550 nm).

Thermal treatments such as thermal annealing have a significant effect on the optical properties of ZnO, Chen et al has shown that the optical absorption of ZnO in the violet and UV region increases considerably after annealing in air or in an atmosphere of nitrogen, and that the intensity of the green emission strongly depends on the conditions of elaboration and the annealing

temperature, this intensity varies according to the annealing temperature in respect to an Arrhenius law:

$I = I_0 \exp(-E_a/KT_r)$ with: Tr: annealing temperature and Ea: activation energy (Ea= 1.035 eV).[28]

e. Chemical and catalytic properties:

The ability of a substance to be a catalyst in a specific system depends on its chemical nature and surface properties. The effectiveness of zinc oxide depends on its method of preparation. It is essentially due to the degree of perfection of the crystal lattice, and to the semiconducting properties (gaps, atoms in interstitial positions ...) [29].

Zinc oxide is used as a trap and chemical gas sensor (H_2S, CO_2, H_2, and CH_4) [30]. Suspended in water, it can act as a photochemical catalyst for a number of reactions such as oxidation of oxygen to ozone, ammonia oxidation to nitrate, reduction of methylene blue, synthesis of hydrogen peroxide [31], or the oxidation of phenols [32]. Thin films of ZnO were also used to catalyze the reaction of copper deposition [33].

More recent work is investigating new ZnO shaping for applications as catalysts or sensors with good chemical properties. This new porous material was obtained at low temperature in an acoustic reaction from $Zn(OH)_2$. The process is based on the initiation of the reaction between NH_3 and $Zn(OH)_2$ by ultrasonic activation in aqueous medium [34].

I.5.3 Potential application of Zinc oxide:

Table I.6 summaries some applications of zinc oxide under different forms namely thins films and nanoparticles.

Table I.6: some applications of zinc oxide

ZnO thin films	ZnO Nanoparticles
UV-protection [35]	**Photo catalysis [41]**
Gas sensors [36]	**antimicrobial defense [42]**
Biosensors [37]	**Water purification [43]**
Light-Emitting Diodes [38]	**Gas sensors [44]**
Laser [39]	**Biosensors [45]**
Photo detector [40]	**Sunscreen [46]**
✓ **Schottky photo diode**	**Biomedical [47]**
✓ **Photoconductor**	
✓ **P-N Heterojunctions Photodiode**	

I.5.4 Presentation of Nickel oxide NiO:

NiO known as (bunsenite) [48] is a very acidic oxide improved to mild. It is in the form of a greenish gray powder according to the mode of presentation, more or less dense and less black.

The impure nickel oxides are nickel sinters and granular nickel oxide (green nickel oxide), also called nickel protoxide [49].

Nickel oxide is a metal and antiferromagnetic transition material, well-studied cell positive electrode, antibacterial applications. Nickel oxide has a substructure (cubic centered body, perovskite, cubic face centered). It has thermodynamic stability and excellent chemical stability. NiO is also a material anodic and positive potential. They are used in electrochromic device, ceramic dye, batteries and chemical reaction catalysts [50].

Nickel oxide is obtained by pyrolysis of nickel hydroxide, Ni $(OH)_2$. Some NiO phases are defined as follow:

a) <u>Phase β-Ni $(OH)_2$:</u>

Nickel hydroxide (II) [Ni $(OH)_2$] occurs in several types. There are mainly two different phases which are illustrated in Fig I.3 The β-Ni $(OH)_2$ phase is brucite Mg (OH)2 and crystallizes in the hexagonal system described as an hcp structure (hexagonal close-packed) of hydroxyl ions (AB oxygen fill) with Ni (II) occupying half of the octahedral interstices. This structure is actually a layered structure. Each layer consists of a hexagonal planar arrangement of Ni (II) ions with octahedral oxygen coordinated. The inter layer distance corresponds to the cell parameter c=4.605Å and the distance Ni-Ni within a layer is given by a=3.126Å [51].

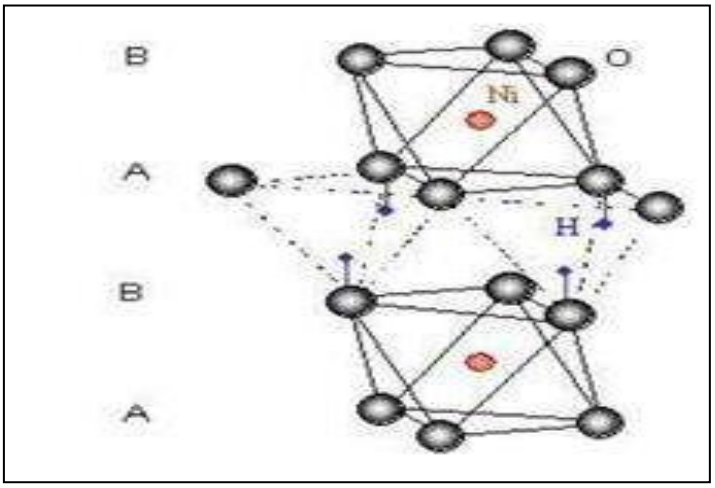

Figure I.3: Nickel hydroxide phase β-Ni $(OH)_2$ [52]

b) <u>Phase α-Ni $(OH)_2$:</u>

Phase α-Ni $(OH)_2$ has a type structure brucite Mg $(OH)_2$ where the layers (001) are superimposed on the c axis, but separated by water molecules. Other authors, they rejected this well-organized building in favor of a structure where the Ni $(OH)_2$ layers are equidistant by about 8Å and parallel as in the case of phase β, but randomly oriented and separated by water molecules linked to hydroxyl groups by hydrogen bonds. Phase β can be obtained from the phase solution

ageing α through a redissolution of phase α followed by nucleation and growth of the phase β. It is necessary to specify that α or β hydroxides used by the electrochemists cannot be considered as well-defined materials [53].

I.5.5 Physicochemical properties of NiO:

Among the TCOs, nickel oxide (NiO) is a transition metal and antiferromagnetic oxide [50] Their Neel temperature is 523K, it is a temperature that characterizes the antiferromagnetic materials; below this temperature the sub-lattice atoms spontaneously magnetize in the manner of a ferromagnetic lattice [51].

a) Crystallographic and structural properties:

The crystallographic structure of nickel oxide is shown in Fig. I.4 This compound crystallizes in a cubic face-centered structure type NaCl (CFC); Its crystalline parameter is of the order of a = 4.177 Å and its density is 6.72 g/cm^3 [54]. This cubic structure is composed of two similar sub-networks A and B such that any atom of the sub-network A only has neighbors belonging to the sub-network B and vice versa. The anion subnet (O^{-2}) and the cation subnet (Ni^{+2}) have a CFC structure. The ionic rays: R (Ni^{+2}) =0.72 Å and R (O^{-2}) = 1.40 Å [5]. The plane (100) is a mixed plane that is composed of 50% nickel and 50% oxygen. The planes (111) are alternately pure Ni, pure O. The face (111) is a polar face (not-stable) against the face (100) is a not-polar face (stable). The inter-reticular distance between two different planes is 0.120 nm and is almost double between two planes of the same nature [55].

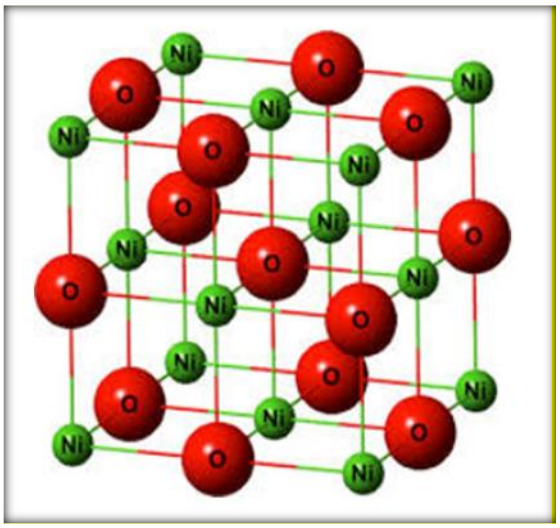

Figure I.4: Crystal structure of nickel oxide [**55**]

b) Electronic band structure:

The electronic structure of Oxygen and Nickel which are constituted the NiO semiconductor:

O: $1s^2\ 2s^2\ 2p^4$

Ni: $1s^2\ 2s^2\ 2p^6\ 3s^2\ 3p^6\ 3d^8\ 4s^2$

The band structure of NiO molecular and bulk are represented in Fig I.5.and 6. respectively. In fact, nickel oxide is an insulator with an optical band gap ranged in 3.6-4 eV (see Fig I.5 and 6), with resistivity more than 106 Ω.cm [56]. Conduction mechanism of NiO has not clearly explained yet, so there is no common agreement about its electrical properties [57].

Firstly, it was believed that stoichiometric NiO is Mott insulator [58]. Then, it is corrected that it behaves as Mott-Hubbard type insulator [59]; It is considered as p-type conductor [60]. In general, some results reveal that conduction mechanism and electronic structure of NiO is quite complex [61].

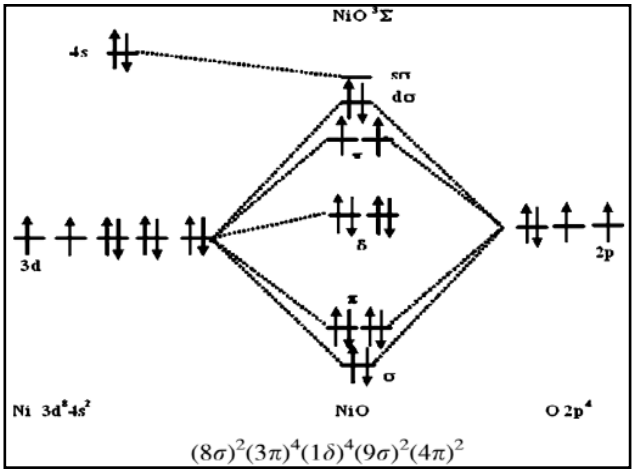

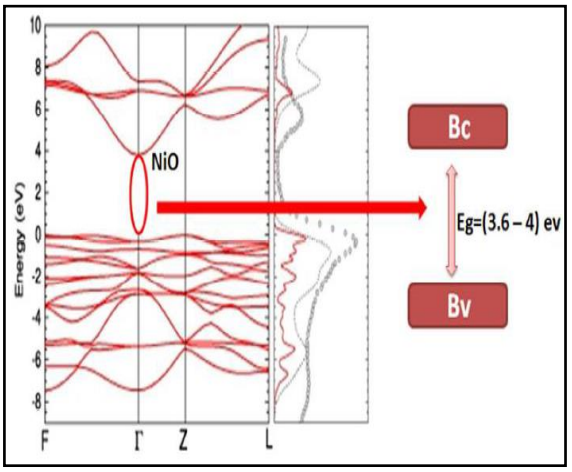

FigureI.5: Diagram molecular of the fundamental state of NiO**[62]FigureI.6:** Diagram of band structure of NiO **[63]**

c) Electrical properties:

Nickel oxide is a p-type semiconductor [56]. Studies have shown that its conductivity varies between 10^{-2} $(\Omega.cm)^{-1}$ and 10_{-1} $(\Omega.cm)^{-1}$ at 500 K and 300K respectively [5]. The following Table I.7 gives experimental results concerning the electrical properties of NiO. The NiO film in its stoichiometric (NiO) form is an insulator with a very high resistivity at room temperature.

Table I.7: Some electrical property of nickel oxide

Conductivity σ $(\Omega.cm)^{-1}$	**0.1-1≤10 [64]**
Mobilité μ (cm^2/V.s)	**0.1-1 [64]**
Electronic density N (cm^3)	**10^{18} - 10^{19} [64]**
Band gap energy Eg (eV)	**3.6 – 4 [5]**
Dielectric constant	**11.9 [65]**

d) Optical properties:

As we said earlier, nickel oxide is a transparent material in the visible and in the general case; this compound has a direct gap of 3.6 to 4 eV [5]. The transmittance is varied between 40-80% and the refractive index is of the order of 2.33 [56]. Table I.8 gives results of the optical gap of NiO experimentally obtained by studies using the spray method from different conditions

(solution, precursor, molarity, substrate temperature).

Table I.8: Experimental results of optical proprieties of NiO films made by spray

Precursors Solutions	T(%)	D (nm)	Eg (eV)	Eu (meV)	References
$NiCl_2.6H_2O$	30-60	//	3.7-3.84	281-337	[66]
$Ni(NO_3)_2.6H_2O$	57-88	180-200	3.68-3.56	300-450	[67]
$(C_2H_3CO_2)_2.4H_2O$	80-90	800-900	3.61	//	[68]

I.5.6 Doping of NiO:

In a p-type doping, the dopant atom causes an electronic deficiency in the ionic bonding, thus creating an empty acceptor energy level just above the valence band, which can accept an electron from the valence band, and leaves behind it a positive charge (hole). This allows conduction via doping species to a bulk semiconducting or insulating lattice structure [69].

a) Extrinsic doping (substitutional):

It is done by changing the original ions Ni^{2+}or oxygen ions O^{2-} (anions) with ions having respectively a higher or lower valence, the charge carrier concentration can be increased. The introduction of impurities into the crystal lattice creates energy levels in the gap and either donors or acceptors, which are responsible for changing the optical and electrical properties. There are also linear defects (dislocation) and plane defects (grain boundaries). Huge dielectric response has been observed for (Li, Fe) and (Li, V) doped NiO [70]. The effects of transition metal like Fe, Cu, Co, Mn etc. doping can drive a non-magnetic semiconductor into a semiconductor with ferromagnetism [71-74].

b) Intrinsic doping:

By introducing excess of oxygen atoms in the interstitial position, or by creating nickel gaps. The major defects in nickel oxide are cationic vacancies Ni^{2+}. NiO can be written $Ni_{1-y}O$, or there is the difference in the stoichiometry. The conductivity of nickel oxide increases with temperature, that is to say their semiconductor behavior is interpreted by the presence of defects in the crystal lattice. When there are vacant crystallographic sites, in this case, it is possible to envisage an electrical conduction by jump, a cation (Ni^{2+}) passing from an occupied site to a vacant site produces the displacement of the vacant site, and such a displacement of charges is more efficient at high temperature.

I.5.7 Potential applications of NiO:

Nickel oxide is a material which has a set of physical properties likely to use it in many applications. Table I.9, summaries few NiO applications as thin films or nanostructure.

Table I.9: NiO applications under thin films and nano structures

NiO thin films	NiO Nanoparticles
Semiconductor (of whole type conductivity) in solar cells and super capacitors [75].	NiO based composites have considered as good solar absorber coatings [76].
Gas sensor for H_2 [77]. Anode in oxygen fuel cells [79].	As efficient materials for the fabrication of nanotubes, and for networks for storing hydrogen [78]. biomedical applications [80].

I.6 Thin films deposition techniques :

It is possible to identify a thin film of a material that is an element of this material so that its thickness is significantly reduced, which is expressed with micrometers or nanometers. (film quasi-two dimensionality). The small distance between the two frontier surfaces gives a perturbation of physical, chemical and mechanical properties of the elaborated thin films which differ from the bulk.

A selective appropriate deposition technique will be taken in consideration in the following step. There are many methods for obtaining thin films, which can be generally classified into two groups, namely, physical and chemical deposition processes. The physical methods include magnetron sputtering [81], physical vapor deposition (PVD), laser ablation [82] and molecular beam epitaxy [83]. While the chemical methods comprise gas phase and liquid phase deposition methods. The gas phase methods are chemical vapor deposition (CVD) and atomic layer epitaxy (ALE) [84], however the liquid phase methods are included spray pyrolysis [85], sol-gel [86], electro deposition [87], chemical bath deposition (CBD) [88], liquid phase epitaxy (LPE) [89], spin- coating [90] and dip-coating [91].

Many deposition techniques have been used to produce ZnO and NiO thin films. The most useful of these techniques are: RF magnetron sputtering [92, 93**]**, Pulsed Laser Deposition (PLD) [94, 95], Sol–gel process [96, 97], chemical vapor deposition (CVD) [98, 99], and spray pyrolysis [100, 52]. In the following will be provide a description of these techniques respectively. In this thesis only spray pyrolysis is taken in consideration to elaborate our samples.

I.7 Spray pyrolysis technique (SPT):

I.7.1 Introduction:

The spray pyrolysis technique involves spraying of fine droplets of metal salts solutions (chlorides, nitrates or acetates, which are easily soluble in water or in alcohol), onto a preheated surface which called substrate. There is a chemical reaction on the hot surface of the substrate which makes it possible to obtain a deposit after the evaporation of the volatile products of the reaction. SPT represents a very simple and cost method, especially regarding equipment; it does

not necessitate high-quality substrates or chemicals. SPT has been used for several decades in solar cell production to deposit electrically conducting electrodes. The first use of the spray pyrolysis was by researchers Chamberlin and Skarman in 1966 when they were prepared CdS thin films for solar cells application [101]. After that, many research articles related to spray pyrolysis method and the wide applications range of thin films deposited by this method have appeared.

I.7.2 SPT schematic representation:

Fig I.7 shows the schematic representation of SPT equipment which is generally used. The fundamental SPT equipment consist of an atomizer, Spray solution (precursor solution), Heater of surface (substrate heater), temperature controller, an air compressor or any other source of gas carrying.

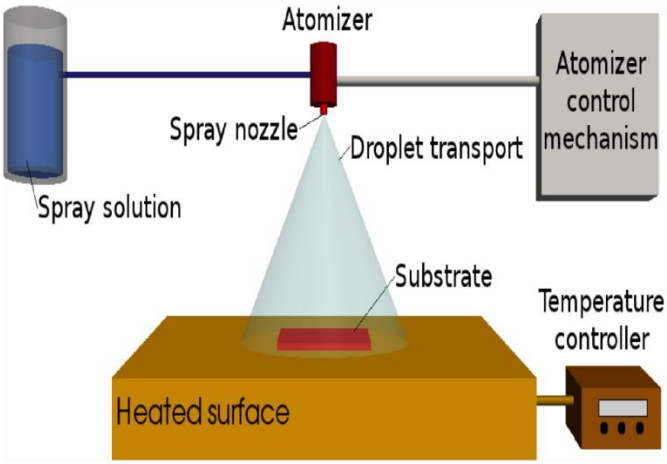

Figure I.7: Schematic diagram of SPT equipment [95-97]

I.7.3 Advantages of spray pyrolysis technique:

In this presented work (SPT) has been chosen for preparation of ZnO and NiO thin films because it has a number of advantages among of them are [5]:

a. It is a relatively simple and inexpensive technique and doesn't require the use of pumping group like most other methods.
b. It is an effective technique that leads to thin films with a considerable deposition rate and large surface area with good uniformity and controlled thick.
c. It is a method developed for conductive oxide for many applications such as solar cells.
d. The method was used for the deposition of multi layers.
e. The deposition rate and the thickness of the films can be easily controlled over a wide range by changing the spray parameters.
f. It allows controlling the chemical composition of the material.
g. Possibility to use more than one product at the same time, especially for doping

I.7.4 Main processing steps of SPT:

Spray pyrolysis involves a lot of processes happening either simultaneously or sequentially.

There are essential steps of the thin films formation by spray which are presented as follows:

1. Precursor solution preparation (Source)
2. Precursor solution atomization
3. Aerosol transport of the droplet
4. Decomposition of the precursor

I.7.4.1 Precursor solution preparation (Source) :

The composition of the starting solution is determined by the precursors dissolved in the solvent with predetermined stoichiometric ratio. Chemical materials at formal nitrates, chlorides and acetates usually used as precursors [5].

Distilled water or alcohol is often used as solvent. In the basic solution it is necessary to eliminate the problems of solubility and phase segregation, where the different components rush at different times. To overcome this and to obtain homogeneous solutions. A small amount of acid (for example: nitric acid) is recommend to be added during the preparation [102]. The overall concentration of the solution can be varied from 0.01 to some mole/l.

The preheating and agitation of the solution can accelerate the reaction on the substrate and this increases the deposition rate and improves the quality of the resulting films.

I.7.4.2 Precursor solution atomization:

The atomization procedure is the second step in the spray pyrolysis deposition after the preparation of precursor solution. It depends on generating droplets from the spray solution and focalize them, with primary velocity, towards the substrate surface. Two methods are generally used to spray the solution: Ultrasonic spraying and Pneumatic spraying: the pneumatic spraying has been chosen in this work. this is the fog produced by a compressed gas that sucks and burst the liquid.

The gas carrier can be controlled with great sensitivity. However, for most compound semiconductors, nitrogen N_2 gas is used to avoid chemical reactions, between compound materials and solvent, which would lead to the addition of impurities. In some cases, to prevent the oxidation of materials, a binary mixture of N_2 and H_2 is used as a gas carrier [103].

The atomizers differ in resulting droplet size, rate of atomization, and the primary velocity of the droplets. It has been shown that the size of the generated droplet is not related to any fluid property of the precursor solution and depends solely on the fluid charge density level. The mass of a droplet m, assuming a spherical shape depends on its density ρ_q [104]:

The primary leaving velocity of the droplet is a significant parameter as it determines the rate at which the droplets arrive at the substrate surface, the heating speed of the droplet, and the quantity of time the droplet remains in transport. Due to its ease of production, a pressure, or air blast, atomizer uses high speed air in order to generate an aerosol from a precursor solution.

Increasing the air pressure causes a direct decrease in the generated mean droplet diameter. Inversely, increasing the liquid pressure causes a direct increase in the mean droplet diameter [105].

I.7.4.3 Aerosol transport of the droplet:

After the droplet leaves the atomizer, it moves through the ambient with a primary velocity determined by the atomizer. In the aerosol form, the droplets are transported with the aim of as many droplets as possible reaching the surface. As the droplets move through the ambient, they obey a physical and chemical changes as depicted in Fig I.8. As the droplet traverses the ambient, there are four forces simultaneously acting on it, describing its path. Those forces are gravitational [102], electrical [103], thermophoretic [104] and the Stokes force [105] (see Fig I.8).

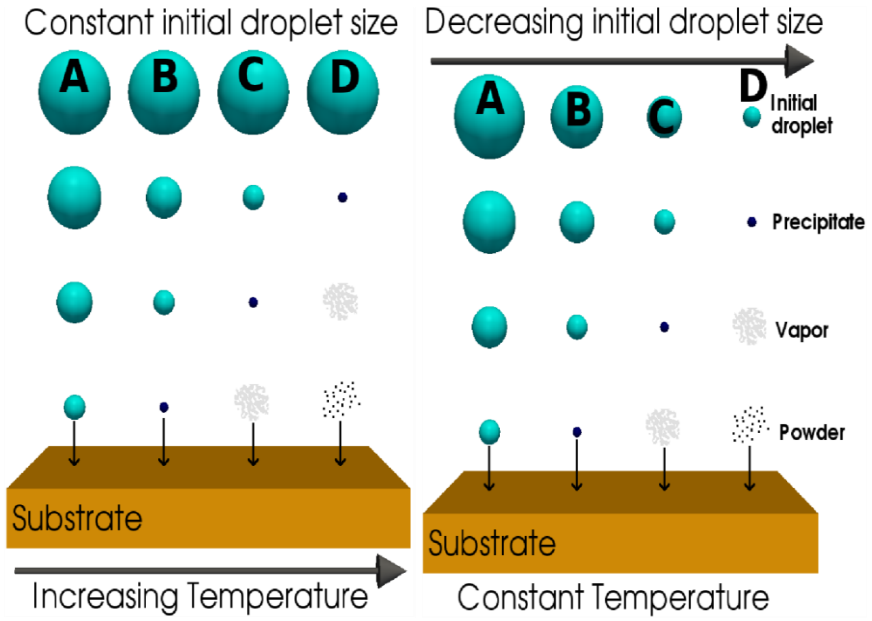

Figure I.8: Diagram of the different process stages for the aerosol droplet evolution as it approaches the hot substrate for two cases: (a) Constant initial droplet size and increasing substrate temperature, and (b) constant substrate temperature and decreasing initial droplet size [110].

I.7.4.4 Precursor decomposition:

The precursor, as it moves through the heated ambient undergoes various changes, which are shown in Fig I.8 (a) and (b). Evaporation, precipitate formation, and vaporization all occur depending on the droplet size, ambient temperature and atomizer to substrate distance. Fig I.8

and (b) shows the four physical forms in which the droplet may interact with the substrate surface, although all processes occur during deposition. Process C is the optimal process for obtaining dense and homogeneous films, like the CVD deposition is desired to yield a dense high quality film [111], as it will be explained in the following section.

a) <u>Process A: (low temperature/large initial droplet)</u>

When the large droplets come close to the heated substrate and the temperature is not sufficiently high to fully evaporate the solution, they will impact with the substrate and decompose. Upon contact, the droplet is completely evaporated and a dry precipitate is left behind. This process has a weak sticking probability [112].

b) Process B: (Low intermediate temperature/Large medium droplet size)

When large medium droplet sizes are initially formed, some evaporation occurs. Just as the droplet reaches the surface, however, it forms a precipitate as an amorphous salt and a dry precipitate hits the surface, where decomposition occurs. Some particles evaporate and condense into gaps between particles, where surface reaction occurs. However, this process has a medium sticking probability [111, 113].

c) Process C: (A medium temperature/A medium droplet size):

When the processing environment causes droplets to evaporate prior to reaching the substrate vicinity, a precipitate will form early. As the precipitate reaches the immediate vicinity of the substrate, it is converted into a vapor state and it undergoes a heterogeneous reaction through the following steps [105, 111, 114]:

1- Reactant molecules diffuse to the surface.

2- Adsorption of some molecules at the surface.

3- Surface diffusion and a chemical reaction, incorporating the reactant into the lattice.

4- Desorption and diffusion of the product molecules from the surface.

This is a classical CVD reaction, which results in a high quality film deposition and a high sticking probability.

d) Process D: (A high temperature/A small droplet size):

When small initial droplets are formed, or the temperature is high enough, the droplet quickly forms a precipitate. As the precipitate approaches the substrate, it is vaporized and a chemical reaction subsequently occurs in the vapor phase. This homogeneous reaction leads to the condensation of molecules into crystallites in the form of a powder precipitate. The powder falls to the substrate surface, but without a deposition reaction [113].

I.7.5 Effect of some SPT parameters on the resulting films quality:

There are many parameters affecting the quality of deposited films. In this section, some main parameters on properties of the deposited films will be taken in consideration.

I.7.5.1 Effect of substrate temperature Ts:

The deposition temperature is involved in all mentioned processes, except in the aerosol generation. As a result, the substrate surface temperature is the most important parameter that determines the form and properties of the film [114]. By increasing the temperature, the film morphology can change from a cracked to a porous microstructure. In many studies the deposition temperature was reported indeed as the most important spray pyrolysis parameter. The properties of deposited films can be varied and thus controlled by changing the deposition temperature; As well known it influences the structural, optical and electrical properties of thin films [115].

The influence of substrate temperature on the structural, optical and electrical properties of ZnO films prepared by the spray pyrolysis method using aqueous solution of zinc acetate has been investigated [4, 116, 119]. X-ray diffraction measurements show that all the films are polycrystalline with hexagonal Wurtzit structure and a strong preferred orientation along the (002) plane, which is strongly dependent on the substrate temperature. Optical absorption spectra, show high transparency of the film (90–95% transmission) in the visible range, with a sharp absorption edge around 375 nm wavelength of light which closely corresponds to the intrinsic band gap of ZnO (3.3 eV). ZnO films with the lowest resistivity, which is due to the increased mobility resulting from the improvement of the crystallinity of the films, can be prepared at a substrate temperature of 490°C.

Characterization of nickel oxide films deposited at different substrate temperatures using spray pyrolysis using aqueous solution of nickel chloride has been investigated by [120, 125]. X ray diffraction showed that, The NiO films obtained at low substrate temperature are amorphous, whereas at higher Ts≥ 275°C cubic structure of NiO with preferred orientation along the (111) plane. The absorption spectra analysis reveals that the electronic transitions are clearly affected by substrate temperature and the dark electrical resistivity decreases noticeably from 10^4 to 10Ωm when the temperature increases.

I.7.5.2 Effect of precursor solution type:

The precursor solution is the second important parameter. It's worth noting that solvent, salt type and salt concentration affect the physical and chemical properties of the precursor solution. So many properties of the deposited film can be changed by changing the composition of the precursor. Such as film thickness, morphology, chemical structure, and electrical and optical properties [112].

The influence of precursor solution properties for ZnO thin films deposition by spray pyrolysis was a main work investigation, where the authors have studied the effect of precursor solution and some kind of zinc salts [113, 118, 126]; They used three or four starting solutions namely: zinc acetate, zinc chloride, zinc nitrate, and zinc carbonate. The obtained results indicate

that the dissociation energy of the starting solution plays an important role on films growth rate.

A linear relationship between the solution dissociation energy and the growth rate activation energy was found, However, the surface tension of the used solution controls the droplet shape impact. Both solution surface tension and dissociation enthalpy alter the microstructure of the formed film. Films deposited with zinc acetate are characterized by a smooth surface, dense network and high transparency, while films deposited with zinc chloride have a better crystallinity and low optical transmittance.

Properties of NiO thin films deposited by chemical spray pyrolysis using different precursor solutions have been investigated by L. Cattin [118, 127, 128]. NiO thin films have been deposited using a perfume atomizer to grow the aerosol. The influence of the precursors, nickel chloride hexahydrate ($NiCl_26H_2O$), nickel nitrate hexahydrate (Ni $(NO_3)_26H_2O$), nickel hydroxide hexahydrate (Ni $(OH)_26H_2O$), nickel sulfate tetrahydrate ($NiSO_44H_2O$), on the thin films properties has been studied M]. In the experimental conditions used (substrate temperature 350°C, precursor concentration 0.2–0.3 M, etc.), pure NiO thin films crystallized in the cubic phase can be achieved only with $NiCl_2$ and Ni $(NO_3)_2$ precursors.

I.7.5.3 Effect of distance between nozzle and substrate:

When spraying is done in the air, compounds that are as stable as or more stable than oxides are easily detected. In fact, the thickness of the sample is controlled by the concentration of solutions, the temperature of the substrate, and the distance between the spray and the surface of the substrate. J. C. Vigui and J. Spitz [129] they studied the classification of the group of processes that occur with increasing temperature as shown in Fig I.9.

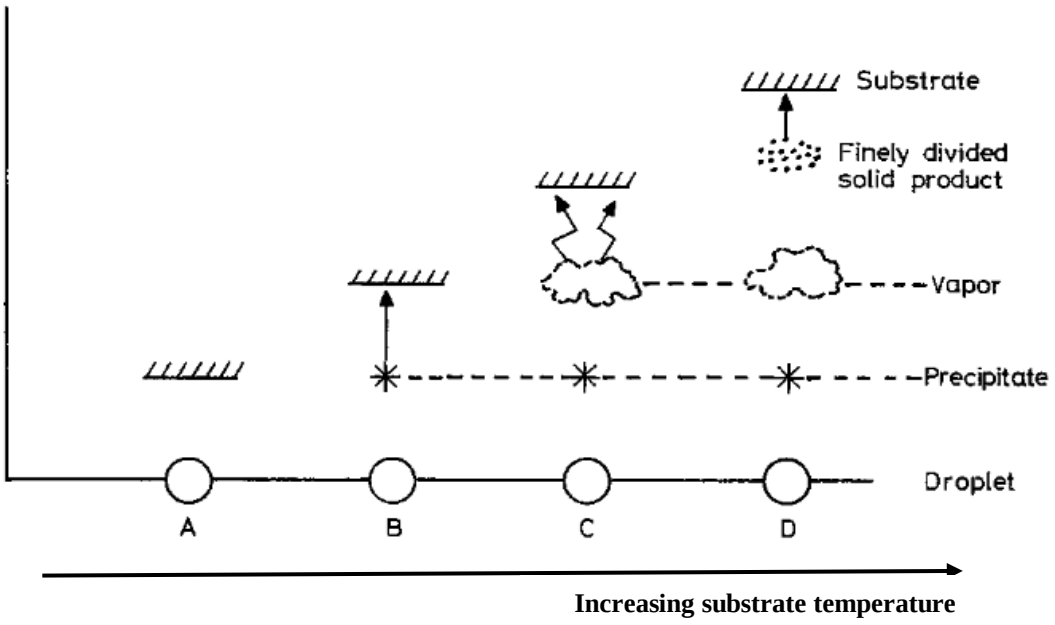

Figure I.9: Description of the deposition processes initiated with increasing substrate temperature [129]

I.7.6 Keys to promote metal oxide crystallization:

Metal oxide crystallization is controlled by nucleation. As a result, one of the earliest tactics for improving crystallization kinetics in metal oxide thin films was based on the seeding effect (see Fig I.10) [130]. The key principle is to reduce the energy barrier necessary for the development of the crystalline phase by encouraging its nucleation at a specific surface region (heterogeneous nucleation) [130]. This can be accomplished by adding a seeding layer (i.e., a buffer layer of a different material that has already crystallized) on top of the substrate. When such nanoseeds are present, the density of nucleation sites inside the as-deposited film increases relative to spontaneous nuclei production. This promotes the crystallization of the metal oxide by nucleation on the surfaces of the particles dispersed throughout the film [130].

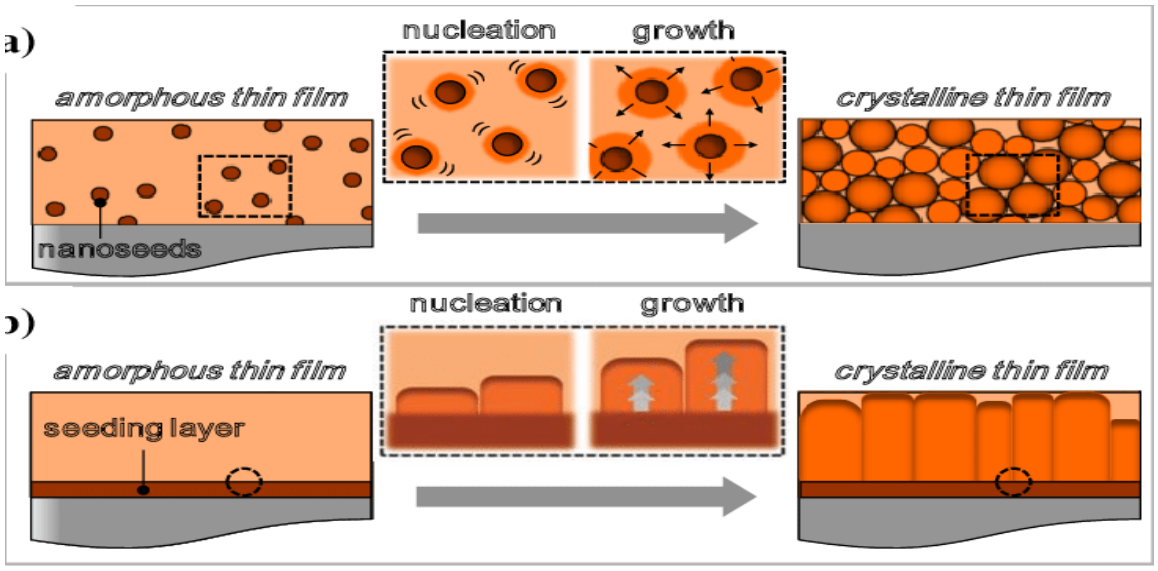

Figure I.10: Schematic examples of the nucleation and growth events in metal oxide thin films aided by the seeding effect, using (a) a seeding layer previously developed on the substrate and (b) crystalline nanoseeds previously inserted into the bulk film [130]

I.8 Conclusion:

In the first part of this chapter, main properties and some areas of the applications of transparent conductive oxides (TCOs) and present the criteria for the choice of zinc oxide ZnO, nickel oxide NiO were recalled. Then in the last part of this chapter the different used methods zinc oxide and nickel oxide depositions were exhibited SPT and the different steps of preparing thin films of this technique were mentioned as well as the advantages of using this method in the domain of thin films were cited. In the last part of this chapter the different methods of manufacturing zinc oxide and nickel and were explained. Method of thermal spraying and different steps as well as the advantages of using this method in the field of thin films were mentioned with the effect of certain parameters such as substrate temperature, type of theprecursor solution used and the distance between the atomizer and substrate.

References :

[1] Benzarouk, H. (2008). Synthèse d'un oxyde transparent conducteur (OTC) par pulvérisation chimique (ZnO, NiO). Mémoire de Magister, Université Badji Mokhtar Annaba.

[2] D. Lamb and S. Irvine, near infrared transparent conduction cadmium oxide deposited by MOCVD, Thin Solid Films, vol. 518, no. 4, pp. 1222-1224, 2009.

[3] J. Anderson, Chris G Van de Walle, Fundamentals of zinc oxide as a semiconducting, Rep. Prog. Phys. 72 (2009) 126501-29.

[4] Benramache, S., Benhaoua, B., & Chabane, F. (2012). Effect of substrate temperature on the stability of transparent conducting cobalt doped ZnO thin films. Journal of Semiconductors, 33(9), 093001.

[5] B. Rafia, Caractérisation Spectroscopique des Couches minces d'oxyde de Nikel (NiO) Elaborées par Spray. Doctoral thesis, Kasdi Merbah Ouargla University, 2017

[6] B. Benhaoua, S. Abbas, A. Rahal and others, Effect of film thickness on the structural, optical and electrical properties of SnO2: F thin films prepared by spray ultrasonic for solar cells applications, Superlattices and Microstructures, **83** (2015), p 78-88.

[7] Ahmed, F. S., Ahmed, N. Y., Ali, R. S., Habubi, N. F., Abass, K. H., & Chiad, S. S. (2020). Effects of substrate type on some optical and dispersion properties of sprayed CdO thin films. NeuroQuantology, 18(3), 56.

[8] Costa, M. S., Baptista, V., Minas, G., Veiga, M. I., & Catarino, S. O. (2021). Effect of the Materials' Properties in the Design of High Transmittance and Low FWHM SiO2/TiO2 Thin Film Optical Filters for Integration in a Malaria Diagnostics Device. BIODEVICES, 1, 21-31.

[9] Lin, C. P., Chen, H., Nakaruk, A., Koshy, P., & Sorrell, C. C. (2013). Effect of annealing temperature on the photocatalytic activity of TiO2 thin films. Energy Procedia, 34, 627-636.

[10] Pathak, T. K., Pal, P. K., Gupta, H., Matta, G., Kumar, A., Kumar, R., & Purohit, L. P. (2015). Synthesis and Characterization of ZnO Thin Films Fabricated by Sol-Gel Method. ESSENCE-international Journal for Environmental Rehabilitation and Conservation, 6(2), 184-188

[11] S. Benramache, B. benhaoua, N Khechai, F. Chabane, Matériaux & Techniques 100 (2012) 573-580.

[12] Mass, J., Bhattacharya, P., & Katiyar, R. S. (2003). Effect of high substrate temperature on Al-doped ZnO thin films grown by pulsed laser deposition. Materials Science and Engineering: B, 103(1), 9-15.

[13] Du, X. Y., Fu, Y. Q., Tan, S. C., Luo, J. K., Flewitt, A. J., Maeng, S., & Milne, W. I. (2007, July). ZnO f device. In Journal of Physics: Conference Series (Vol. 76, No. 1, p. 012035). IOP Publishing.

[14] Badgujar, A. C., Yadav, B. S., Jha, G. K., & Dhage, S. R. (2022). Room temperature sputtered aluminum-d application in solar cells and for low-band-gap optoelectronic devices. ACS omega, 7(16), 14203-14210.

[15] Islam, M. M., Ishizuka, S., Yamada, A., Matsubara, K., Niki, S., Sakurai, T., & Akimoto, K. (2011). Thickn a window layer in Cu (In1− xGax) Se2 thin film solar cell. Applied Surface Science, 257(9), 4026-4030.

[16] Dimitrov, I. G., Dikovska, A. O., Atanasov, P. A., Stoyanchov, T. R., & Vasilev, T. (2008, May). Al doped ZnO thin films for gas sensor application. In Journal of Physics: Conference Series (Vol. 113, No. 1, p. 012044). IOP Publishing.

[17] Herrero, J., & Guillen, C. (2004). Improved ITO thin films for photovoltaic applications with a thin ZnO layer by sputtering. Thin Solid Films, 451, 630-633.

[18] Ma, L., Ai, X., Huang, X., & Ma, S. (2011). Effects of the substrate and oxygen partial pressure on the microstructures and optical properties of Ti-doped ZnO thin films. Super lattices and Microstructures, 50(6), 703-712.

[19] Menaglia, A., Bara, B., & Zerrouki, S. (2015). Elaboration et caractérisation des couches minces de znO pures et dopées fe par la voie sol-gel.

[20] Özgür, Ü., Alivov, Y. I., Liu, C., Teke, A., Reshchikov, M. A., Doğan, S., ... & Morkoç, A. H. (2005). A comprehensive review of ZnO materials and devices. Journal of applied physics, 98(4).

[21] V.A. Coleman, C. Jagadish. Zinc Oxide Bulk Thin Films and Nanostructures Processing Properties and Applications Gainesville. FL, USA, 206, p. 1–20.

[22] W.H. HIRSCHWALD et al. Current Topics in Materials Science 7 (1981) 143–482.

[23] A.F. Kohn, G. Ceder, D. Morgon, C. G. Van de Walle, Phys. Rev.B., 61 (2000) 15019–15024.

[24] Schröer, P., Krüger, P., & Pollmann, J. (1993). First-principles calculation of the electronic structure of the wurtzite semiconductors ZnO and ZnS. Physical Review B, 47(12), 6971.

[25] These ZnO Z. Fan, J.G. Lu, Zinc Oxide Nanostructures: Synthesis and Properties, Irvine, CA 92697, USA, 2005.

[26] H. Lekiket, These de magister, Elaboration et Caract2rusation des hétérojonctions à base de couches minces de ZnO et ZnS, Université de Constantine, Algeria 2008.

[27] Lambert K. van Vugt, Thèse de doctorat, Optical Properties of Semiconducting Nanowires, University Utrecht, Pays-Bas 1977.

[28] Omri, K., Najeh, I., & El Mir, L. (2016). Influence of annealing temperature on the microstructure and dielectric properties of ZnO nanoparticles. Ceramics International, 42(7), 8940-8948.

[29] Lee, K. M., Lai, C. W., Ngai, K. S., & Juan, J. C. (2016). Recent developments of zinc oxide based photocatalyst in water treatment technology: a review. Water research, 88, 428-448.

[30] Gadkari, A. B., Shinde, T. J., & Vasambekar, P. N. (2010). Ferrite gas sensors. IEEE Sensors journal, 11(4), 849-861.

[31] Elsayed, M. A., Gobara, M., & Elbasuney, S. (2017). Instant synthesis of bespoke nanoscopic photocatalysts with enhanced surface area and photocatalytic activity for wastewater treatment. Journal of Photochemistry and Photobiology A: Chemistry, 344, 121-133.

[32] Shukla, P., Fatimah, I., Wang, S., Ang, H. M., & Tadé, M. O. (2010). Photocatalytic generation of sulphate and hydroxyl radicals using zinc oxide under low-power UV to oxidise phenolic contaminants in wastewater. Catalysis Today, 157(1-4), 410-414.

[33] Zhao, J., Nunn, W. T., Lemaire, P. C., Lin, Y., Dickey, M. D., Oldham, C. J., & Parsons, G. N. (2015). Facile conversion of hydroxy double salts to metal–organic frameworks using metal oxide

particles and atomic layer deposition thin-film templates. Journal of the American Chemical Society, 137(43), 13756-13759.

[34] Y. Iida, AIST Today 3 (2003) 14–17.

[35] Johansson, W., Peralta, A., Jonson, B., Anand, S., Österlund, L., & Karlsson, S. (2019). Transparent TiO_2 and ZnO thin films on glass for UV protection of PV modules. Frontiers in Materials, 6, 259.

[36] Paliwal, A., Sharma, A., Tomar, M., & Gupta, V. (2017). Carbon monoxide (CO) optical gas sensor based on ZnO thin films. Sensors and Actuators B: Chemical, 250, 679-685.

[37] Saha, S., & Gupta, V. (2011). Influence of surface defects in ZnO thin films on its biosensing response characteristic. Journal of Applied Physics, 110(6).

[38] Hwang, D. K., Oh, M. S., Lim, J. H., & Park, S. J. (2007). ZnO thin films and light-emitting diodes. Journal of Physics D: Applied Physics, 40(22), R387.

[39] Znaidi, L., Illia, G. S., Benyahia, S., Sanchez, C., & Kanaev, A. V. (2003). Oriented ZnO thin films synthesis by sol–gel process for laser application. Thin solid films, 428(1-2), 257-262.

[40] Chen, K. J., Hung, F. Y., Chang, S. J., & Young, S. J. (2009). Optoelectronic characteristics of UV photodetector based on ZnO nanowire thin films. Journal of Alloys and Compounds, 479(1-2), 674-677.

[41] Di Mauro, A., Fragalà, M. E., Privitera, V., & Impellizzeri, G. (2017). ZnO for application in photocatalysis: From thin films to nanostructures. Materials Science in Semiconductor Processing, 69, 44-51.

[42] Fahimmunisha, B. A., Ishwarya, R., AlSalhi, M. S., Devanesan, S., Govindarajan, M., & Vaseeharan, B. (2020). Green fabrication, characterization and antibacterial potential of zinc oxide nanoparticles using Aloe socotrina leaf extract: A novel drug delivery approach. Journal of Drug Delivery Science and Technology, 55, 101465.

[43] Spoială, A., Ilie, C. I., Trușcă, R. D., Oprea, O. C., Surdu, V. A., Vasile, B. Ș., ... & Dițu, L. M. (2021). Zinc oxide nanoparticles for water purification. Materials, 14(16), 4747.

[44] Mascini, M., Gaggiotti, S., Della Pelle, F., Di Natale, C., Qakala, S., Iwuoha, E., ... & Compagnone, D. (2018). Peptide modified ZnO nanoparticles as gas sensors array for volatile organic compounds (VOCs). Frontiers in chemistry, 6, 105.

[45] Umar, A., Rahman, M. M., Vaseem, M., & Hahn, Y. B. (2009). Ultra-sensitive cholesterol biosensor based on low-temperature grown ZnO nanoparticles. Electrochemistry Communications, 11(1), 118-121.

[46] Smijs, T. G., & Pavel, S. (2011). Titanium dioxide and zinc oxide nanoparticles in sunscreens: focus on their safety and effectiveness. Nanotechnology, science and applications, 95-112.

[47] Jiang, J., Pi, J., & Cai, J. (2018). The advancing of zinc oxide nanoparticles for biomedical applications. Bioinorganic chemistry and applications, 2018.

[48] Barir, R., Benhaoua, B., Benhamida, S., Rahal, A., Sahraoui, T., & Gheriani, R. (2017). Effect of precursor concentration on structural optical and electrical properties of NiO thin films prepared by spray pyrolysis. Journal of Nanomaterials, 2017.

[49] S. Perusin, Conséquences de l'oxydation haute température sur l'injection de défauts et le comportement mécanique des matériaux métalliques, Thése de Doctorat, Institut National Polytechnique de Toulouse, (2004).

[50] J. Wang, P. Yang, X. Wei, Z. Zhou, Preparation of NiO two-dimensional grainy films and their high-performance gas sensors for ammonia detection, Nanoscale research letters, **10** (2015) 119.

[51] V.P. Michel A.Petit, Electrochemical study of iridium oxide layers in anhydrous propylene carbonate by cyclic voltammetry and "mirage effect" analysis, Journal of Electroanalytical Chemistry, **379** (1994) 165-172.

[52] Park, D. H. (2010). Optimization of nickel oxide-based electrochromic thin films (Doctoral dissertation, Université Sciences et Technologies-Bordeaux I).

[53] Moulki, H. (2013). Matériaux et dispositifs électrochromes à base de NiO modifié en couches minces (Doctoral dissertation, Bordeaux 1).

[54] Stanescu, S. (2002). Structure and morphology of NiO/Cu (111) and NiO/FeNi/Cu (111) ultra-thin layers and nanostructures (Doctoral dissertation, Université Louis Pasteur-Strasbourg I).

[55] Bouzoubaa, A. (2008). Modélisation atomistqiue des interactions entre les ions chlorures et la surface du nockel passivé (Doctoral dissertation, Chimie Paris Tech).

[56] Benhamida, S. (2018). Caractérisation Des Couches Minces D'oxyde De Nickel (NiO) Elaboré Par Spray Pyrolyse (Doctoral dissertation, Université Mohamed Khider-BISKRA).

[57] Schuler, T. M., Ederer, D. L., Itza-Ortiz, S., Woods, G. T., Callcott, T. A., & Woicik, J. C. (2005). Character of the insulating state in NiO: A mixture of charge-transfer and Mott-Hubbard character. Physical Review B, 71(11), 115113.

[58] Mott, N. F. (1949). The basis of the electron theory of metals, with special reference to the transition metals. Proceedings of the Physical Society. Section A, 62(7), 416.

[59] The effect of temperature on the properties of NiO thin layers produced by solar pyrolysis spray. Authors: زكريا, دو · اسامة, دباب · سعد, بوصبيع العايش.

[60] Reguig, B. A., Regragui, M., Morsli, M., Khelil, A., Addou, M., & Bernede, J. C. (2006). Effect of the precursor solution concentration on the NiO thin film properties deposited by spray pyrolysis. Solar Energy Materials and Solar Cells, 90(10), 1381-1392.

[61] Obaida M., Fathi A.M., Moussa I. et al. Characterization and electrochromic properties of NiO thin films prepared using a green aqueous solution by pulsed spray pyrolysis technique. Journal of Materials Research 37 (2022)2282–2292.

[62] Suman Nandy, Biswajit Saha, Manoj K. Mitra, K. K. Chattopadhyay, Effect of oxygen partial pressure on the electrical and optical properties of highly (200) oriented p-type Ni 1–xO films by DC sputtering, J Mater Sci (2007) 42:5766–5772

[63] Long Zhang, Peter Staar, Anton Kozhevnikov, Yun-Peng Wang, DFT+DMFT calculations of the complex band and tunneling behavior for the transition metal monoxides MnO, FeO, CoO and NiO, Phys. Rev. B 100, 035104 – Published 8 July 2019

[64] Lany, S., Osorio-Guillén, J., & Zunger, A. (2007). Origins of the doping asymmetry in oxides: Hole doping in NiO versus electron doping in ZnO. Physical Review B, 75(24), 241203.

[65] Le Pévédic, S. (2007). Etude de la formation et de l'oxydation de couches minces d'alliages Al-Ni après dépôt d'Al sur un monocristal de Ni (111) (Doctoral dissertation, Université Pierre et Marie Curie- Paris VI).

[66] Mrabet, C., Amor, M. B., Boukhachem, A., Amlouk, M., & Manoubi, T. (2016). Physical properties of La-doped NiO sprayed thin films for optoelectronic and sensor applications. Ceramics International, 42(5), 5963-5978.

[67] J. Wang, P. Yang, X. Wei, Z. Zhou, Preparation of NiO two-dimensional grainy films and their high-performance gas sensors for ammonia detection, Nanoscale research letters, 10 (2015) 119.

[68] Desai, J. D., Min, S. K., Jung, K. D., & Joo, O. S. (2006). Spray pyrolytic synthesis of large area NiO_x thin films from aqueous nickel acetate solutions. Applied Surface Science, 253(4), 1781-1786.

[69] M. R. Waugh, "The Synthesis, Characterization and Application of Transparent Conducting Thin Films", Doctorate Thesis, College London University, (2011), England.

[70] Mrabet, C., Amor, M. B., Boukhachem, A., Amlouk, M., & Manoubi, T. (2016). Physical properties of La-doped NiO sprayed thin films for optoelectronic and sensor applications. Ceramics International, 42(5), 5963-5978.

[71] Belahssen, O., M. Ghougali, and A. Chala. "Effect of iron doping on physical properties of NiO thin films." Journal of Nano-and Electronic Physics 10.2 (2018).

[72] Ghougali, M., et al. "Investigation of the physical properties of nanostructured CO: NiO thin films." Chalcogenide Letters 18.12 (2021): 765-775.

[73] Ghougali, Mebrouk. Elaboration and characterization of nanostructuring NiO thin films for gas sensing applications. Diss. University of Mohamed Khider, BISKRA, 2019.

[74] Khodair, Ziad T., Asaad A. Kamil, and Yamamah K. Abdalaah. "Effect of annealing on structural and optical properties of $Ni_{(1-x)}Mn_xO$ nanostructures thin films." Physica B: Condensed Matter 503 (2016): 55-63.

[75] Hu, Z., Chen, D., Yang, P., Yang, L., Qin, L., Huang, Y., & Zhao, X. (2018). Sol-gel-processed yttrium-doped NiO as hole transport layer in inverted perovskite solar cells for enhanced performance. Applied Surface Science, 441, 258-264.

[76] Gebretinsae, H. G., Tsegay, M. G., Welegergs, G. G., Maaza, M., & Nuru, Z. Y. (2022). Effect of rotational speed on the structural, morphological, and optical properties of biosynthesized Nickel Oxide thin films for selective solar absorber nanocoatings. Energies, 15(23), 8960.

[77] Stamataki, M., Tsamakis, D., Brilis, N., Fasaki, I., Giannoudakos, A., & Kompitsas, M. (2008). Hydrogen gas sensors based on PLD grown NiO thin film structures. physica status solidi (a), 205(8), 2064-2068.

[78] Green, M., & O'Brien, P. (2001). The preparation of organically functionalised chromium and nickel nanoparticles. Chemical Communications, (19), 1912-1913.

[79] M.Messaouda, Mémoire de master, Université Larbi Tébessi- Tébessa (Algérie), 2015.

[80] Ezhilarasi, A. A., Vijaya, J. J., Kaviyarasu, K., Maaza, M., Ayeshamariam, A., & Kennedy, L. J. (2016). Green synthesis of NiO nanoparticles using Moringa oleifera extract and their biomedical applications: Cytotoxicity effect of nanoparticles against HT-29 cancer cells. Journal of Photochemistry and Photobiology B: Biology, 164, 352-360.

[81] S. Pevedic, Thèse de doctorat, Université Pierre et Marie Curie-PARIS VI (France), 2007.

[82] H.Benzarouk, Mémoire de magister, Université d'Annaba (Algérie), (2008).

[83] S. Perusin, Thèse de doctorat, Université Toulouse, 2004.

[84] A. Bouzoubaa, Thèse de Doctorat, Université Pierre et Marie Curie-Paris VI (France), 2008.

[85] M. Belkhir, Thèse de doctorat, Université de Metz, 1988.

[86] B.A. Reguig, M. Regragui, M. Morsli, A. Khelil, M. Addouc, J.C. Bernède, Solar Energy Materials & Solar Cells. 2006,90, 1381–1392.

[87] Amor, M. B., Boukhachem, A., Boubaker, K., & Amlouk, M. (2014). Structural, optical and electrical studies on Mg-doped NiO thin films for sensitivity applications. Materials science in semiconductor processing, 27, 994-1006.

[88] Sato, H., Minami, T., Takata, S., & Yamada, T. (1993). Transparent conducting p-type NiO thin films prepared by magnetron sputtering. Thin solid films, 236(1-2), 27-31.

[89] GROUNDWATER, C. O. G. A. I. (2017). Bondu, R., Cloutier, V., Rosa, E., Benzaazoua, M. (2016). A review and evaluaion of the impacts of climate change on geogenic arsenic in groundwater from fractured bedrock aquifers. Water, Air, & Soil Pollution, 227 (9), 296. Mise en garde, 98.

[90] Sato, H., Minami, T., Takata, S., & Yamada, T. (1993). Transparent conducting p-type NiO thin films prepared by magnetron sputtering. Thin solid films, 236(1-2), 27-31.

[91] Berkat, L., Cattin, L., Reguig, A., Regragui, M., & Bernede, J. C. (2005). Comparison of the physico-chemical properties of NiO thin films deposited by chemical bath deposition and by spray pyrolysis. Materials chemistry and physics, 89(1), 11-20.

[92] H.Kamel, E.K, Elmaghraby, S.A.Ali, K.Abdel-Hady, Journal of Crystal Growth. 2004, **262**, 424- 434.

[93] Carcia, P. F., McLean, R. S., Reilly, M. H., & Nunes Jr, G. (2003). Transparent ZnO thin-film transistor fabricated by rf magnetron sputtering. Applied Physics Letters, 82(7), 1117-1119.

[94] Nandy, S., Maiti, U. N., Ghosh, C. K., & Chattopadhyay, K. K. (2009). Enhanced p-type conductivity and band gap narrowing in heavily Al doped NiO thin films deposited by RF magnetron sputtering. Journal of Physics: Condensed Matter, 21(11), 115804.

[95] Fasaki, I., Koutoulaki, A., Kompitsas, M., & Charitidis, C. (2010). Structural, electrical and mechanical properties of NiO thin films grown by pulsed laser deposition. Applied Surface Science, 257(2), 429-433.

[96] Jin, B. J., Bae, S., Lee, S. Y., & Im, S. (2000). Effects of native defects on optical and electrical properties of ZnO prepared by pulsed laser deposition. Materials Science and Engineering: B, 71(1-3), 301-305.

[97] Benramache, S., Benhaoua, B., Chabane, F., & Guettaf, A. (2013). A comparative study on the nanocrystalline ZnO thin films prepared by ultrasonic spray and sol gel method. Optik-International Journal for Light and Electron Optics, 124(18), 3221-3224.

[98] Kong, J., Cassell, A. M., & Dai, H. (1998). Chemical vapor deposition of methane for single-walled carbon nanotubes. Chemical physics letters, 292(4-6), 567-574.

[99] Son, I. H., Song, H. J., Kwon, S., Bachmatiuk, A., Lee, S. J., Benayad, A., ... & Rümmeli, M. H. (2014). CO2 enhanced chemical vapor deposition growth of few-layer graphene over NiO x. ACS nano, 8(9), 9224-9232.

[103] Nakaruk, A. S. C. C., & Sorrell, C. C. (2010). Conceptual model for spray pyrolysis mechanism: fabrication and annealing of titania thin films. Journal of Coatings Technology and Research, 7, 665-676.

[104] Perednis, D., & Gauckler, L. J. (2004). Solid oxide fuel cells with electrolytes prepared via spray pyrolysis. Solid state ionics, 166(3-4), 229-239.

[105] Li, W., & Davis, E. J. (1995). Measurement of the thermophoretic force by electrodynamic levitation: Microspheres in air. Journal of aerosol science, 26(7), 1063-1083.

[106] SALMI, A. (2021). Synthesis and characterization of copper doped nickel oxide thin films by spray pyrolysis technique (Doctoral dissertation).

[107] Falcony, C., Aguilar-Frutis, M. A., & García-Hipólito, M. (2018). Spray pyrolysis technique; high-K dielectric films and luminescent materials: a review. Micromachines, 9(8), 414.

[108] SALMI, A. (2021). Synthesis and characterization of copper doped nickel oxide thin films by spray pyrolysis technique (Doctoral dissertation).

[109] Fachini, F. F. (2007). Effects of the initial droplet temperature on the vaporization process at high pressure. Journal of the Brazilian Society of Mechanical Sciences and Engineering, 29, 91-98.

[110] Siefert, W. (1984). Properties of thin In_2O_3 and SnO_2 films prepared by corona spray pyrolysis, and a discussion of the spray pyrolysis process. Thin solid films, 120(4), 275-282.

[111] Perednis, D., & Gauckler, L. J. (2005). Thin film deposition using spray pyrolysis. Journal of electroceramics, 14, 103-111.

[112] Filipovic, L., Selberherr, S., Mutinati, G. C., Brunet, E., Steinhauer, S., Köck, A., ... & Grogger, W. (2013). A method for simulating spray pyrolysis deposition in the level set framework. Eng. Lett, 21(4), 224-240.

[113] PrasannaKumari, K., & Thomas, B. (2018). Synthesis of nano-structured tin oxide thin films with faster response to LPG and ammonia by spray pyrolysis. Materials Research Express, 5(1), 014007.

[114] Zahedi, F., Dariani, R. S., & Rozati, S. M. (2013). Effect of substrate temperature on the properties of ZnO thin films prepared by spray pyrolysis. Materials Science in Semiconductor Processing, 16(2), 245-249.

[115] Karthik, T. V. K., Hernández, A. G., Kudriavtsev, Y., Gómez-Pozos, H., Ramírez-Cruz, M. G., Martínez-Ayala, L., & Escobosa-Echvarria, A. (2020). Sprayed ZnO thin films for gas sensing: effect

of substrate temperature, molarity and precursor solution. Journal of Materials Science: Materials in Electronics, 31, 7470-7480.

[119] Swapna, R., & Kumar, M. S. (2012). The role of substrate temperature on the properties of nanocrystalline Mo doped ZnO thin films by spray pyrolysis. Ceramics International, 38(5), 3875-3883.

[120] Kamal, H., Elmaghraby, E. K., Ali, S. A., & Abdel-Hady, K. (2004). Characterization of nickel oxide films deposited at different substrate temperatures using spray pyrolysis. Journal of crystal growth, 262(1-4), 424-434.

[121] Godbole, B., Badera, N., Shrivastava, S. B., Jain, D., & Ganesan, V. (2007). Investigation of Fe-doped and-undoped NiO nanocrystalline films. Surface Review and Letters, 14(06), 1113-1119.

[122] Krunks, M., Soon, J., Unt, T., Mere, A., & Mikli, V. (2014). Deposition of p-type NiO films by chemical spray pyrolysis. Vacuum, 107, 242-246.

[123] Romero, R., Martin, F., Ramos-Barrado, J. R., & Leinen, D. (2010). Synthesis and characterization of nanostructured nickel oxide thin films prepared with chemical spray pyrolysis. Thin Solid Films, 518(16), 4499-4502.

[124] Jlassi, M., Sta, I., Hajji, M., & Ezzaouia, H. (2014). Synthesis and characterization of nickel oxide thin films deposited on glass substrates using spray pyrolysis. Applied Surface Science, 308, 199-205.

[125] Lehraki, N., Aida, M. S., Abed, S., Attaf, N., Attaf, A., & Poulain, M. (2012). ZnO thin films deposition by spray pyrolysis: Influence of precursor solution properties. Current Applied Physics, 12(5), 1283-1287.

[126] Arca, E., Fleischer, K., & Shvets, I. V. (2009). Influence of the precursors and chemical composition of the solution on the properties of ZnO thin films grown by spray pyrolysis. The Journal of Physical Chemistry C, 113(50), 21074-21081.

[127] Gomaa, M. M., Yazdi, G. R., Schmidt, S., Boshta, M., Khranovskyy, V., Eriksson, F., ... & Yakimova, R. (2017). Effect of precursor solutions on the structural and optical properties of sprayed NiO thin films. Materials Science in Semiconductor Processing, 64, 32-38.

[128] Arabi, H., & Moghadam, N. K. (2013). Nanostructure and magnetic properties of magnesium ferrite thin films deposited on glass substrate by spray pyrolysis. Journal of Magnetism and Magnetic Materials, 335, 144-148.

[129] J. C. Vigui and J. Spitz, Chemical Vapor Deposition at Low Temperatures, Journal of the Electrochemical Society, (1975) 122 585.

[130] In˜igo Bretos, Ricardo Jime´nez, Jesu´s Ricote and M. Lourdes Calzada, Low-temperature crystallization of solution-derived metal oxide thin films assisted by chemical processes, Chemical Society Reviews 2018, 47, 291-

II.1. Introduction:

In this chapter a presentation will take place for various steps followed about the elaboration of ZnO, Al and Na codoped NiO and ZnO/$Ni_{(1-x)}$ Cu_xO heterojunctions thin films by spray pyrolysis process. Then the principles operating of different characterization techniques which have used in this context to analyze the structural, optical and electrical properties of elaborated thin films, then a discussed along with their principles and instrumentations are exhibited.

These analytical techniques are X-ray diffraction (DRX) and scanning electron microscopy (SEM) coupled with Energy Dispersion Spectroscopy (EDS), FTIR (Fourier Transformed Infrared), leading to deduce the chemical structure of materials (the chemical bond in the thin films), whereas (SEM) allows to have the morphology of the films and use of EDS mode giving the elemental composition. UV-visible spectroscopy that measures film thicknesses, optical gap and other measurements of optical properties of the prepared thin films such as the transmittance. Also, the four-point method for measuring the sheet resistance of the films will take place.

II.2. Experimental montage of homemade SPT system:

The homemade SPT system is shown in Fig II. 1, which is used to prepare ZnO and NiO samples as well as ZnO/NiO (n-p) heterojunctions samples. Actually, it exists in applied chemistry laboratory in Biskra University; this device is built from a simple and easy experimental equipment to make homogeneous and transparent films.

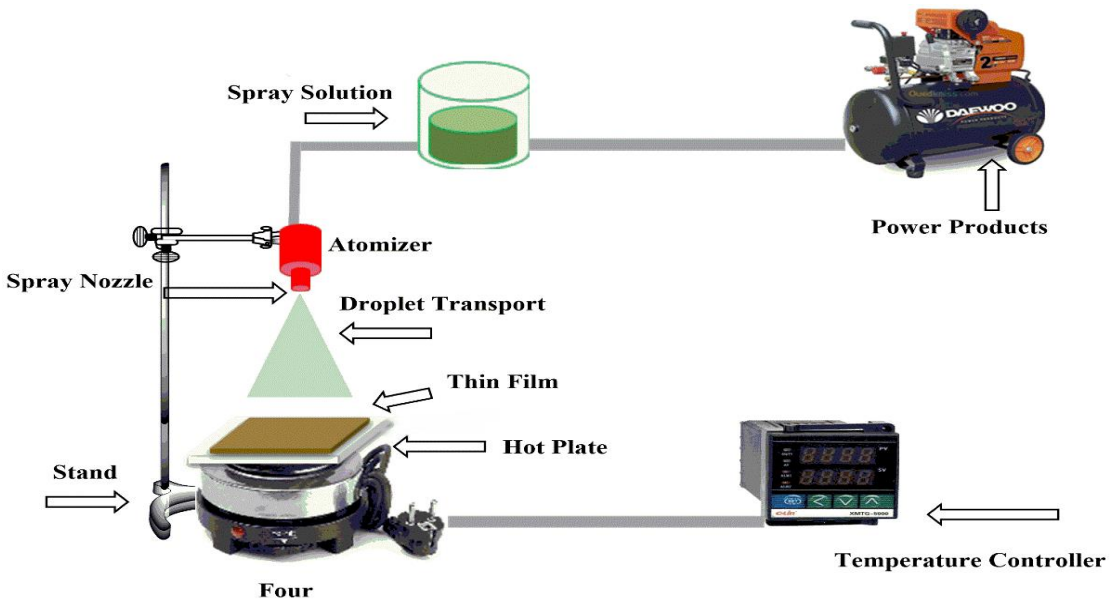

Figure II.1: The Illustration SPT system

II.3 Deposition parameters:

In the chemical spray deposition technique, the structure, composition and other characteristics of the deposited films depend on a number of process variables (deposition parameters). The variable quantities such as the substrate temperature, solution concentration and air flow rate, deposition time, quality of the substrate material, size of atomized droplets, distance between substrate and atomizer, etc. Those variables have effects on the film properties. To study the effect of any one of these parameters on the film properties we keep the other parameters fixed. For the deposition of thin film, all the above-mentioned parameters were kept at their optimum values (see Table II. 1)

Table II. 1: The values of the fixed parameters used for preparing study samples

Parameters	Optimum values
Air pressure	2 bar
Deposition rate	1 ml/min
Distance between the atomizer precursors solution	37.5 cm
Deposition time	10 min
Precursor solution volume	10 ml

II.4 Experimental procedure :

II.4.1 Choice of deposit substrates:

Based on an economic reason, the chosen substrates to deposit the thin films are microscope slides (see Fig II.2), having dimension of 2.5x7.5x0.3cm^3 which is cut for by pointed pen to glass slides having a surface (2.5 x 1.5) cm^2 for future measurement of the properties.

In addition to the economic reason, the choice of the glass for the type of the substrate is because of the good agreement of thermal expansion that it presents with NiO and ZnO (α_{verre} = 8.5 x 10^{-6} K^{-1}, α_{NiO} = 3.2 x 10^{-5} K^{-1} [1], α_{ZnO} = 7.2 x 10^{-6} K^{-1} [2]. in order to minimize the stresses at the layer-substrate interface and this type of glass is limited by a temperature of 600°C, as well as the glass substrates adapt well for the optical and electrical characterization of our films.

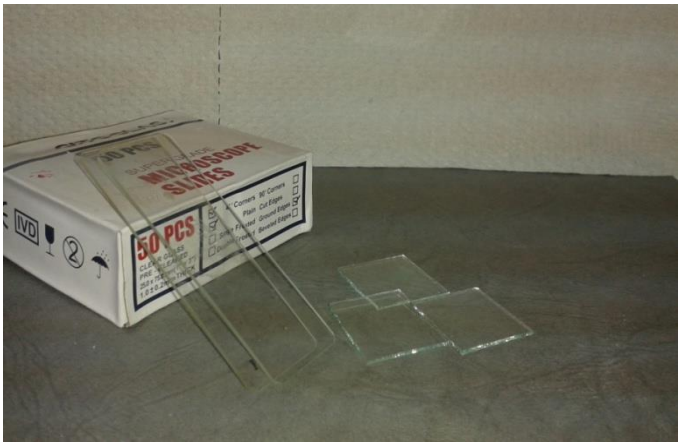

Figure II.2: Glass substrates.

II.4.2 The substrate surface cleaning:

Indeed, the best quality of deposition (uniformity of thickness) requires the cleanliness of the substrate surface (grease, dust ...) which is the necessary step that precede the depositing step.

In this work the substrates were cleaned according to the following steps:

a. Wash with double distilled water
b. Wash with methanol and then with acetone for 2 min.
c. Carrying out another wash using distilled water.
d. Drying with an optical paper.
e. Avoid touching the surface of the substrate to avoid all contamination.

II.4.3 Choice of precursors solutions:

For ZnO samples, Na and Al codoped NiO samples, and **$ZnO/Ni_{(1-X)}Cu_XO$** heterojunctions, some salts were chosen as follow:

1. **Pure ZnO samples:** zinc acetate dehydrate was chosen;
2. **Na and Al codoped NiO samples:** nickel chloride hexahydrate was chosen; sodium chloride dehydrate and aluminum chloride dehydrate as two sources of dopant.
3. **heterojunctions $ZnO/Ni_{(1-X)}Cu_XO$ samples:** zinc acetate dehydrate, nickel dinitrate hexahydrate and copper dinitrate trihydrate as doping source were chosen.

Some physical and chemical properties of the sources are given in six tables as shown below:

II.4.3.1 Physical and chemical properties of used salts:

- **Zinc acetate dehydrate:**

Table II.2: Some physical properties of zinc acetate dehydrate [3]

Property	Value
Physical state	Solid
The molecular formula	$Zn(C_2H_3O_2)_2.2H_2O$
Molar mass	219.50g/mol
Melting point	237°C
Boiling point	Decomposes
Density	$1.735g/cm^3$ at 20°C
Water solubility	Soluble
Purity	98%

❖ **Nickel (II) nitrate hexahydrate**:

Table II. 3: Some physical properties of nickel (II) nitrate hexahydrate [4]

Property	**Value**
Physical state	Solid
The molecular formula	Ni $(NO_3)_2.6H_2O$
Molar mass	290.79g/mol
Melting point	56.70°C
Boiling point	136.70°C
Density	2.05g/cm^3
Water solubility	soluble
Purity	98%

❖ **Nickel Chloride hexahydrate**:

Table II. 4: Some physical properties of nickel chloride hexahydrate [5]

Property	**Value**
Physical state	Solid
The molecular formula	$NiCl_2.6H_2O$
Molar mass	237.69 g/mol
Melting point	140°C
Boiling point	*973°C*
Density	1.92 g/cm^3
Water solubility	Very soluble in H_2O
Purity	99%

❖ **The doping sources :**

✓ **Sodium Chloride dehydrate $NaCl_2.2H_2O$:**

Table II. 5: Some physical properties of sodium chloride dehydrate [6]

Property	Value
Physical state	Solid
The molecular formula	$NaCl_2$, $2H_2O$
Molar mass	58.44 g/mol
Melting point	800.7 °C
Boiling point	1465 °C
Density	2.17 g/cm^3
Water solubility	soluble in water
Purity	99.7%

❖ **Aluminum chloride dehydrate $AlCl_2.2H_2O$:**

Table II. 6: Some physical properties of aluminum chloride dehydrate [7]

Property	Value
Physical state	Solid
The molecular formula	$AlCl_2$, $2H_2O$
Molar mass	169.37 g/mol
Melting point	192.4° C
Boiling point	120° C
Density	2.48 g/cm^3
Solubility	*Soluble in water* and alcohol
Purity	99%

❖ **copper (II) nitrate trihydrate:**

Table II. 7: Some physical properties of Copper (II) nitrate trihydrate [8]

Property	Value
Physical state	Solid
The molecular formula	Cu $(NO_3)_2.3H_2O$
Molar mass	241.6g/mol
Melting point	114°C.
Boiling point	170°C
Density	2.32g/cm^3
Solubility	soluble in water at 0°C
Purity	99.5%

II.5 Thin films deposition steps:

II.5.1 Preparation of precursors solutions:

a) Used solvent:

For the preparation of all the above precursors solutions it was used the following group of solvents, for instance 10ml of solution it was used:

- 3ml of Bi-distilled water
- 2ml of Acetic acid CH_3COOH
- 5ml of Isopropyl alcohol C_3H_7OH

b) Magnetic stirring for 15 minutes at room temperature.

c) HCl (Agitation for 2 hours at 50 °C) is added dropwise to increase the solubility of precursors in the solvents and leads to a transparent and homogeneous solution

II.5.2 Deposition conditions of pure ZnO thin films:

Zinc acetate dihydrate Zn $(CH_3COO)_2.2H_2O$ was weighted according to its stoichiometric percentage of (0.1M) using an automatic scale of the type (KERN PLS360-3 Fig. (II.6), precision

10^{-3}g), and then it is dissolved in the above solvents. The ZnO films were deposited at a temperature ranging from 350 to 410°C for 8 minutes as illustrated in Table II. 8.

To produce ZnO thin film, a chemical reaction may take place on the previously heated substrate as following

$$Zn\ (CH_3COO)_2.2H_2O \longrightarrow ZnO + CO_2 + CH_4 + Steam$$

When a droplet of the solution reaches the substrate, a chemical reaction happens between the zinc acetate and water solution under the stimulated temperature, which provides the formation of ZnO thin films.

Table II.8 illustrates the experimental conditions of elaboration of undoped ZnO thin films.

Table II. 8: Summary of experimental conditions of ZnO

First series	T_s(°C)	C (mol/l)
1	380	0.05
2		0.075
3		0.1
4		0.125
First series	**C (mol/l)**	**T_s(°C)**
1	0.1	350
2		380
3		410

II.5.3 Deposition conditions of Na and Al codoped NiO thin films:

Na and Al codoped NiO solutions were prepared by dissolving 0.1M nickel chloride hexahydrate ($NiCl_2$, $6H_2O$) and Na/Ni = 2% of sodium chloride dehydrate ($NaCl_2$, $2H_2O$) and x% of aluminum chloride dehydrate ($AlCl_2$, $2H_2O$) with the ratio of Al/Ni = 0, 0.01, 0.02, 0.03 and 0.04. The mixtures solutions were dissolved in a solvent containing equal volumes of absolute ethanol solution (99.995%) purity. The HCl solution was added to stabilize the solution; which was stirred at 50°C for 120 min to yield a clear and transparent solution. The final solution of NiO was obtained according to the following equations:

$$NiCl_2 + 6H_2O \rightarrow 2HCl + Ni\ (OH)_2 + 4H_2O$$

$$NiCl_2 + 6H_2O \rightarrow 2HCl + NiO + 5H_2O$$

Na and Al codoped NiO solutions were deposited on heated glass substrates at 420°C by spray pneumatic method, which is transforms the liquid into a stream formed with uniform and fine droplets of 25 µm average diameters.

Table II. 9 illustrates the experimental conditions for elaboration of NiO codoped Na and Al thin films.

Table II. 9: Summary of experimental conditions of Na and Al codoped NiO thin films

Depot at T_s = 420°C	Na%	Al%
1	2%	0%
2	2%	1%
3	2%	2%
4	2%	3%
5	2%	4%

II.5.4 Deposition conditions of $ZnO/Ni_{1-x}Cu_xO$ thin heterojunctions:

The nickel dinitrate hexahydrate (Ni $(NO_3)_2.6H_2O$) is also weighed according to its stoichiometric percentage 0.1M. The doping source of NiO is copper dinitrate trihydrate (Cu $(NO_3)_2.3H_2O$), the molar ratio of the dopant varies from 1 to 4% Cu/Ni. The NiO films were deposited at a temperature ranging from 350°C to 500°C for eight minutes. Table II.10 illustrates the experimental conditions of $Ni_{1-x}Cu_xO$ thin films of elaboration on ZnO support prepared previously (C= 0.1M/L and 380°C).

Table II.10: Summary of experimental conditions of preparation of undoped hetero junctions ZnO/NiO

Depot of undoped NiO under conditions: C=0.1M/l and ZnO as support prepared at C= 0.1M/L and 380°C	**T_{sNiO}(°C)**
1	350
2	400
3	450
4	500

Table II.11: Summary of experimental conditions of Cu doped hetero junctions $ZnO/Ni_{1-X}Cu_XO$

Depot of NiO under conditions: C=0.1M/l and ZnO as support prepared at C= 0.1M/L and T_s=380°C	**Cu (%)**	**T_{sNiO} °C**
1	2	350
2		400
3		450
4		500

Depot of NiO under conditions: C=0.1M/l and ZnO as support prepared at C= 0.1M/L and 380°C	**T_{sNiO} °C**	**Cu (%)**
1	450	2
2		3
3		4

II.5.5 Samples preparation:

After preparing the earlier mentioned solutions. magnetic stirring and HCl agitation, is taken place, after that the solution is placed in the flask.

After the preparation of the substrate, the substrate carrier is placed on top of a heating element (resistance) controlled by a temperature regulator to prevent the thermal shock of the substrates; the substrate carrier is heated progressively from the room temperature to the chosen temperature for the deposition. When the heating is carried out, the defect of the solution is fixed, very fine droplets are sprayed on the heated substrate thus allowing activation of the chemical reaction between the compounds; the volatiles evaporate due to the endothermic reaction while the two compounds react with each other to form the thin film. At the end of the deposition, the substrates are cooled on the substrate carrier to room temperature.

1) The distance between sprayer and substrate is fixed and equal to 37 Cm.
2) While each spraying time took five seconds separated by another five seconds as a break time to keep the heat of the substrate's constant.

II.6 Characterization techniques:

Characterization techniques play important role in semiconducting materials which are synthesized by different methods. The structural and electronic properties as well as the primary particle size distribution are strongly dependent on the preparation method. Once the synthesis of an appropriate material is done, the first goal is to perform the characterizations of that particular material. In order to perform this in a systematic way, one needs a diverse array of characterization techniques. An important issue is the correct interpretation of the experimental results obtained by characterization tools. To confirm this, in this element we will describe the various characterization techniques utilized in this work.

II.6.1 Structural characterizations:

II.6.1.1 X-rays diffraction:

X-rays diffraction (XRD) is a characterization technique that can be used to determine the crystallographic properties of the prepared thin films such as: the crystalline structure, the growth orientation of the crystallites in the sample, the crystallites sizes, … etc.

Crystalline state studies of the present work have been made systematically on all the films. These studies were carried out by X-ray diffraction using tow diffractometers, the first one is type of (Rigaku Mini Flex 600) in Biskra university and the second one is type of PROTO in Eloued university as shown in Fig II.3. X-rays were produced from a copper-anode Cu Kα radiation source with a wavelength of $\lambda = 1.5405A°$, with an acceleration voltage of 30-40KV and a current of 20-30 mA.

The positions and intensity of the diffraction lines of most known materials have been

studied and are recorded in databases in the form of data files for example (JCPDS: Joint Committe for Powder Diffraction Standards). The comparison of an experimental spectrum with these data makes it possible to identify the nature of each constituent phase of the thin films.

Figure II.3: (a) Diffractometer type (Rigaku-MiniFlex600). **(b)** Diffractometer type PROTO

II.6.1.2 Principle of XRD analysis:

When a monochromatic X-ray beam is directed at a polycrystalline material, it is partially reflected by the atomic planes of some crystals Fig II.4. The diffraction will take place only in the crystallized materials and when the Bragg low is verified [3]:

$$2d_{hkl}\sin\theta = n\lambda \qquad \text{(II.2)}$$

Where d_{hkl}: is the inter-reticular distance, that is, the distance between two crystallographic planes.

θ: the angle of incidence and therefore of reflection with respect to these plans.

n: the order of reflection in our studies will be limited to the first order.

λ: the wavelength of the X-ray beam.

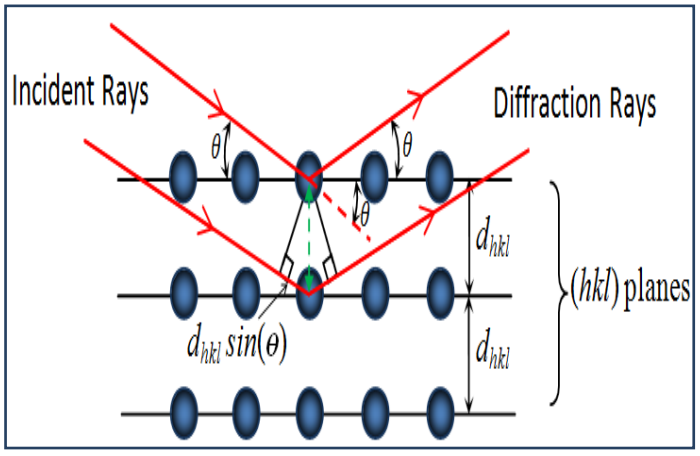

Figure II.4: Schematic of X-ray diffraction According to Bragg

II.6.1.3 Information obtained from XRD spectrum:

There is much information that we may deduce from the XRD pattern, some of which are presented below.

II.6.1.3.a Grain size:

From the spectra given by X-rays diffraction the width generated in the most intensity peak which known as full width at half maximum (FWHM) (See Fig II.5), can be used to calculate the average crystallites sizes of the film in a direction perpendicular to the respective (*hkl*) planes, by using the Scherrer's formula [4], which is given as follow:

$$D = \frac{(0{,}9.\lambda)}{\beta cos\theta_{hkl}} \qquad \text{(II.3)}$$

Where D: is the average grain size obtaining from the peak (*hkl*), λ: Wavelength of the X-ray beam (λ=0.15406 nm), θ_{hkl}: is the diffraction angle expressed by radian, β_{hkl}: is the full width at half maximum intensity of the peak (*hkl*) expressed by radian

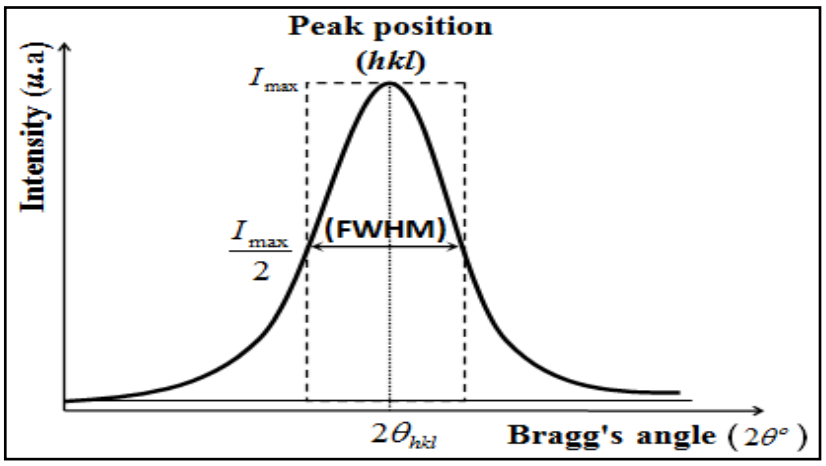

Figure II.5: Schematic diagram showing Full Width at Half Maximum (β)

II.6.1.3.b Lattice parameters:

We know that for a lattice, there is a relation connecting the planes (hkl), the inter-reticular distance d_{hkl} and the lattice parameters of the sample a,b and c.

a) On the first case, it is the hexagonal lattice of ZnO whose expression is given in the following form [5]:

$$\frac{1}{d_{hkl}} = \left(\frac{4}{3}\frac{h^2+hk+k^2}{a^2} + \frac{l}{c^2}^2\right)^{\frac{1}{2}} \qquad \text{(II.4)}$$

Where **a** and **c** are the lattice parameters.

From this formula, we can determine the parameter **a** taking in the measurement h=1, k=l=0 So we take the pick (100): $\frac{1}{d_{hkl}^2} = \frac{4}{3a^2}(1)^2 + \frac{0^2}{c^2}$ (II.5)

$$a = \sqrt{\frac{4d_{(100)}^2}{3}} = \sqrt{\frac{4}{3}}d_{100} \qquad \text{(II.6)}$$

The parameter **c** taking in the measurement h = k = 0, l = 2

So, we take the pick (002):

$$\frac{1}{d^2_{(002)}} = \frac{4}{3a^2}(0)^2 + \frac{2^2}{c^2} = \quad \text{(II.7)}$$

$$c = \sqrt{4d^2_{(002)}} = 2d_{(002)} \quad \text{(II.8)}$$

b) On the second case, for NiO films, the lattice is cubic (cfc) whose expression is given in the following form [6]:

$$d_{hkl} = \frac{a}{\sqrt{h^2+k^2+l^2}} \quad \text{(II.9)}$$

$$a = d_{hkl}.\sqrt{h^2 + k^2 + l^2} \quad \text{(II.10)}$$

If we take the pick (111):

$$a = \sqrt{3}d_{111} \quad \text{(II.11)}$$

II.6.1.3.c The main strain:

The strain (ε) values of the films were estimated from the observed shift, in the diffraction peak between their positions in the XRD spectra.

a) For the hexagonal lattice of ZnO the formula is given as follow [7]:

$$\varepsilon = (c^{exp} - c^{the})/c^{the} \quad \text{(II.12)}$$

Where (ε) is the strain in the film in the direction of the c-axis**,** $c^{exp}$is the lattice constant of ZnO thin films**,** and c^{the} is the lattice constant of the bulk (0.5205 nm).

The films possessing values of c greater than the bulk value exhibit a positive (or extensive) strain, while those with lower values display a negative (or compressive) strain [8].

b) For the cubic lattice of NiO the strain formula is given as follow [9].

$$\varepsilon = (a^{exp} - a^{the})/a^{the} \quad \text{(II.13)}$$

Where (ε) is the mean strain in NiO thin films**,** $a^{exp}$is the calculated lattice constant NiO thin films**,** and a^{the} is the standard lattice constant of the bulk (a^{the}= 4.1769 Å) according to standard carte (JCPDS, N_0 47-1049).

II.6.1.3.d Dislocation density:

A dislocation is a flaw found within a crystal and is linked to the misalignment of the lattice in one portion of the crystal with that in another section. Unlike vacancies and interstitial atoms, dislocations do not represent equilibrium defects, meaning that their significance cannot be solely explained by thermodynamic factors [10]. The dislocation density (δ) is the dislocation lines per unit area of the crystal can be evaluated from the grain size (D) using the formula [11].

$$\delta = 1/D^2\ (Lines/m^2) \quad \text{(II.14)}$$

II.6.1.4 Scanning Electron Microscope (SEM) is equipped with Energy Dispersive Spectroscopy (EDS) system.:

A scanning electron microscope provides information in the form of bright images, result of interaction of an electron beam with a microscopic volume of the studied sample.

The general principle of operation of an SEM comprises scanning sequentially, line by line, the surface of the sample with an electron beam and transmit the sensor signal to a cathode ray tube whose scan is precisely synchronized with the beam electronic incident.

The system consists of a secondary vacuum chamber or the electrons are emitted by a tungsten filament brought to high temperature (200 °C) in an electron gun.

1- In a gun electron are accelerated by a potential of the order of 0.5 to 30 eV.
2- The flow of electrons is then limited by the diaphragms and focused on the surface of the sample using different electromagnetic lenses in the form of a spot.
3- Deflector coils in X and Y allow the electric brush to be moved on the surface of the sample (XY plane).

The SEM analysis process is based on the detection of:

- **Primary electrons:** Some electrons are backscattered from the electron gun; others transmit part of their energy which will give rise to so-called secondary electrons and to X-rays.
- **Secondary electrons:** The secondary electrons are created by the passage of an incident electron near an atom. The incident electron can transmit a part of its energy to a little bound electron of the conduction band thus causing ionization by ejection of the latter electron. The kinetic energy of the latter cannot exceed 50 eV. Each incident electron can create several secondary electrons.

  Die of their low energy, only the secondary electrons emitted near the surface (<10 nm) can escape from the sample and be collected by the detector.

  The slightest topographic variation will modify the amount of secondary electrons collected [12].
- **The backscattered electrons:** the backscattered electrons are caused by the collision between an incident electron and an atom in the sample. These are primary electrons that reacted elastically with nuclei of atoms in the sample. They are scattered in all directions with little loss of energy.
  - ✓ Due to their high energy, the backscattered electrons recovered can come from a greater depth than that of the secondary electrons. They have a much lower topographic sensibility.
  - ✓ Due to their origin, the quantity of backscattered electrons increases with the atomic number of the constituent atoms of the target [17].
  - **X-rays (photon X):**

The emission of an X photon allows an ionized atom, under the impact of the electron beam, to return to the ground state. When an electron from an inner layer of an atom has been ejected, an electron from a more outer layer will fill the gap. The difference in energy between these two layers will cause the emission of a photon X (secondary emission) or an Auger electron as it is shown schematically in Fig II.6.

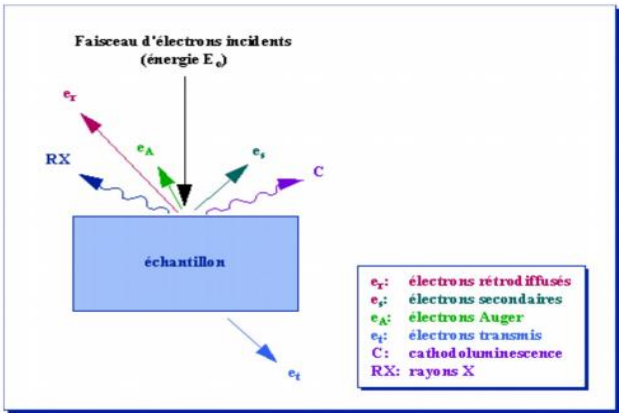

Figure II.6: Schematic representation of the interaction between an electron beam and the surface of a sample [13]

These X photons have a characteristic energy specific to each element which emitted them. These photons are collected and classified according to their energies. Electron Dispersion Spectroscopy (EDS) can provide information about the chemical composition of the sample under study. They are very penetrating and are emitted from an interaction pear of the order of a micron cube. The number of electrons arriving at the detector depends on the morphology of the surface where the detection is made.

The scanning electron microscope (SEM) is an analytical tool capable of swiftly providing morphology information. When utilized in EDS mode, it becomes feasible to ascertain the chemical composition of a solid object.; Taking in consideration that the measurement depth does not surpass a few hundred nanometers. [12].

For this study, the SEM images were obtained by an apparatus of type (TESCAN-VEGA3**)** Fig (II.7) from Biskra University.

Figure II.7: Scanning electron microscope typeTESCAN-VEGA3

II.6.1.6 FTIR characterization technique:

Infrared radiation is electromagnetic waves occurring between 0.8µm and 1mm that is to say between visible radiations and microwaves; the infrared radiation is subdivided into near infrared (0.8µm to 1µm), medium infrared (1.4µm to 3µm) and far infrared (3µm to 1000µm).

The molecular groups or networks constituting the material have a number of characteristic modes of vibration. Their vibration frequencies are determined by the masses of the constituent atoms, the interatomic forces and the geometry of the arrangements, that is to say the structure. The vibrations modify the dipolar electric moment, which causes the absorption of electromagnetic waves in the region of 1 to 100 µm which corresponds to the field of infrared spectroscopy.

The study by infrared spectroscopy makes it possible to obtain certain information on the structural organization of materials. The absorption bands being directly related to the binding force constant between atomic nuclei. The transmission limit is limited by the multiphonon break expressed by Hooke relation which expressed as follow [14]:

$$\nu = \frac{1}{2\pi c}\sqrt{\frac{k}{\mu}} \qquad \text{(II.15)}$$

Where µ: the reduced system mass ($\mu = \frac{1}{m_A} + \frac{1}{m_B}$),k: Force constant of the vibratory link (k=5.105 dyne.cm^{-1}) and m_A and m_B = atomic mass between two A atoms and B

C: speed of light.

The transmission specters of our samples were recorded between 4000 and 400 cm^{-1} via an FTIR spectrophotometer type of Cary 630 FTIR which is presented in Fig II.7. The principle of this technique is schematized in Fig II.8

Figure II.8: Fourier Transform Infrared Spectrophotometer apparatus type of Cary 630 FTIR

The modes which we worked are the modes of infrared absorption on KBr pastis which contains scraped powders of the prepared thin films, the measurements are taken at room temperature.

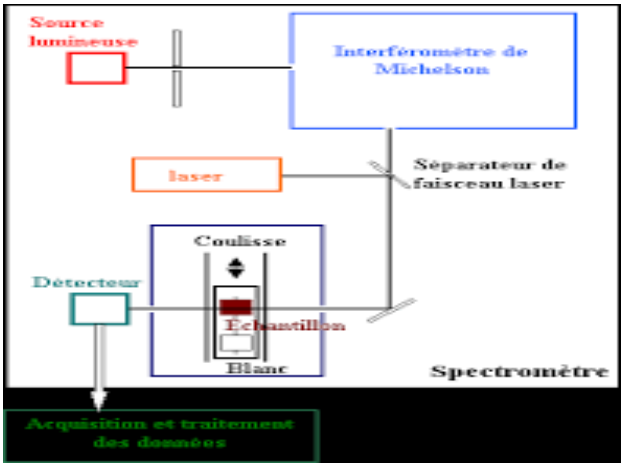

Figure II.9: Diagram of Fourier Transform Infrared spectroscopy [15]

II.6.2 Optical characterization:

II.6.2.1 UV-visible spectroscopy:

spectroscopy domains of are typically well-known according to the wave lengths interval utilized for measurements. The following areas can be distinguished: UV-visible, UV-visible-near infrared, infrared and microwave. The used apparatus is an UV-VIS spectrophotometer type of SHIMADZU UV-1900 i which recorder with double beams Fig II.10, its principle operational is illustrated in Fig II.11. By using this apparatus, we generated graphs representing the variation of the transmittance, as a function of the wavelength in the spectral domain from 200 to 900nm, the ultraviolet (UV) portion is studied from 200 to 400 nm, and the visible section is ranged in 400-800 nm. If the sample does not absorb light of a given wavelength, $I=I_0$. Furthermore, if the sample absorbs light then I is less than I_0, and this variation may be plotted on a graph versus wavelength.

Absorption was displayed as transmittance ($T = I/I_0$) or absorbance ($A = \log I_0/I$). If no existence of absorption so T = 1. and A= 0 [16]

By utilizing these curves, it's possible to calculate approximately the film's thickness and to determinate its optical characteristics including the optical absorption threshold, absorption coefficient, band gap width Eg, Urbach energy Eu and refractive index [17].

Figure II.10: UV-VIS spectrophotometer type of SHIMADZU UV-1900 i

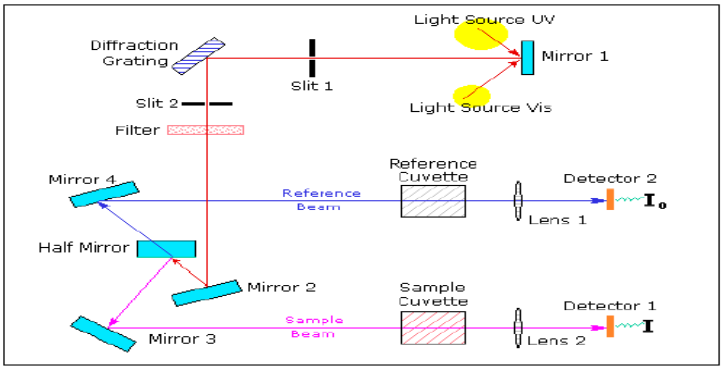

Figure II.11: Schematic representation of the UV-visible spectrophotometer [17]

II.6.2.1.A The transmittance spectra:

The transmission coefficient, or transmittance T, is defined as being the ratio of the transmitted light intensity to the incident light intensity. For the measurement of transmittance, our ZnO and NiO films were deposited on glass substrates. The latter is essential because it doesn't absorb the light in the spectral domain studied. A blank substrate is used in the reference beam of the spectrophotometer for the spectral plot, a computer connected to this device reproduces the spectra representing the transmittance T (%) of thin film as a function of the wavelength λ(nm) of the incident beam.

As an example, in Fig II.12, we reported a typical spectrum obtained in one of our

elaborated thin films [17], where we distinguish two domains:

a) The sudden decrease in transmission observed the shorter wavelengths in the range of 300 to 370 nm [18], corresponds to the absorption energy threshold of our NiO. This phenomenon can be attributed to the transition occurring between the valence band and the conduction band of this material.

b) The transmittance of the thin film is determined by calculating the average value in the range of 400 to 700 nm.

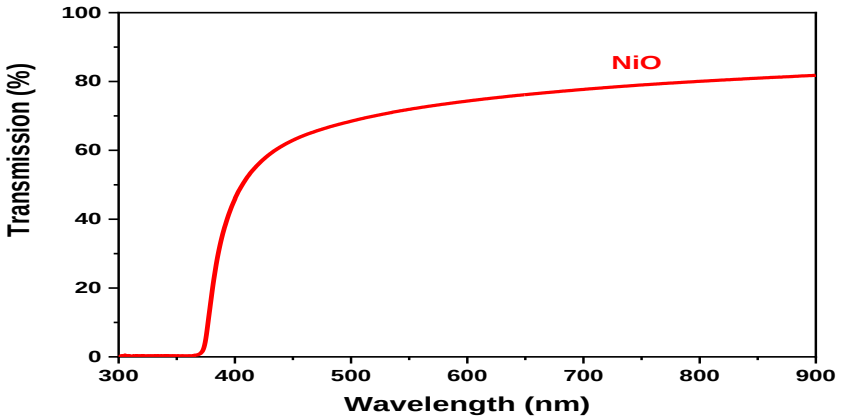

Figure II.12: Typical transmittance spectrum of NiO thin films deposited by spray [18]

II.5.2.1.B Measurement of optical properties:

a) Determination of the thickness of film:

The method which estimates the thickness (t) is the gravimetric method of difference of weight taking into account that the density ρ of ZnO and NiO is equal to 5.6 g/cm^3 and 6.7 g/cm^3 respectively, one defined by [19]:

$$t = \Delta m / A.\rho \qquad \text{(II. 16)}$$

With t: is the thickness of the film

Δm: is the different masses (before-after) deposition

ρ: is the density

A: is the surface of the thin film

b) Determination of the absorption coefficient:

In the range spectral where light is absorbed, and after knowing the thickness of the film. It is possible to determine the absorption coefficient for each value of the transmittance T (%), which is given by Beer-Lambert-Bouguer's law [20]:

$$\log(I_0/I) = \varepsilon cl \qquad \text{(II. 17)}$$

Where $\alpha t = \varepsilon c l$

Where I_0: Intensity of incident light, I: Intensity of light transmitted by the sample, c: sample concentration, l: sample path length. ε: molar absorption coefficient, α is the absorption coefficient, and t is the thickness of the film.

The ratio I/I_0 is known as the transmittance (T) of the sample expressed in (%).

As a consequence:

$$-\log(I/I_0) = -\log T = \alpha.t \qquad \text{(II. 18)}$$

Consequently**:**

$$\alpha t = \log(1/T) \qquad \text{(II. 19)}$$

$$\alpha = \frac{1}{t}\log\left(\frac{1}{T}\right) \qquad \text{(II. 20)}$$

Where: t is the thickness of the film, T is the transmittance in (%), α: is the absorption coefficient in (cm^{-1})

This relation can be written as follow:

This approximate relationship is established, neglecting reflections at all interfaces; air /film, air / substrate and film/ substrate [21].

c) Measurement of optical band gap width:

Many authors have focused on describing the distribution functions of energy states (Eg) in energy bands. In the case of crystalline materials, the energy separating the valence band from the conduction band is perfectly defined by E_v and E_c. The E_c-E_v energy corresponds to the energy of the forbidden band which is determined for semiconductors such as ZnO and NiO by Tauc's relation, which is given as follow:[22]

$$(\alpha h\nu)^2 = B(h\nu - E_g) \qquad \text{(II. 21)}$$

where B is a constant, (hν) is the photon energy, Eg is the band gap energy of the sample.

By plotting the function: $(\alpha h\nu)^2 = f(h\nu)$ and extending the linear part of α^2 to the abscissa axis (That is to say for $\alpha^2 = 0$), we obtain the value of E_g, see Fig II.13.

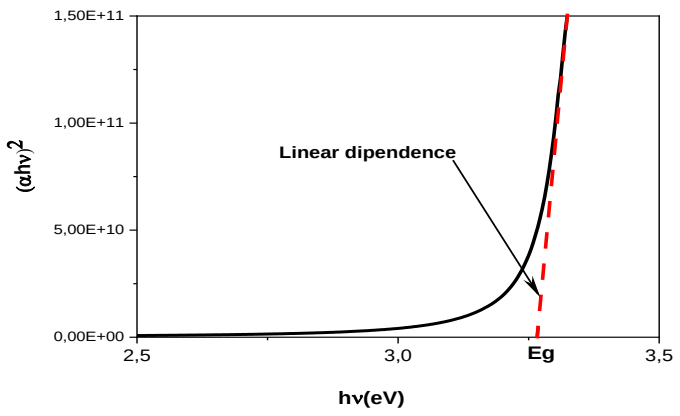

Figure II.13: Determination of the gap energy of ZnO thin film [23]

d) Measurement of Urbach energy :

Another important parameter that characterizes the disorder of the material is the Urbach's tail energy (E_u) [24]. which is corresponded the transitions between the extended states of the valence band and the localized states in the conduction band, as per Urbach's law, the expression of the absorption coefficient takes the following form [25]

$$\alpha = \alpha_0 exp\left(\frac{h\nu}{E_U}\right) \qquad \text{(II. 22)}$$

So , $$ln\alpha = \frac{1}{E_u}(h\nu) + ln\alpha_0 \qquad \text{(II. 23)}$$

Where: α_0 is the pre-exponential factor, (hv) the photon energy and (Eu) is the Urbach's energy. By drawing the curve of $ln\alpha = f(h\nu)$, The Urbach energy, or the disorder, can be estimated from the inverse slope of the linear plot see Fig II.14.

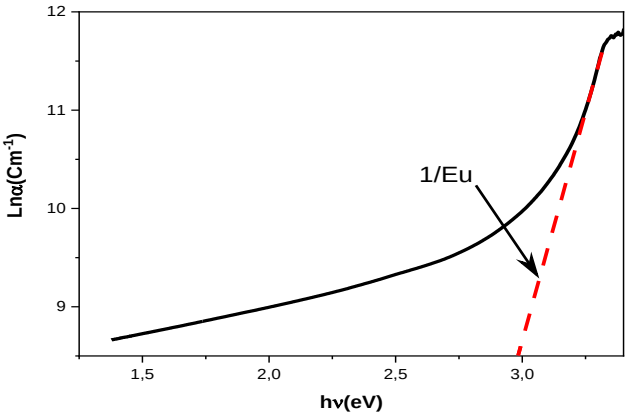

Figure II.14: Determination of Urbach energy for a prepared ZnO sample

II.5.3 1 The four-probe method:

The four-probe method is an appropriate technique for directly calculating the surface resistance or as well-known sheet resistance. This device is shown in Fig II.15.

During the measurement, four metal tips were affixed to the sample where the spacing between the probes was 1mm (see Fig II.16). Then an electric current its intensity I=1nA is applied between the external probes which has been used to pass the current through the internal two probes. A voltmeter is used to measuring the voltage (V) between the internal probes. As a result, the sheet resistance of the thin film can be calculated by using this relation [26]:

$$R_{Sh} = \frac{\pi}{Ln2} * \frac{V}{I} = 4.53236 \qquad \text{(II. 24)}$$

where the factor (π/Ln2) is included to account of the influence of the current extending, V is the measured voltage and I is the applied current.

The resistivity (ρ) and the conductivity (σ) of the thin film can be obtained from the following relation:

$$\rho = \frac{1}{\sigma} = R_{sh} * t \qquad \text{(II. 25)}$$

Where t is the film thickness.

We take into account that the calculated value is the average of three measured values, in order to minimize the measured errors [27].

Figure II.15: Four-point device type of Signatone PRO4

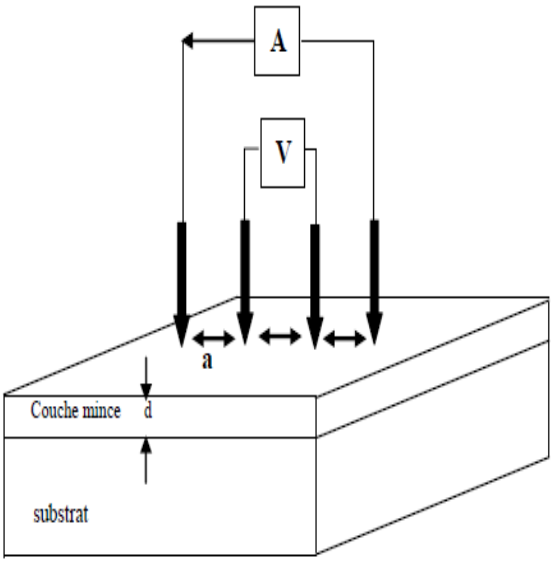

Figure II.16: Schematic diagram of a four-point device

II.8 Conclusion:

In this chapter we have presented the criteria for choosing the adopted method of deposition thin films on a glass substrate using spray pyrolysis. Then, we have demonstrated the various characterization technique (in this case XRD, SEM, FTIR, UV-Visible, and four probes) used to determine the structural, optical, and electrical properties.

Reference:

[1] Zaouche, C. (2021). THE ROLE OF Ni AND Zn ON DILUTED MAGNETIC SEMICONDUCTOR Ni1-x Znx O THIN FILMS (Doctoral dissertation, Université de mohamed kheider biskra).

[2] Kouidri, N. (2019). Contribution à l'étude de couches minces d'oxydes transparents conducteurs à base de zinc et cobalt par spray pneumatique (Doctoral dissertation, University of Mohamed Khider, BISKRA).

[3] Fares, Z. (2021). Effect of solution molarity on physical properties of Nickel oxide thin films prepared by spray pyrolysis method (Doctoral dissertation).

[4] Gumus, C. E. B. R. A. İ. L., Ozkendir, O. M., Kavak, H., & Ufuktepe, Y. Ü. K. S. E. L. (2006). Structural and optical properties of zinc oxide thin films prepared by spray pyrolysis method. *Journal of optoelectronics and advanced materials*, *8*(1), 299.

[5] Juwhari, H. K., Ikhmayies, S. J., & Lahlouh, B. (2017). Room temperature photoluminescence of spray-deposited ZnO thin films on glass substrates. *International Journal of Hydrogen Energy*, *42*(28), 17741-17747.

[6] Cattin, L., Reguig, B. A., Khelil, A., Morsli, M., Benchouk, K., & Bernede, J. C. (2008). Properties of NiO thin films deposited by chemical spray pyrolysis using different precursor solutions. *Applied Surface Science*, *254*(18), 5814-5821.

[7] Bouaichi, F. (2019). Deposition and analysis of Zinc Oxide thin films elaborated using spray pyrolysis for photovoltaic applications (Doctoral dissertation, University Mohamed Khider of Biskra).

[8] Benramache, S., Temam, H. B., Arif, A., Guettaf, A., & Belahssen, O. (2014). Correlation between the structural and optical properties of Co doped ZnO thin films prepared at different film thickness. *Optik*, *125*(7), 1816-1820.

[9] Fares, Z. (2021). Effect of solution molarity on physical properties of Nickel oxide thin films prepared by spray pyrolysis method (Doctoral dissertation).

[10] Bakr, N. A., Khodair, Z. T., & Alghalabi, I. A. Effect of Co doping on structural and optical properties of ZnO thin films prepared by chemical spray pyrolysis method. International Journal of Current Research, 7, 12411-12417.

[11] M. Karunakaran, S. Maheswari, K.Kasirajan and S. Dineshraj, "Physical properties of nanocrystalline Tin Oxide thin film by chemical spray syrolysis method", International Journal for Research in Applied Science & Engineering Technology, Vol. 4, No. 7, (2016), 691-695.

[12]بن عمرة , & 2013) .حبيبة). L'effet de la température du substrat et de la molarité sur les propriétés des couches minces de sulfure de zinc déposées par spray ultrasonique (Doctoral dissertation, Université Mohamed Khider-Biskra).

[13] Castignolles, M. (2004). Etudes de la synthèse et de la structure par microscopie et spectroscopie électroniques de nanotubes de carbone purs et dopés à l'azote (Doctoral dissertation, Montpellier 2).

[14] Muthukumaran, S., & Gopalakrishnan, R. (2012). Structural, FTIR and photoluminescence studies of Cu doped ZnO nanopowders by co-precipitation method. *Optical Materials*, *34*(11), 1946-1953.

[15] George, B. (1987). P. McIntyre Infrared Spectroscopy.

[16] Vanalakar, S. A. (2010). chemical synthesis of cds, ZnO and CdS sensitized ZnO thin films and their characterization for photo-electrochemical solar cells.

[17] F. Ynineb, Contribution à l'élaboration de couches minces d'Oxydes Transparents Conducteurs (TCO), Mémoire du Magister, Université Mentouri-Constantine, (2010).

[18] Benramache, S., Guezzoun, H., & Benhaoua, B. (2020). Synthesis and characterizations of nanocrystalline Na and Al codoped NiO thin films. International Journal of Integrated Engineering, 12(1), 204-209.

[19] Benhaoua, B., Abbas, S., Rahal, A., Benhaoua, A., & Aida, M. S. (2015). Effect of film thickness on the structural, optical and electrical properties of SnO2: F thin films prepared by spray ultrasonic for solar cells applications. *Superlattices and Microstructures*, *83*, 78-88.

[20] Bakr, N. A., Salman, S. A., & Ali, M. N. (2016). Effect of fluorine doping on structural and optical properties of SnO_2 thin films prepared by chemical spray pyrolysis method. *Advances in Materials*, *5*(4), 23-30.

[21] Joshi, B. N., Yoon, H., & Yoon, S. S. (2013). Structural, optical and electrical properties of tin oxide

thin films by electrostatic spray deposition. *Journal of Electrostatics*, *71*(1), 48-52.

[22] Tauc, J., Grigorovici, R., & Vancu, A. (1966). Optical properties and electronic structure of amorphous germanium. *physica status solidi (b)*, *15*(2), 627-637.

[23] Gahtar, A., Rahal, A., Benhaoua, B., & Benramache, S. (2014). A comparative study on structural and optical properties of ZnO and Al-doped ZnO thin films obtained by ultrasonic spray method using different solvents. *Optik*, *125*(14), 3674-3678.

[24] Boubaker, K. (2011). A physical explanation to the controversial Urbach tailing universality. *The European Physical Journal Plus*, *126*, 1-4.

[25] Urbach, F. (1953). The long-wavelength edge of photographic sensitivity and of the electronic absorption of solids. *Physical review*, *92*(5), 1324.

[26] Benramache, S., Aoun, Y., Lakel, S., Benhaoua, B., & Torchi, C. (2019). The calculate of optical gap energy and urbach energy of Ni 1− x Co x O thin films. *Sādhanā*, *44*, 1-6.

[27] Pinit, J., Paradee, N., & Sirivat, A. (2016). Electrochromic characteristics of poly (o-toluidine) coated onto flexible indium tin oxide: Effect of H_2SO_4 and 1-butyl-3-methylimidazolium chloride electrolytes. *Thin Solid Films*, *616*, 381-387.

III.1 Introduction:

The aim of the work in the present chapter to investigate the both effects of substrate temperature and solution concentration on the crystalline quality of ZnO thin films with a good structural and optical properties. In this present study, two series of ZnO thin films were prepared and investigated as follows: the first one is prepared at a constant substrate temperature of 380°C, and the precursor solution concentration is varied as: 0.05, 0.075, 0.1 and 0.125. For the second one, it was prepared at a constant solution concentration, and the substrate temperature was varied from 350, 380, and 410°C.

The obtained films were characterized by different techniques using X-ray diffraction, FTIR spectroscopy, and UV-vis spectroscopy.

The obtained results concerning the influence of precursor concentration (Molarity) and substrate temperature T_S on the structural and optical properties of ZnO thin films will be presented and discussed later.

III.2: Study the effect of precursor solution molarity:

III.2.1 Structural properties :

III.2.1.1 X-rays diffraction analyses :

X rays diffraction spectra of the undoped ZnO films prepared at various precursor solution concentration are shown in the Fig III.1, which was obtained in the scanning range (2θ) from 20° to 80°. These spectra are processed by X'Pert High Score software.

In this analysis we observed seven diffraction peaks are recorded for diffraction angles 2θ equal to 31, 34, 36, 47, 56, 63 and 68 which corresponding to (100) (002) (101) (102) (110) (103) and (112) planes, and well matched with standard (JCPDS No 036-1451). The strongest peak was observed at 2θ = 34.49° which corresponding to (002) plane. Additionally, this peak is the highest and sharpest one, which means that the films are polycrystalline and hexagonal structure with a strong preferred orientation along the (002) plane. [1-3]. We also can see that the peak (002) become higher and narrower as precursor concentrations increases, suggesting that the ZnO crystalline quality is better.[4] the crystallization of C=0.1 mol/l gives the most crystallized sample with the strongest peaks.

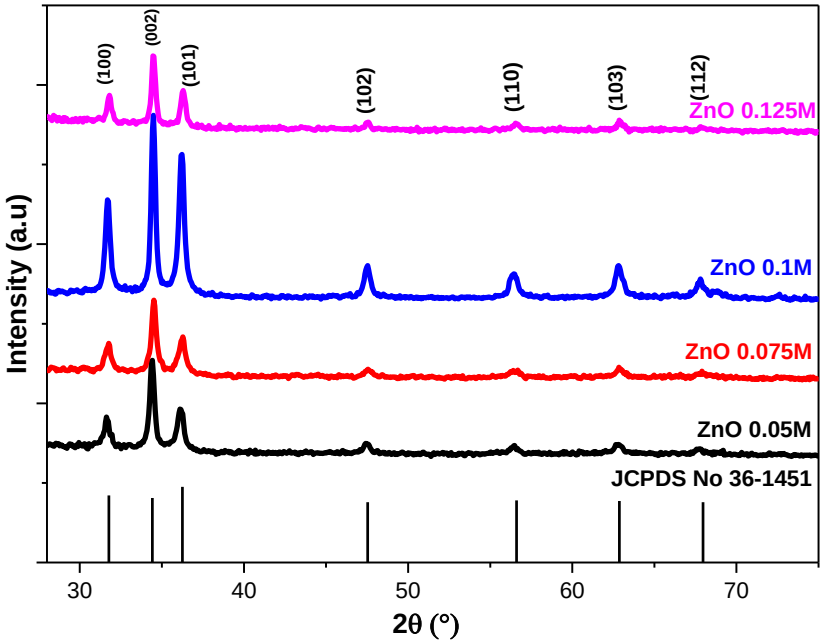

Figure III.1: X-rays diffraction specters of ZnO samples at different precursor concentrations

To obtain more structural information, different structural parameters were calculated, such as lattice parameters a and c, (hkl) Miller indices, inter planar lattice distance d_{hkl}, grain size (crystallite size) D, the average strain ε and dislocation density δ of ZnO thin films deposited at various precursor concentrations were also determined. In the hexagonal Wurtzite structure, recalling all the calculation equations in chapter II (Eq.4-8,12, and 14), the following table III.1 summarizes the variations of different structural parameters of ZnO thin films prepared at different precursor concentrations.

Table III.1: structural parameters of ZnO thin films at different precursor concentrations

C(mol/l)	$2\theta_{hkl}$ (°)	(h k l)	d_{hkl}	a (Å)	c (Å)	β_{hkl} (°)	D(nm)	ε (%)	δ (lines/m^2)
0.05	34.37	(002)	2.61	3.27	5.22	0.22	28.45	0.0041	-0.9545
0.075	34.52		2.60	3.26	5.20	0.22	29.44	0.0009	-0.2095
0.1	34.48		2.60	3.27	5.20	0.22	32.73	0.0041	-0.9545
0.125	34.49		2.60	3.24	5.20	0.21	34.71	-0.0052	1.2106

In addition, Fig III.2 show the change in the values of grain size as a function of the concentration solution. We can see that the size of the grain is increase when the precursor concentration increase, and this because with the increasing of molarity, the solution contains more zinc ions that react and this leads to an increase in films mobility, especially enhancing the growth rate of ZnO films and grain sizes, where many researchers indicated that in the literatures [5-7]. Also, the increase in grain size indicates a decrease in structural defects, which reduces internal stress and dislocation density as observed in Table (III.1) [8].

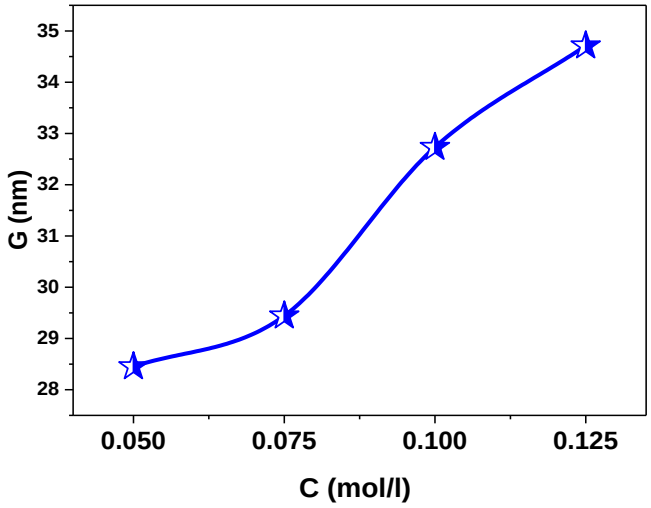

Figure III.2: Variation of grain size as function of precursor concentration of ZnO thin films

III.2.1.2 FTIR Spectroscopy results:

To confirm the DRX results of elaborated ZnO films, the samples were studied by FT-IR spectroscopy (Fourier Transform Infrared). The specters of ZnO samples measured in the range of 400-4000 cm^{-1}using a spectrophotometer infrared type of (Cary 630 FTIR).

The analysis by FTIR spectroscopy was carried out in the spectral range of 1200-400 cm^{-1} because its specters can give a precise idea of the oxide's molecular bonds. The reason for choosing this limited domain is that metal oxides generally give absorption in the region bellow 1000 cm^{-1}[19], Fig III.3 shows the FTIR spectra of ZnO thin films with varying precursor concentrations (0.05, 0.075, 0.1 and 0.125) respectively.

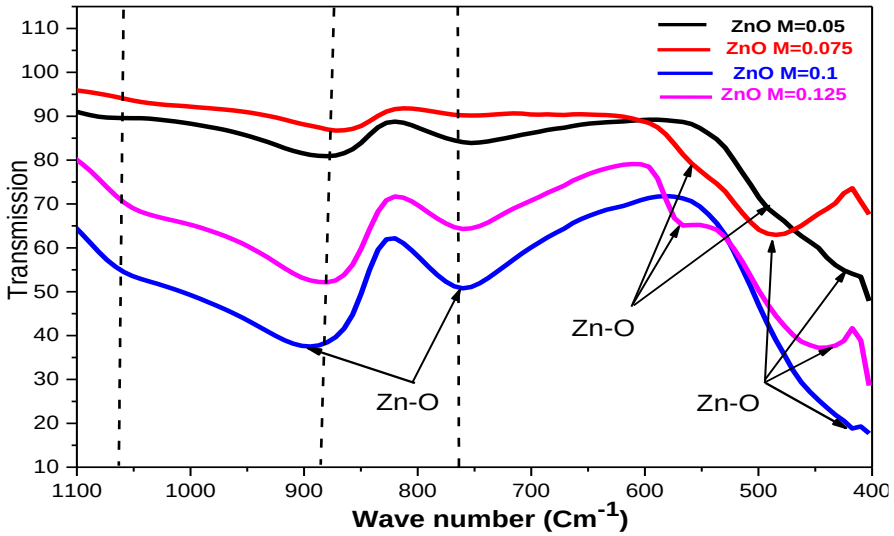

Figure III.3: Specters FTIR of ZnO thin films in different precursor solution concentration

As shown in the specters, for all samples, the characteristic peaks are 418, 420, 443, 485, 567, 755, 756, 758, 760, 877, 868, 883, and 895cm^{-1} correspond to the Zn-O stretching vibration

mode as indicated in literatures [9-19], While the weak band situated at: 1055, 1060, and 1082 is due to C=O or C-H bonds [10, 15]. a pic at 1037 $cm^{-1}$is exhibited, which can be attributed to Si–O bonding due to Si substrate used [17]. Table III.2 summarizes obtained results of this study, which confirms the existence of ZnO bond.

Table III.2: Vibratory modes of undoped ZnO thin films of different molarity

Vibration modes	**Position (Cm^{-1})**			
Molarity	**0.05**	**0.075**	**0.1**	**0.125**
Zn-O	420, 485, 877, 755	868, 758	418, 760, 895	443, 567, 883, 757
C=O or C-H bonds	1082		1060	1055
Si-O bonds		1037		

III.2.2 Optical characterization:

III.2.2.1 Transmission specters:

The optical transmittance specters of ZnO films prepared at a constant substrate temperature T_s=380°C were registered in the interval of the wavelength varies between 300 and 900nm. The transmittance specters as a function of precursor concentration are depicted in Fig III.4. We note that the higher of precursor concentration value higher the transmission this means that our samples are very transparent, where the highest registered value of transmittance is (T=83%) [20]. The transmission values are listed in the Table III.2, the law transmittance value is (T=44%) of the sample with the low precursor concentration C=0.05 (mol/l), which is due to the sample is relatively amorphous because of small concentration.

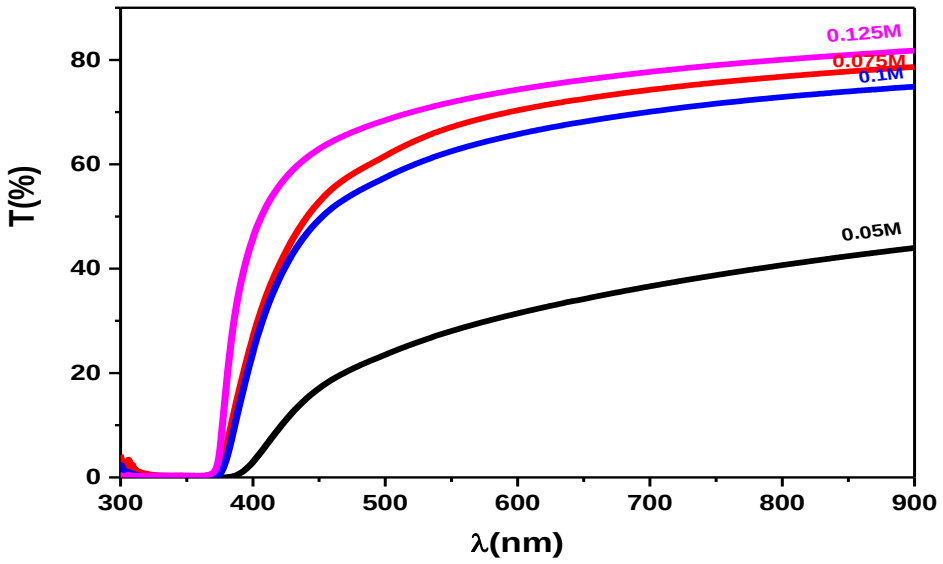

Figure III.4: Transmission specters of ZnO thin films as a function of precursor molarity

III.2.2.1 Determination of Optical gap energy and disorder Urbach energy:

The optical band gap values were deduced from transmission measurements using Tauc's relationship (II. 20). As seen in Fig III.5, for all the films which prepared at different precursor concentration, the values of Eg were determined by drawing of $(\alpha h\nu)^2$ as a function of $(h\nu)$ and extrapolating of the linear portion of $\alpha h\nu^2$ to the x-axis ($\alpha h\nu^2=0$). The plot of $ln\alpha$ as a function of photon energy $(h\nu)$ was used according to relation (II. 22) to deduce the Urbach's energy Eu, as illustrated in Fig III.6.

Tab III.3 summarizes the calculated optical properties of undoped ZnO thin films prepared at various precursor concentration.

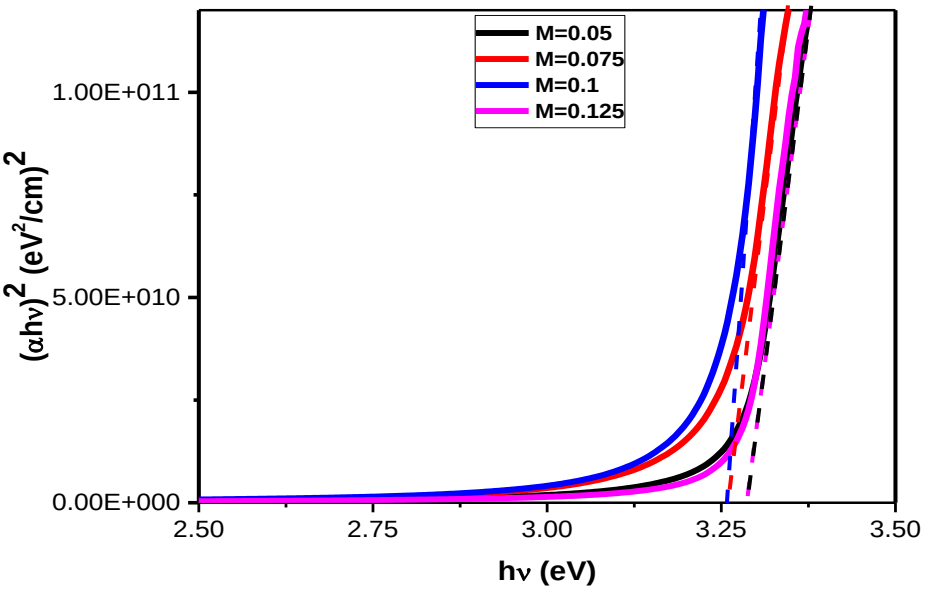

Figure III.5: Drawn of $(\alpha h\upsilon)^2$versus $h\upsilon$ to determinate of optical gap energy in ZnO thin films

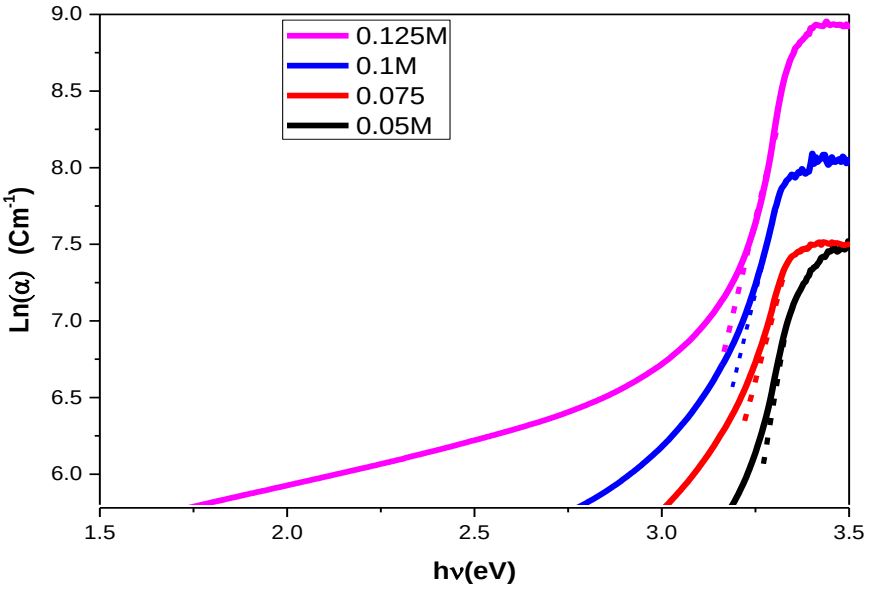

Figure III.6: Plot of Ln(α) versus (hυ) to determinate Urbach energy in ZnO thin films

Table III.3: summarizing of optical properties of ZnO thin films according to precursor concentration

C (M)	G (nm)	T (%)	Eg(eV)	Eu(eV)
0.05	28.45	44	3.29	0.09
0.075	29.44	79	3.26	0.13
0.1	32.73	75	3.26	0.14
0.125	34.71	82	3.29	0.08

III.2.2.2 Interpretation of the obtained Eg and Eu results:

The obtained values of optical band gap are in good agreement with other reports [21-24], Furthermore the increase of Eg values with the increase of precursor concentration can be taped of the increase in the grains size and the decrease of structural disorder in the ZnO films as it was seen from the Urbach energy analysis, then the increase of the precursor concentration (C=0.125 mol/l) causes the decrease of Eg and the increase of Eu [25].

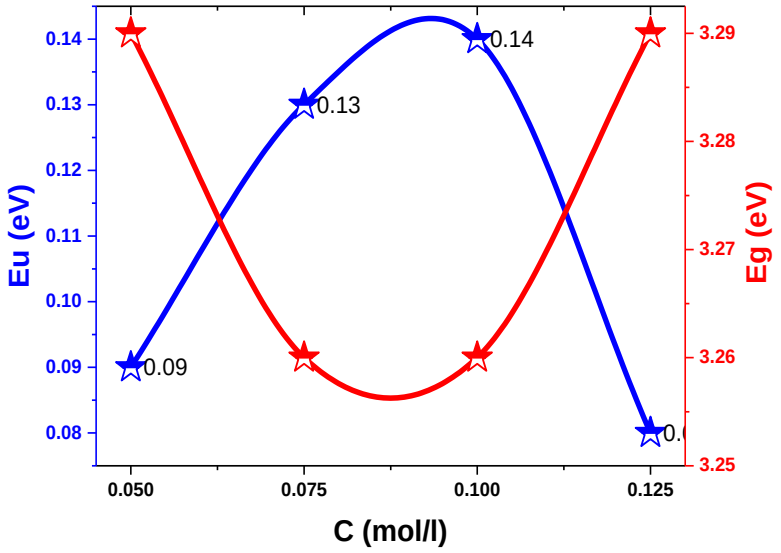

Figure III.7: The variation of Gap energy Eg and Urbach energy Eu as a function of precursor solution concentration of ZnO thin films

III.3 Study the effect of substrate temperature:

III.3.1 Optical properties:

III.3.1.1Transmission specters:

The optical transmittance specters of ZnO films were registered in the interval of the wavelength varies between 300-900 nm. Fig III.8 shows the transmittance at three different substrate temperature, As can be noted, an increase in substrate temperature from 350°C to 410°C has improved the optical transmission which has increased significantly from 44% to 80%, this means an enhancement in film crystallinity deposited at higher substrate temperature which causes an enhancement in emissions [26].

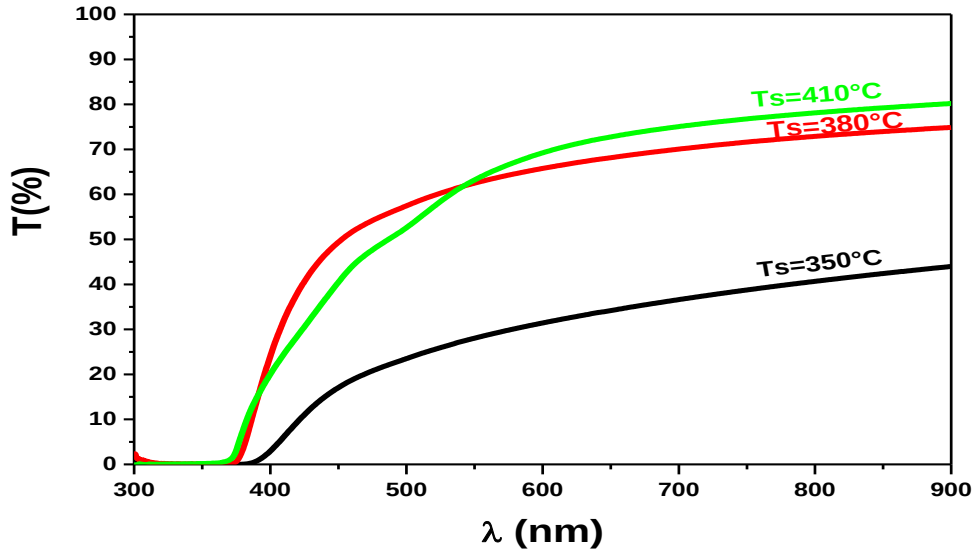

Figure III.8: Transmission specters of ZnO thin films as a function of substrate temperature

III.3.1.2 Determination of Optical gap energy and Urbach energy:

The optical band gap values were deduced from transmission measurements using Tauc's relationship (II-20). As seen in Fig III.9, for all the films which prepared at different substrate temperature, the values of Eg were determined by drawing of $(\alpha h\nu)^2$ as a function of $(h\nu)$ and extrapolating of the linear portion of $\alpha h\nu^2$ to the x-axis ($\alpha h\nu^2=0$). The plot of $ln\alpha$ as a function of photon energy $(h\nu)$ was used according to relation (II. 22) to deduce the Urbach's energy Eu, as illustrated in Fig III.10.

Tab III.3 summarizes the calculated optical properties of undoped ZnO thin films prepared at various substrate temperature.

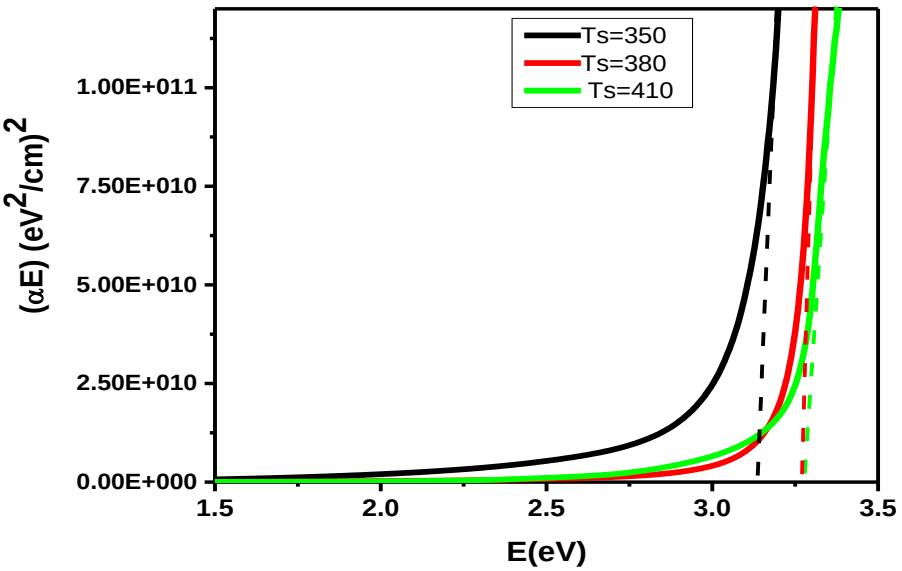

Figure III.9: Drawn of $(\alpha h\upsilon)^2$ versus $h\upsilon$ to determinate optical gap energy in ZnO thin films in different substrate temperature

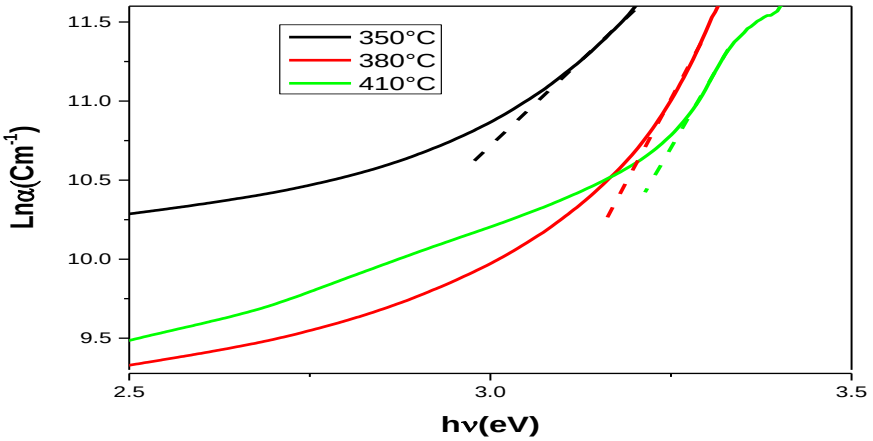

Figure III.10: Plot of Ln(α) versus (hυ) to determinate of Urbach energy in ZnO thin films

Table III.4 listed the optical band gap values (**Eg**), and Urbach energy of this films of ZnO

Ts (°C)	T (%)	Eg(eV)	Eu(meV)
350	44	3.15	0.2
380	75	3.25	0.13
410	80	3.27	0.12

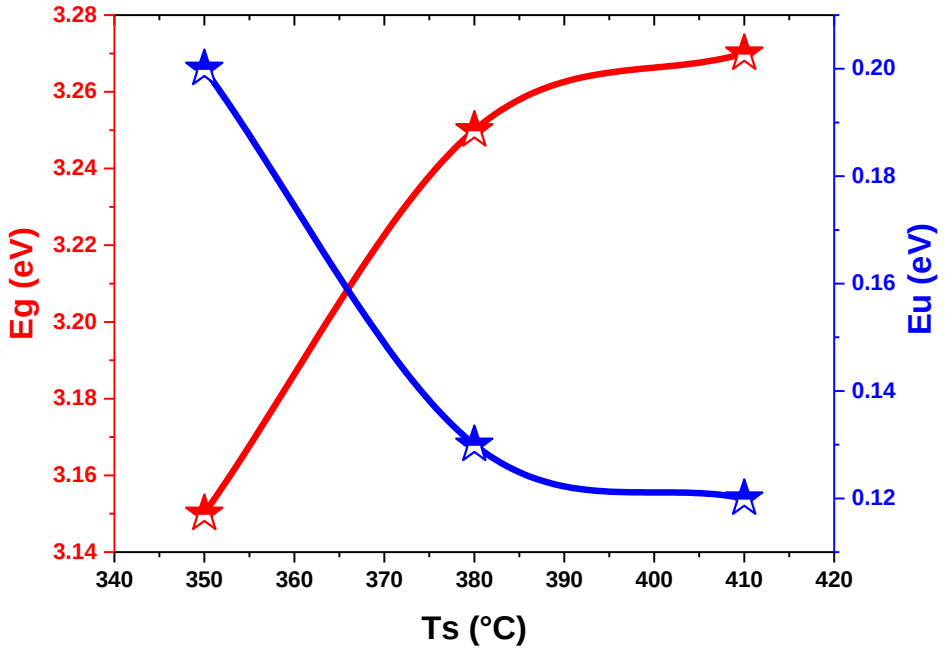

Figure III.11: The variation of Gap energy Eg and Urbach energy Eu as a function of substrate temperature of ZnO thin films

III.3.1.3 Interpretation of the obtained Eg and Eu results discussion:

From one hand, it can be observed that the values of Eg is increased considerably from 3.15 to 3.27 eV with increasing the substrate temperature in the range of temperature (350-410°C). On the other hand, the value of Urbach energy Eu is decreased from 0.2 to 0.12 meV, this means the existence of inter band states (structural disorder) in the prepared film at low temperature. However, the decrease in Urbach energy values in the prepared films at higher temperatures 380°C and 410°C indicates that these temperatures are adequate for less disorder in the film. As expressed in the literatures [27-29].

III.4. Conclusion:

In this chapter, pure ZnO thin films were fabricated using spray pyrolysis technique varying precursor concentrations and substrate temperatures. Upon investigating the impact of this parameters, we observed a significant influence on the film's structural composition and optical properties. When utilizing a low precursor concentration and low deposition temperature, the obtained films appeared relatively amorphous, characterized by the presence of small ZnO crystallites. However, as we increased the precursor molarity and raised the substrate temperature, a remarkable transformation occurred, the films became more transparent and adopted a polycrystalline structure, with (002) preferential orientation.

Reference

[1] Baneto, M., Enesca, A., Lare, Y., Jondo, K., Napo, K., & Duta, A. (2014). Effect of precursor concentration on structural, morphological and opto-electric properties of ZnO thin films prepared by spray pyrolysis. *Ceramics International*, *40*(6), 8397-8404.

[2] Gahtar, A., Rahal, A., Benhaoua, B., & Benramache, S. (2014). A comparative study on structural and optical properties of ZnO and Al-doped ZnO thin films obtained by ultrasonic spray method using different solvents. *Optik*, *125*(14), 3674-3678.

[3] Morinaga, Y., Sakuragi, K., Fujimura, N., & Ito, T. (1997). Effect of Ce doping on the growth of ZnO thin films. *Journal of crystal Growth*, *174*(1-4), 691-695.

[4] Abdulrahman, A. F., Ahmed, S. M., Ahmed, N. M., & Almessiere, M. A. (2020). Enhancement of ZnO nanorods properties using modified chemical bath deposition method: effect of precursor concentration. *Crystals*, *10*(5), 386.

[5] Znaidi, L. (2010). Sol–gel-deposited ZnO thin films: A review. *Materials Science and Engineering: B*, *174*(1-3), 18-30.

[6] Vimalkumar, T. V., Poornima, N., Kartha, C. S., & Vijayakumar, K. P. (2010). Effect of precursor medium on structural, electrical and optical properties of sprayed polycrystalline ZnO thin films. *Materials Science and Engineering: B*, *175*(1), 29-35.

[7] Meryem, Lamri Zeggar, Nour El Houda Touidjen, Mohammed Salah Aida, Nabila Aouabdia, and Sawsen Rouabah. "Growth of undoped ZnO thin films by spray pyrolysis: effect of precursor

concentration." *Journal of Optics* (2023): 1-7.

[8] Castro-Lopes, S., Guerra, Y., Silva-Sousa, A., Oliveira, D. M., Gonçalves, L. A. P., Franco, A., ... & Peña-Garcia, R. (2020). Influence of pH on the structural and magnetic properties of Fe-doped ZnO nanoparticles synthesized by sol gel method. *Solid State Sciences*, *109*, 106438.

[9] TOUATI TLIBA, M. *Etude des propriétés optiques et électroniques des couches minces de ZnO dopé et non dopé: élaboration et application* (Doctoral dissertation, Université Kasdi Merbah Ouargla).

[10] Shammon Batros Jamil, S. (2010). The optical and structural properties of ZnO films prepared by spray pyrolysis. *Engineering and Technology Journal*, *28*(20), 6061-6073.

[11] Khan, Z. R., Khan, M. S., Zulfequar, M., & Khan, M. S. (2011). Optical and structural properties of ZnO thin films fabricated by sol-gel method. *Mater. Sci. Appl*, *2*(05), 340-345.

[12] Ivanova, T., Harizanova, A., Koutzarova, T., & Vertruyen, B. (2010). Study of ZnO sol–gel films: effect of annealing. *Materials letters*, *64*(10), 1147-1149.

[13] Ali, D., Butt, M. Z., Arif, B., Al-Sehemi, A. G., Al-Ghamdi, A. A., & Yakuphanoglu, F. (2017). Li induced enhancement in c-axis orientation and its effect on structural, optical, and electrical properties of ZnO thin films. *Materials Research Express*, *4*(2), 026405.

[14] Kaur, M., Kumar, V., Kaur, P., Lal, M., Negi, P., & Sharma, R. (2021). Effect on the dielectric properties due to In–N co-doping in ZnO particles. *Journal of Materials Science: Materials in Electronics*, *32*, 8991-9004.

[15] Sehgal, P., & Narula, A. K. (2021). Improved optical, electrochemical and photovoltaic properties of dye-sensitized solar cell composed of rare earth-doped zinc oxide. *Journal of Materials Science: Materials in Electronics*, *32*(12), 16612-16622.

[16] Awad, M. A., Ibrahim, E. M. M., & Ahmed, A. M. (2014). Synthesis and thermal stability of ZnO nanowires. *Journal of Thermal Analysis and Calorimetry*, *117*, 635-642.

[17] Ivanova, T., Harizanova, A., Koutzarova, T., & Vertruyen, B. (2015). Optical characterization of sol–gel ZnO: Al thin films. *Superlattices and Microstructures*, *85*, 101-111.

[18] Lanje, A. S., Sharma, S. J., Ningthoujam, R. S., Ahn, J. S., & Pode, R. B. (2013). Low temperature dielectric studies of zinc oxide (ZnO) nanoparticles prepared by precipitation method. *Advanced Powder Technology*, *24*(1), 331-335.

[19] Lagashetty, A., Havanoor, V., Basavaraja, S., Balaji, S. D., & Venkataraman, A. (2007). Microwave-assisted route for synthesis of nanosized metal oxides. *Science and Technology of Advanced Materials*, *8*(6), 484.

[20] Golshahi, S., Rozati, S. M., Martins, R., & Fortunato, E. (2009). P-type ZnO thin film deposited by spray pyrolysis technique: The effect of solution concentration. *Thin solid films*, *518*(4), 1149-1152

[21] Benramache, S., Benhaoua, B., Khechai, N., & Chabane, F. (2012). Elaboration and characterisation of ZnO thin films. *Matériaux & Techniques*, *100*(6-7), 573-580.

[22] Benramache, S., Belahssen, O., Guettaf, A., & Arif, A. (2013). Correlation between electrical conductivity—optical band gap energy and precursor molarities ultrasonic spray deposition of ZnO thin films. *Journal of Semiconductors*, *34*(11), 113001.

[23] Ozutok, F., Demirselcuk, B., Sarica, E., Turkyilmaz, S., & Bilgin, V. İ. L. D. A. N. (2012). Study of ultrasonically sprayed ZnO films: thermal annealing effect. *Acta Physica Polonica A*, *121*(1), 53-55.

[24] Arif, A., Belahssen, O., Gareh, S., & Benramache, S. (2015). The calculation of band gap energy in zinc oxide films. *Journal of semiconductors*, *36*(1), 013001.

[25] Belahssen, O., Benramache, S., & Benhaoua, B. (2014). Effect of Urbach energy with precursor molarity on the crystallite size in undoped ZnO thin film. *Main Group Chemistry*, *13*(4), 343-352.

[26] Nian, H., Hahn, S. H., Koo, K. K., Kim, J. S., Kim, S., Shin, E. W., & Kim, E. J. (2010). Preparation and characterization of sol–gel Li and Al codoped ZnO thin films. *Materials Letters*, *64*(2), 157-160.

[27] Benramache, S., & Benhaoua, B. (2012). Influence of substrate temperature and Cobalt concentration on structural and optical properties of ZnO thin films prepared by Ultrasonic spray technique. *Superlattices and Microstructures*, *52*(4), 807-815.

[28] Daranfed, W., Aida, M. S., Hafdallah, A., & Lekiket, H. (2009). Substrate temperature influence on ZnS thin films prepared by ultrasonic spray. *Thin Solid Films*, *518*(4), 1082-1084.

[29] A. Jain, P. Sagar, R.M. Mehra, Solid State Electronics 50 (2006) 1420–1424.

IV.1 Introduction:

In this study, a presentation of the results will take place concerning Na and Al codoped NiO at various Al concentrations. The thin films of NiO which codoped of Na =2% and Al (Al = 0, 1, 2, 3 and 4%) were deposited on a glass substrate heated to 420 °C by using a spray pyrolysis method using nickel chloride hexahydrate, sodium chloride dehydrate and aluminum chloride dehydrate. Some technical apparatus such as X-rays diffraction, UV-visible spectroscopy and four-point method have been used. to investigate the structural, optical and electrical properties.

IV.2: Structural proprieties:

The structural properties of Na and Al co-doped NiO thin films were investigated using X-rays diffractometer type of Bruker AXS-D8, with Cu Kα radiation (λ = 0.15406 nm). in the scanning range (2θ) from 20° to 70°

IV.2.1: X-rays diffraction analyses :

X rays diffraction spectra of Na and Al co-doped NiO thin films prepared at various Al concentrations are shown in the Fig IV.1. It can be noticed that all the samples have diffraction peaks equal to: (2θ~37° and 43°) which referred to (111) and (200) crystal plans, respectively [1, 2]. The positions of obtaining peaks means that all the films are nanocrystalline of cubic structure type of NaCl, which in agreement with other reports [3-5]. No peaks of Na or Al compounds were observed in our spectra, maybe due to the small doping concentration, which is implied that the structure of the NiO films is not modified by the incorporation of sodium and aluminum doping [6]. Moreover, the good crystalline quality was attained in 2%Na and 1%Al codoped NiO thin film with the strongest peaks.

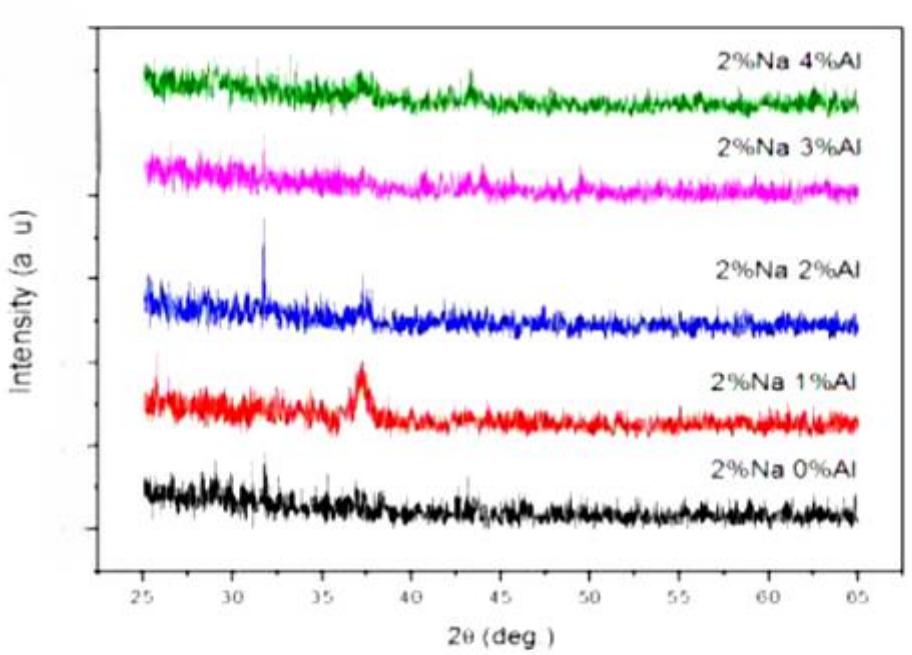

Figure IV.1: X-ray diffraction of Na and Al codoped NiO thin films as a function of Al concentration

IV.3 Optical characterizations:

IV.3.1 Transmission specters:

Fig IV.2 reveals the variation in optical transmittance of Na and Al codoped NiO thin films with various aluminum concentrations; which were measured in an interval of wavelength varies between 300 and 700 nm.

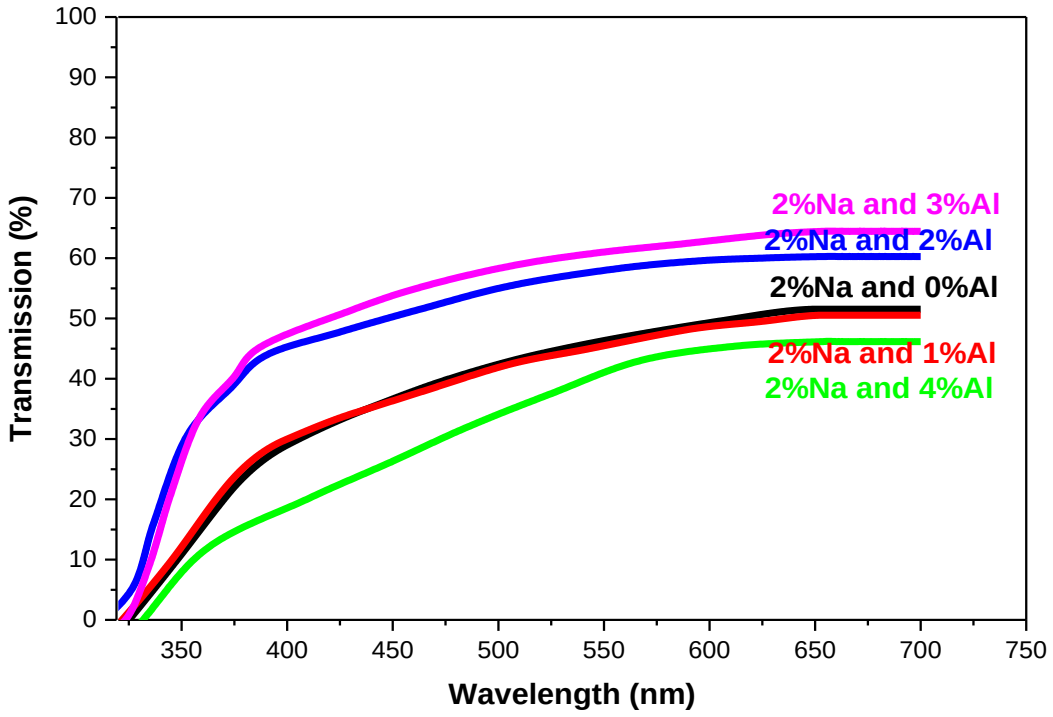

Figure.IV.2: Transmission spectra of Na and Al codoped NiO thin films as function of Al concentration.

As can be seen the NiO films exhibit a good optical transmission (T%), and the average transmission in the visible range increase from 45% to 65% with increasing Al concentration, this increasing in optical transmission can be caused by the increasing in crystallite size as expressed in [5, 7]. However, the samples of NiO co-doped thin films prepared with 2% Al and 3% Al exhibited a high transparency because of the simple corporation between Ni and Al in the substitutional site as mentioned in the research studies [8-10].

IV.3.2 Determination of Optical gap energy Eg and disorder Urbach energy Eu:

The optical band gap values were deduced from transmission measurements using Tauc's relationship (II-20). Fig IV.3. shows the determination of optical band gap energy in the Na and Al co-doped NiO thin films by drawing of $(\alpha h\upsilon)^2$ as function of $(h\upsilon)$ curve and extrapolating the linear portion of its to $\alpha=0$. The Urbach energy (Eu) of Na and Al codoped NiO thin films also can be determined by drawing the curves of $Ln\alpha$ as function of $h\upsilon$ according to relation (II-22), which is shown in Fig IV.4.

Table IV.1 collects the calculated results of optical properties of Na and Al codoped NiO thin films prepared at different Al concentration.

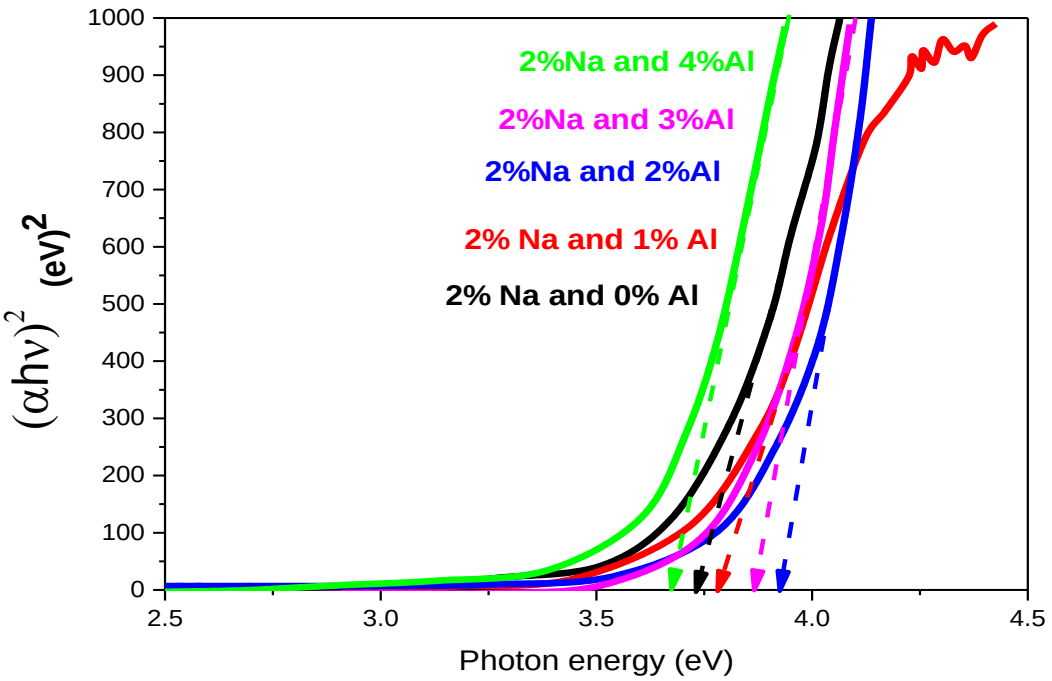

Figure IV.3: Plot of $(\alpha h\upsilon)^2$ versus $(h\upsilon)$ to determinate the optical band gap in Na and Al co-doped NiO thin films in various of Al concentration

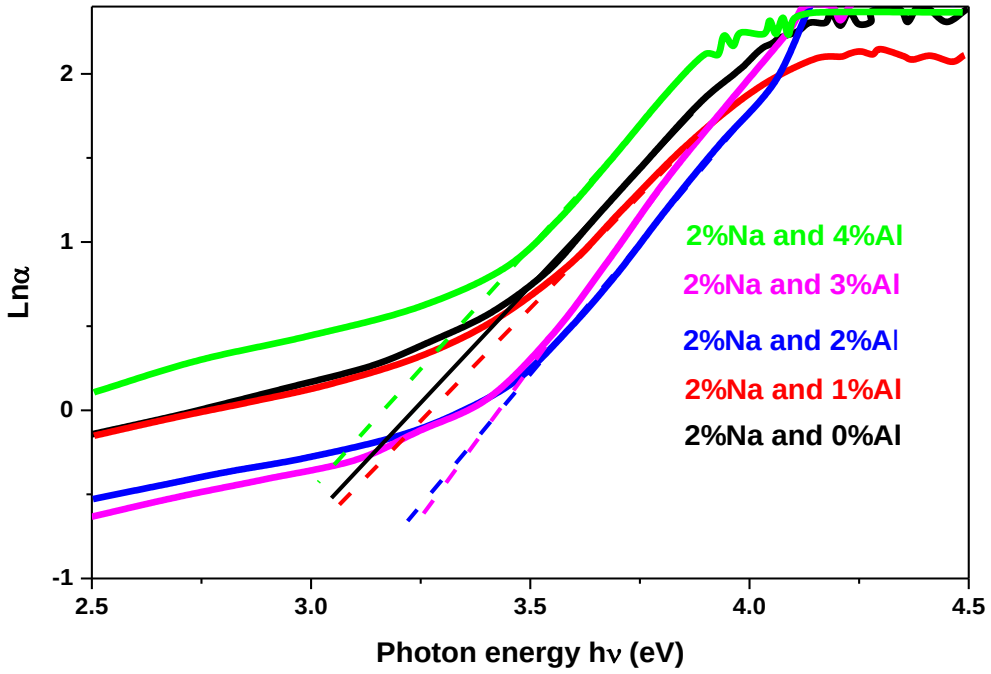

Figure IV.4: The drawn of Ln α as a function of photon energy (hυ), for deduce the Urbach energy in Na and Al codoped NiO thin films

Table IV.1: Results of optical properties of Na and Al co-doped NiO thin films

Al concentration%	T (%)	Eg(eV)	Eu(eV)
0%	52	3.756	0.349
1%	51	3.782	0.344
2%	57	3.927	0.321
3%	65	3.870	0.319
4%	45	3.672	0.358

The variations of the optical gap energy and Urbach energy of Na and Al codoped NiO thin films as a function of Al concentration are illustrated in Fig IV.5

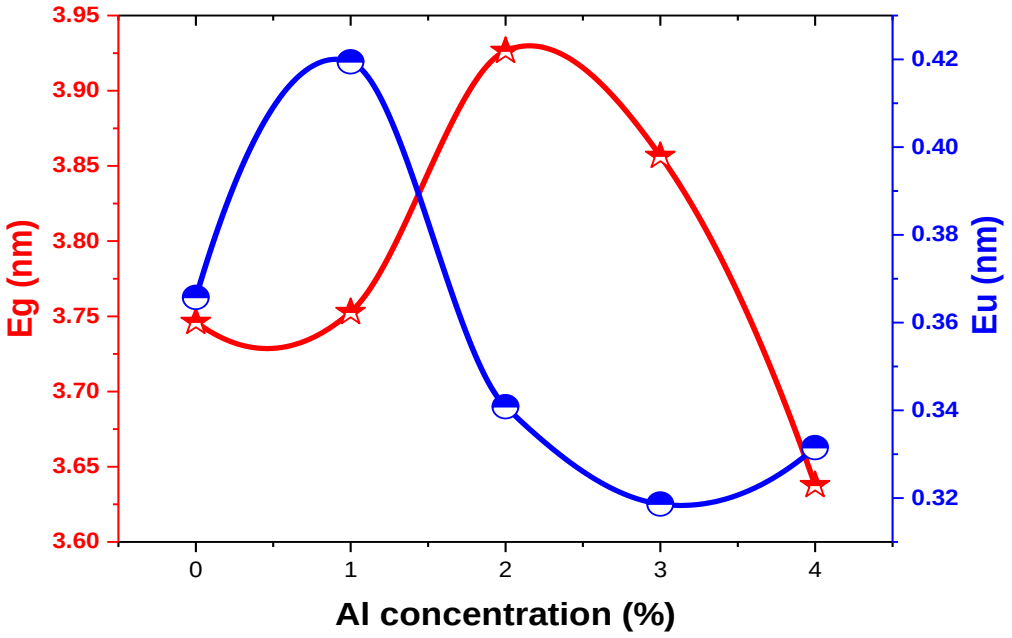

Figure IV.5: Variation of optical gap energy and urbach energy of Na and Al codoped NiO thin films as a function of Al concentration

IV.3.3 Interpretation of the obtained Eg and Eu results:

The values of the optical band gap Eg for Na and Al codoped NiO thin films were estimated to be in the range of 3.672 to 3.926, while the values of Urbach energy change from 0.319 to 0.358, as indicated in Table IV.1. These values correspond closely to the value obtained from bulk NiO [11].

Firstly, the change in the values of optical band gap energy and Urbach energy are opposites. Secondary we can see clearly an increasing in optical gap energy with a decreasing in Urbach energy with the increase in Al concentration from 1%Al to 2%Al which can be explained by the Burstein–Moss effect, which are causes the widen energy band (blue-shift). This phenomenon is that the Fermi level merges into the conduction band with an increase in the carrier concentration. Finally, when the Al concentration rises to 4%, the optical gap energy was decreased, the Urbach energy was increased, and this is due to the oxygen vacancy [9, 12, 13]. The minimum Urbach energy is 0.319 eV, which has been reached for 3%Al.

IV.3.4: The correlation between the optical band gap and Urbach energy:

The widening of the optical band gap is an important parameter to advance materials for potential visible light gas sensing applications involving metal oxide nanostructures. In all deposited films, the optical gap energy can be correlated with Urbach energy to get a new linear fitting; the proposed model is expressed in the following formula:

$$Eg = -0.58Eu + 3.98$$

Fig IV.6 below submitted the variation of the experimental optical gap energy and linear fitting as a function of Urbach energy. The widening of the optical band gap of Na and Al codoped NiO thin films is due to the motion of the valence band Ev downwards and the conduction band Ec upwards which is resulted of the narrowing in the conduction band and the valence band.

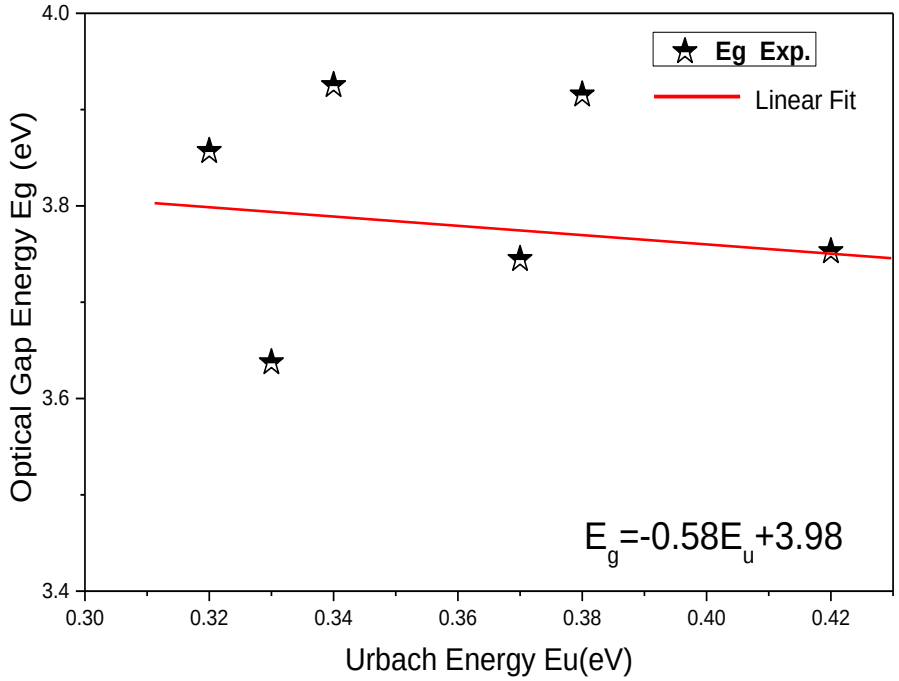

Figure IV.6: The correlation between the optical band gap and Urbach energy of Na and Al codoped NiO thin films

IV.4: Electrical properties:

IV.4.1: Electrical sheet resistance:

The electrical resistance of Na and Al codoped NiO thin films was calculated using four probe method, which was previously explained in chapter II, it is based on measuring the sheet resistance of the films using the relationship (II-23). Fig IV.7 reveals the variation in electrical sheet resistance values of Na and Al co-doped NiO thin films as a function of Al concentration. However, the electrical resistance decreases after codoping to its minimum for 1%Al, it subsequently increases when Al concentration reaches 3%, then while Al concentration increase from 3 to 5%, there is a noticeable decrease in the electrical resistance value. The decrease in the electrical resistance of the Na and Al codoped NiO thin films can be attributed to the displacement of the electrons, which come from the Al^{+3} donor ions occupying the substitutional sites of Ni^{+2}, This leads to formation of the molecular NiNaAlO, which is present on the film's surface [15].

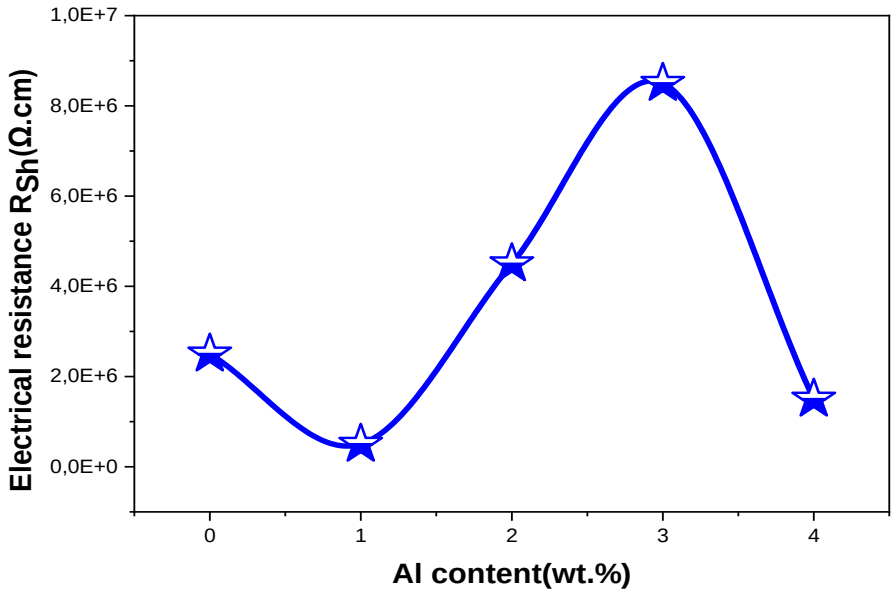

Figure IV.7: The electrical resistance variation of Na and Al codoped NiO thin films as a function of Al concentration

IV.4.1: Application to photovoltaics

To decide this matter is interesting for solar cells application. One can evaluate the figure of merit it means this conjunction of the tow properties needed for solar cells, Transmittance T (%) and Sheet Resistance R_{Sh}, which defined in the relationship (I-4) in chapter I. Table IV.2 summaries these results

Table IV.2: Measurement of figure of merit for Na and Al codoped NiO thin films at different Al concentration

Al concentration %	T (%)	T^{10} x (10^{-3})	R_{Sh} ($\Omega.Cm^{-2}$)	Q (Ω^{-1}) x 10^{-9}
0%	52	1.44	$2.5x10^6$	0.57
1%	51	1.19	$0.5x10^6$	2.38
2%	57	3.62	$4.7x10^6$	0.77
3%	65	13.46	$8.25x10^6$	1.63
4%	45	0.34	$1.25x10^6$	0.27

As conclusion, the NiO thin films codoped Na (2%) and Al (1%) has the lowest electrical resistivity, which may be selected as p type collector for solar cells elaboration. It is so lower than those obtained in the case of n type TCOs collectors [16].

IV.5: Conclusion:

In conclusion, Na and Al codoped NiO thin films with Al percentages ranging from 0% to 4% were effectively deposited onto a glass substrate using the spray pyrolysis method, utilizing nickel chloride hexahydrate, sodium chloride dehydrate. This study explored the influence of Al concentration on the optical, structural, and electrical properties of Na and Al co-doped NiO films.

XRD patterns of the Na and Al codoped NiO thin films show that the obtained thin films have a cubic structure of NiO phase. The transmission spectra revealed that these films exhibit medium optical transparency in the visible region. The band gap energy was increased after co-doping by Al to the maximum value was 3.93 eV for 2%Al. The minimum value of Urbach energy is 0.319 eV for 3%Al. The lowest electrical resistance and figure of merit were found for 1%Al.

Reference:

[1] Sharma, R., Acharya, A.D., Shrivastava, S.B., Shripathi, T., Ganesan, V. (2014). Preparation and Characterization of transparent NiO thin films deposited by spray pyrolysis technique. Optik. 125,6751–6756.

[2] Hoa, N.K., Rahman, H.A., Somalu, M.R. (2018). Influence of Silver Addition on theMorphological and Thermal Characteristics of Nickel Oxide-Samarium Doped Ceria Carbonate(NiO-SDCC) Composite Anode. International Journal of Integrated Engineering. 10(1), 196-201

[3] Sajilal, K., Moses Ezhil Raj A. (2016). Effect of thickness on physico-chemical properties of p-NiO(bunsenite) thin films prepared by the chemical spray pyrolysis (CSP) technique. Optik.127, 1442–1449

[4] Diha, A., Benramache, S., & Benhaoua, B. (2018). Transparent nanostructured Co doped NiO thin films deposited by sol–gel technique. *Optik*, *172*, 832-839.

[5] Aoun, Y., Marrakchi, M., Benramache, S., Benhaoua, B., Lakel, S., & Cheraf, A. (2018). Preparation and characterizations of monocrystalline Na doped NiO thin films. *Materials Research*, *21*.

[6] Chen, S. C., Kuo, T. Y., Lin, Y. C., & Lin, H. C. (2011). Preparation and properties of p-type transparent conductive Cu-doped NiO films. *Thin Solid Films*, *519*(15), 4944-4947.

[7] Siddique, M. N., Ahmed, A., & Tripathi, P. (2018). Electric transport and enhanced dielectric permittivity in pure and Al doped NiO nanostructures. *Journal of Alloys and Compounds*, *735*, 516-529.

[8] Wang, C., Cui, X., Liu, J., Zhou, X., Cheng, X., Sun, P., ... & Lu, G. (2016). Design of superior ethanol gas sensor based on Al-doped NiO nanorod-flowers. *Acs Sensors*, *1*(2), 131-136.

[9] Nandy, S., Maiti, U. N., Ghosh, C. K., & Chattopadhyay, K. K. (2009). Enhanced p-type conductivity and band gap narrowing in heavily Al doped NiO thin films deposited by RF magnetron sputtering. Journal of Physics: Condensed Matter, 21(11), 115804.

[10] Feng, C., Jiang, Z., Chen, B., Cheng, P., Wang, Y., & Huang, C. (2019). Aluminum-doped NiO nanofibers as chemical sensors for selective and sensitive methanol detection. *Analytical Methods*, *11*(5), 575-581.

[11] Avendaño, E. S. T. A. B. A. N., Berggren, L., Niklasson, G. A., Granqvist, C. G., & Azens,

A. (2006). Electrochromic materials and devices: Brief survey and new data on optical absorption in tungsten oxide and nickel oxide films. Thin solid films, 496(1), 30-36.

[12] Shi, J., Lai, L., Zhang, P., Li, H., Qin, Y., Gao, Y., ... & Lu, J. (2016). Aluminum doped nickel oxide thin film with improved electrochromic performance from layered double hydroxides precursor in situ pyrolytic route. *Journal of Solid State Chemistry*, *241*, 1-8.

[13] Mamat, M. H., Parimon, N., Ismail, A. S., Shameem Banu, I. B., Sathik Basha, S., Vijayaraghavan, G. V., ... & Rusop, M. (2019). Structural, optical, and electrical evolution of sol–gel-immersion grown nickel oxide nanosheet array films on aluminium doping. *Journal of Materials Science: Materials in Electronics*, *30*, 9916-9930.

[14] Lou, X., Zhao, X., Feng, J., & Zhou, X. (2009). Electrochromic properties of Al doped B-subsituted NiO films prepared by sol–gel. *Progress in Organic Coatings*, *64*(2-3), 300-303.

[15] Manna, S., Dutta, K., & De, S. K. (2008). High dielectric permittivity observed in Na and Al doped NiO. *Journal of Physics D: Applied Physics*, *41*(15), 155416.

[16] Benhaoua, B., Abbas, S., Rahal, A., Benhaoua, A., & Aida, M. S. (2015). Effect of film thickness on the structural, optical and electrical properties of SnO2: F thin films prepared by spray ultrasonic for solar cells applications. *Superlattices and Microstructures*, *83*, 78-88.

V.1 Introduction:

Based on the more crystallinity of the sample obtained with 0.1M precursor solution depositions of ZnO thin films on such samples are considered as enough wafer in order to elaborate and achieve (n-p) bilayer heterojunctions ZnO/$Ni_{(1-x)}$ Cu_xO (x= 0%, 2%, 3%, and 4%). Growth of undoped and Cu doped NiO thin layers on the ZnO thin films (were previously prepared) proceed at four wafers temperatures, which are 350; 400; 450; and 500°C. Also, the precursor concentration of NiO films was 0.1 (mol/l) [1-6].

The obtained junctions were characterized by various techniques, which are X-rays diffraction, SEM spectroscopy coupled with EDS, and UV-vis spectroscopy.

The obtained results concerning the influence of substrate temperature T_S and the cooper concentration on structural, morphological and optical properties of Cu doped junction ZnO/$Ni_{(1-x)}$ Cu_xO has been studied and investigated in this section.

V.2 ZnO/NiO heterostructures effect of NiO deposition temperature:

In order to study the influence of the NiO deposition temperature on the properties of ZnO/NiO bilayer heterojunctions, NiO films were deposited onto ZnO at Ts=350,400,450, and 500 °C.

V.2.1 Structural characterizations:

V.2.1.1 XRD results:

X-ray diffraction patterns of the ZnO/NiO bilayer heterostructure, where NiO was deposited at Ts=350, 400, 450, and 500 °C is collected in the scanning range (2θ) from 30° to 80°, which was shown in the Fig V.1

The diffractogram of the ZnO/NiO heterostructure, showed nine diffraction peaks at 2Θ of 31.69°, 34.43°, 36.25°, 47.28°, 56.56°, 63.12 and 67.90°, corresponding to the (100), (002), (101), (102), (110), (103), and (112) planes of ZnO, and at 2Θ of 37.16 and 43.28°, corresponding to the (111) and (200) planes of NiO [7], these peaks confirm the presence of crystal planes of both ZnO and NiO in the elaborated heterojunctions.

The detailed explanation of the obtained results at each deposition temperature is as follows:

- **In case of Ts=350°C:** It's clearly observed that a shoulder near the (101) peak of ZnO is due to NiO peak at 2Θ of 37.2 related to (111) NiO plan it means that a refection RX is due to the deeper film of ZnO.
- **In case of Ts=400°C:** The appearance of (111) peak clearly also a small peak at 2Θ of 43.3 related to (002) NiO plan mater of course with the ZnO peaks.

- **In case of Ts=450°C:** When Ts reach 450°C, no appearance of (111) and (002) NiO which may be due to complete covering of deeper ZnO thin film with best crystallization of this films.
- **In case of Ts=500°C:** The same results as 450°C were observed.

As a result, the XRD data confirmed that the NiO crystallites were indeed grown on the ZnO film in the ZnO/NiO junction.

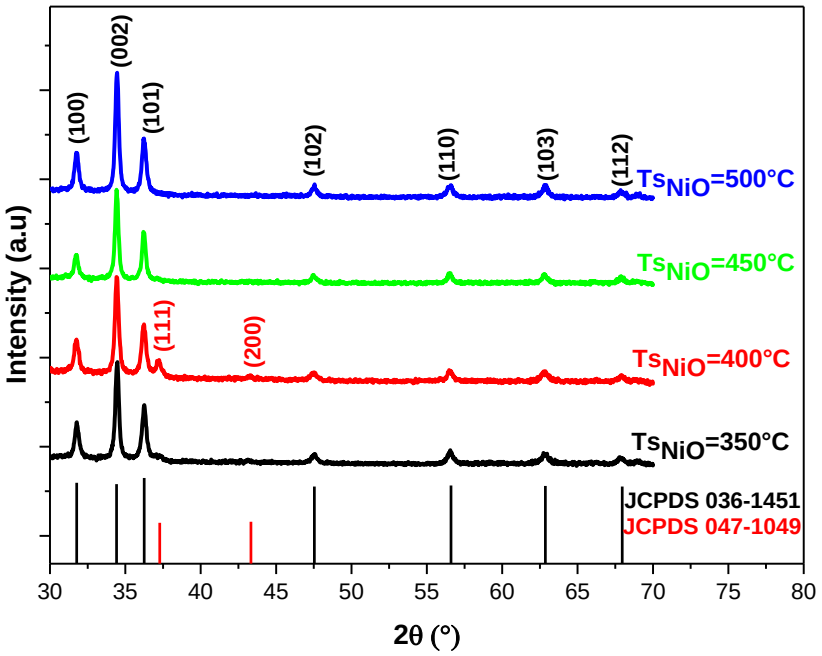

Figure V.1: X rays diffraction specters of ZnO/NiO undoped junction at different deposition temperature of NiO

V.2.1 2 Grain size measurement of ZnO crystallites in ZnO/NiO junctions:

Grain size values of ZnO crystallites in ZnO/NiO junctions were determinate in Table V.1 below which gives the measurements of grain size ZnO crystallites in different deposition temperature of NiO.

Table V.1: Grain size values of ZnO in ZnO/NiO junctions

Ts NiO °C	D (ZnO)
350	47.59
400	55.30
450	47.02
500	47.10

V.2.2 Optical characterization:

V.2.2 1 Transmission specters:

Fig V.2 shows the transmittance specters of undoped ZnO/NiO junctions as a function of substrate temperature deposition of NiO. It can be seen that all these films are exhibited high

transparency when compared to the previous zinc oxide samples (T=70 until 87%), this transparency is a result of double heating effect of ZnO films.

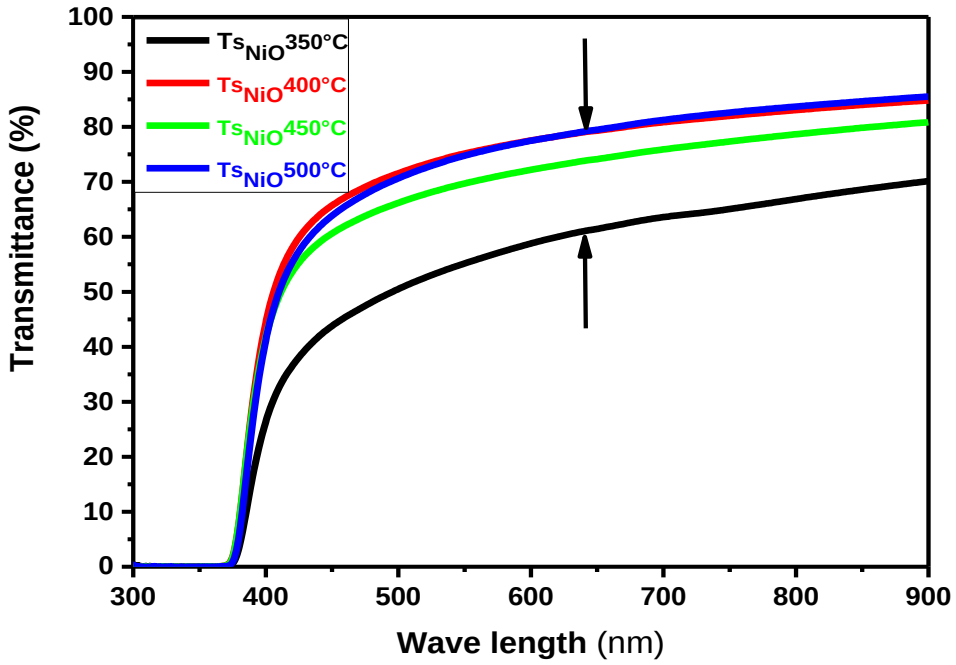

Figure V.2: Transmission specters of ZnO/NiO undoped junctions as a function of Ts of NiO

V.2.2 2 Results of Eg and Eu:

Fig V.3 show the specters of gap energy of the undoped junction ZnO/NiO The transmittance and the optical band gap values Eg of the junctions, are listed in Table V 2, Fig V.4 show the variation of optical gap Eg values in ZnO/NiO undoped junctions at different deposition temperature of NiO.

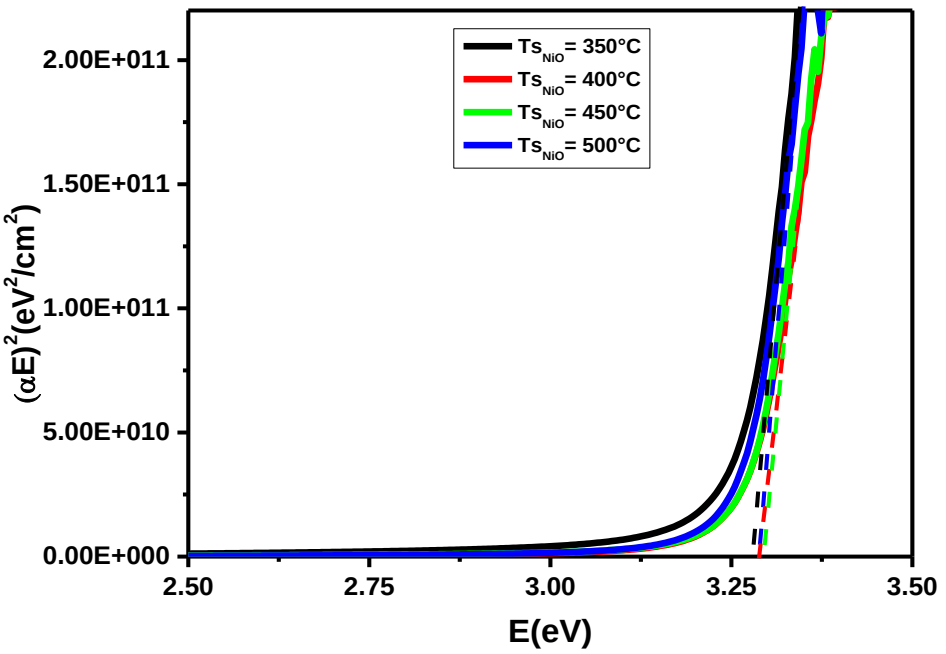

Figure V.3: Determination of Optical gap of ZnO/NiO Junctions as function of substrate temperature of NiO

Table V.2: Values of transmittance and optical gap energy of undoped ZnO/NiO Junctions

Ts $_{NiO}$°C	**T$_{moy}$ (%)**	**Eg (eV)**
350	70	3.27
400	85	3.28
450	81	3.28
500	85	3.28

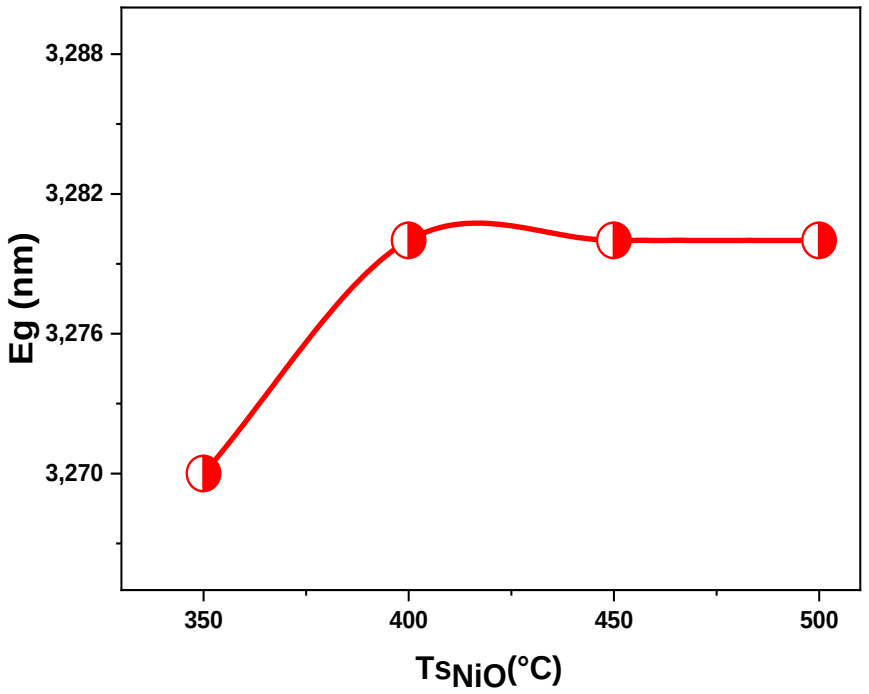

Fig V.4: Variation of optical gab values as function of deposition temperature of NiO in ZnO/NiO Junctions

V.2.2 3 Interpretation of measured Eg and Eu results:

It was remarked that, Eg results of all junction are predominated by Eg of ZnO (Eg=3.27), because ZnO absorb the highest wavelength, as result $Eg_{ZnO}<Eg_{NiO}$ the specters of transmittance are governed by absorption specters of ZnO. In addition, when the deposition temperature of NiO increase to 500°C, we note that the Eg of the junction increase, which has gab energy values of ZnO equal 3.28 nm. As result, the deposition at 500°C treated the junction (thermal treatment).

V.3 ZnO/$Ni_{(1-x)}$ Cu_xO heterostructures effect of Cu concentration:

In order to study the effect of Cu concentration on the structural morphological and optical properties of ZnO/$Ni_{(1-x)}$ Cu_xO heterojunctions, NiO films were deposited onto ZnO films at Ts=350,400,450, and 500 °C. and with different Cu content (Cu=2%, 3% and 4%).

V.3.1. Structural characterization:

V.3.1.1 XRD results:

The diffraction pattern of ZnO/$Ni_{(1-x)}$ Cu_xO with doped junction were collected at different angles ranging from 30° to 80°. Fig V.5 represented diffraction peaks of two junctions doped Cu=2% at two deposition temperature of NiO Ts=350°C and Ts=500°C. It can be seen that all the characteristics peaks of ZnO films were appeared according to the standard JCPDS 036-1451 [8]. In addition, the peaks at positions $2\theta = 37.31°$, and 43.34° appeared noticeably which corresponding to the reflections from (111), (200) according to the standard JCPDS 047-1049 [9].

The results obtained at each temperature can be explained as follows:

At T=350 °C: With doping of Cu, we observe a clear appearance of the two-diffraction peak of NiO (111) and (002) observed at 37.3° and 43.3° respectively whereas previously only the (111) peak appeared in the form of shoulder near the (101) peak of ZnO (see Fig V.1).

At T=500 °C Junction ZnO/$Ni_{(1-x)}$ Cu_xO reveal well the existence of (111) and (002) NiO peaks, after they were completely absent in the undoped junction (see Fig V.1).

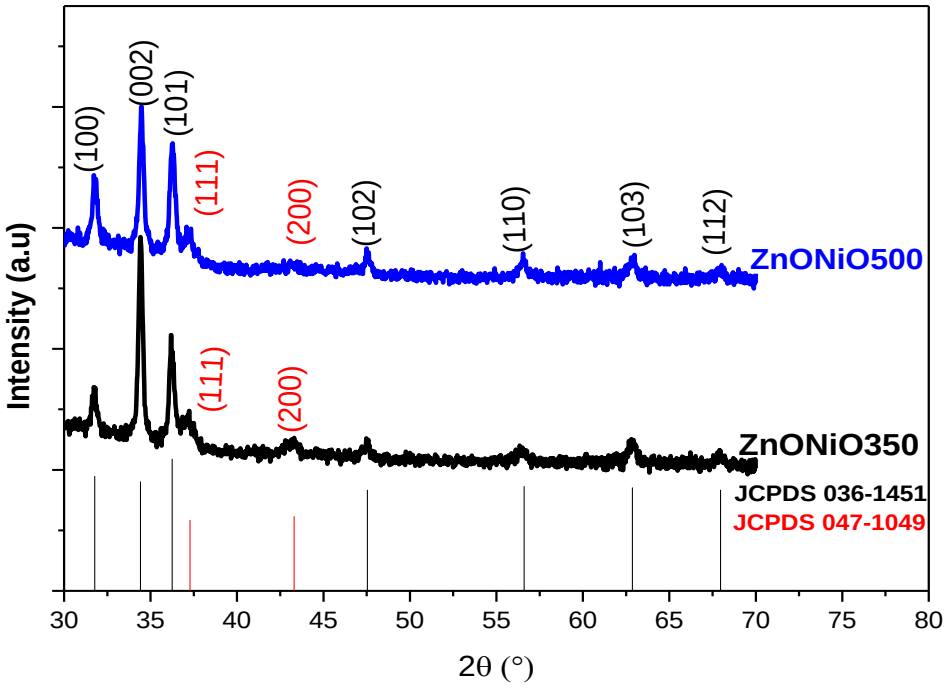

Figure V.5: XRD specters of ZnO/$Ni_{(1-x)}$ Cu_xO junctions with (X=2%) at two different deposition temperature of NiO

V.3.1.2 ZnO grain size measurement in ZnO/$Ni_{(1-x)}$ Cu_xO junctions:

Grain size values of ZnO crystallites in ZnO/$Ni_{(1-x)}$ Cu_xO junctions were determinate in Table V.3 below which gives the measurements of ZnO grain size in ZnO/$Ni_{(1-x)}$ Cu_xO (Cu =2%) in two deposition temperature of NiO Ts=350 and 500 °C

Table V.3: Grain size values of ZnO in ZnO/$Ni_{(1-x)}$ Cu_xO junctions

Ts NiO °C	D (ZnO)
350	73.06
500	60.33

In order to show the evolution in the ZnO grain size. We note that the crystallites size of ZnO nanoparticles in the doped junction is greater than in ZnO thin films (see chapter III), which is due to the best crystallization of ZnO. In addition, Fig V.6 shows the variation in ZnO grain size

values.

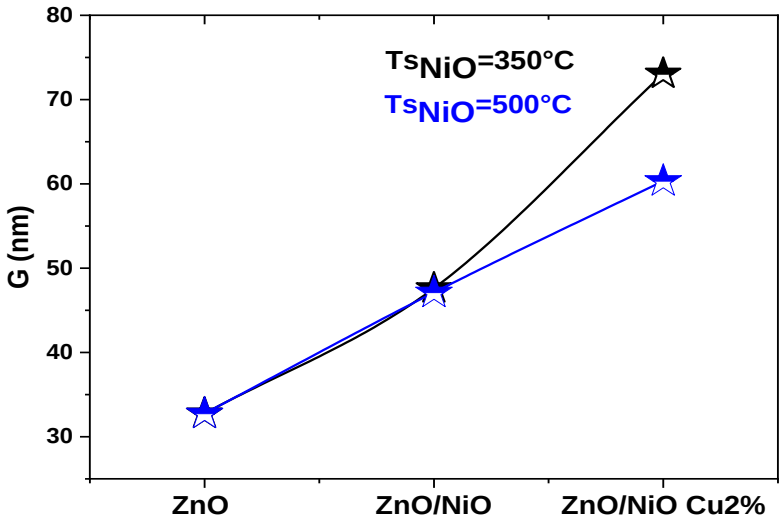

Figure V.6: Variation in ZnO grain size in pure ZnO, undoped and Cu doped ZnO/$Ni_{(1-x)}$ Cu_xOjunction

V.3.2 Morphology and chemical composition of junctions:

V.3.2 1 surface morphology:

The surface morphology of ZnO/$Ni_{(1-x)}$ Cu_xO are recorded using SEM images, for different magnification 20µm and 10µm for each sample. Fig V.7 represents the morphology of surfaces of ZnO/$Ni_{(1-x)}$ Cu_xO junctions with different cooper concentrations (X= 2%, 3% and 4%) and at two deposition temperature of NiO 400 and 450°C which were the adequate temperature in this study. It is worth noting that the surfaces of all are smooth with certain agglomerations.

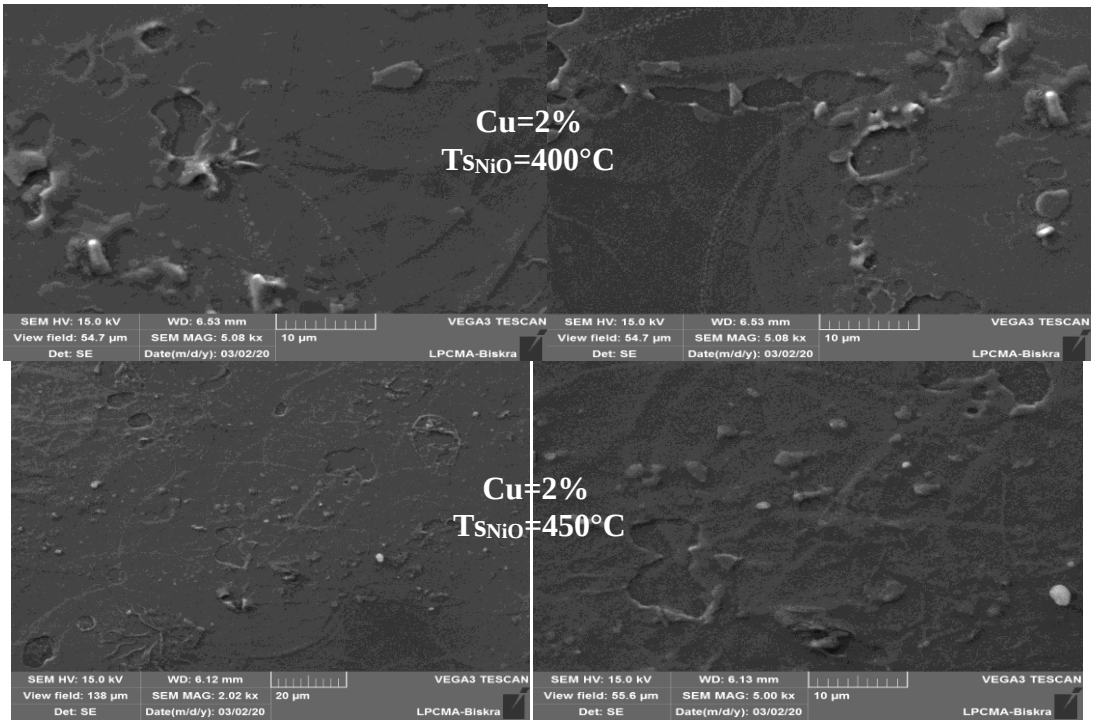

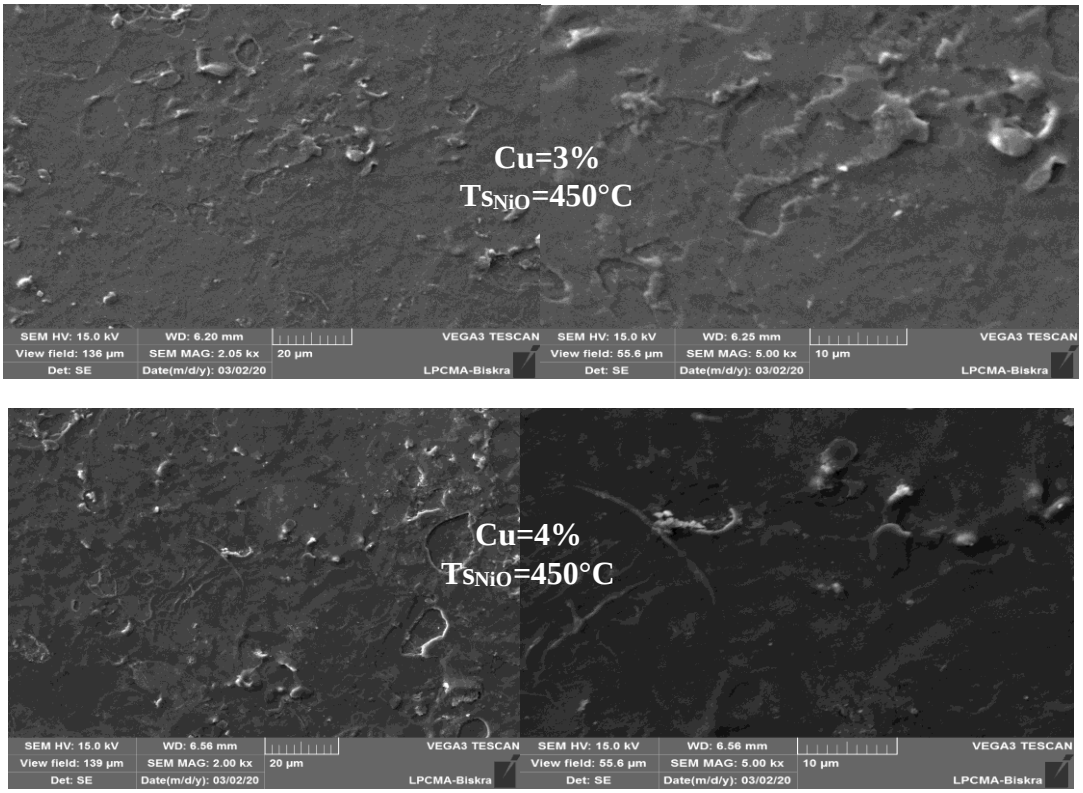

Figure V.7: SEM images of ZnO/$Ni_{(1-x)}$ Cu_xO junctions

V.3.2.2 Energy Dispersion Spectroscopy (EDS) analysis:

The analysis by energy dispersion spectroscopy of the junctions allowed for chemical analyses and to determine the mineralogical chemical composition of the samples which are prepared by spray pyrolysis.

The EDS spectrum shows the presence of each element in the junctions and their proportion. Fig V.8 shows the elemental mapping of the deposited junctions, which confirms that the heterostructures is composed of Zn, Ni, O, Cu and no other impurity

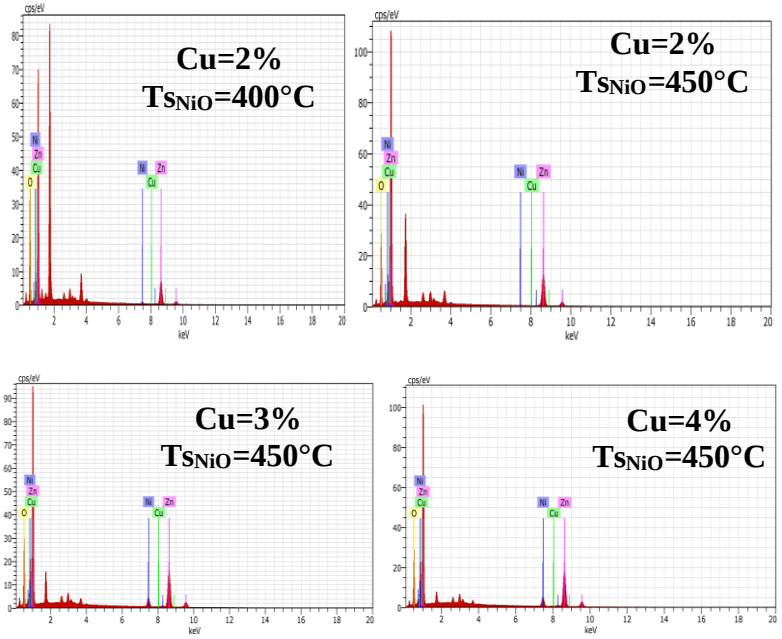

Figure V.8: EDS Specters of ZnO/$Ni_{(1-x)}$ Cu_xO

The detailed results about the elemental composition in terms of atomic percentage are illustrated in Table V.4, which revealed that the deposited junctions are pure.

Table V.4: Elemental composition of ZnO/$Ni_{(1-x)}$ Cu_xO junctions

Samples	**ZnO/$Ni_{(1-x)}$ Cu_xO with Cu=2%, Ts_{NiO}= 400°C**			
Element	Zn	Ni	O	Cu
wt%	51.06	1.7	47.25	0.0
at%	20.75	0.77	78.48	0.0
Samples	**ZnO/$Ni_{(1-x)}$ Cu_xO with Cu=2%, Ts_{NiO}= 450°C**			
element	Zn	Ni	O	Cu
wt%	68.26	0.21	31.53	0.0
at%	34.58	0.12	65.30	0.0
Samples	**ZnO/$Ni_{(1-x)}$ Cu_xO with Cu=3%, Ts_{NiO}= 450°C**			
element	Zn	Ni	O	Cu
wt%	67.13	7.22	25.28	0.36
at%	37.53	4.5	57.76	0.21
Samples	**ZnO/$Ni_{(1-x)}$ Cu_xO with Cu=4%, Ts_{NiO}= 450°C**			
element	Zn	Ni	O	Cu
wt%	68.78	8.10	22.55	0.56
at%	40.32	5.29	54.04	0.34

V.3.3 Optical characterization:

V.3.3 1 Transmission spectra:

The optical transmittance curves of ZnO/$Ni_{1-x}Cu_xO$ (Cu=2%) junctions as a function of wavelength at different deposition temperature of NiO. were plotted in Fig V.9

It is clear that Cu doped ZnO/$Ni_{1-x}Cu_xO$ junctions has resulted an increase in the transmittance rate (T≈90%) in the visible range.

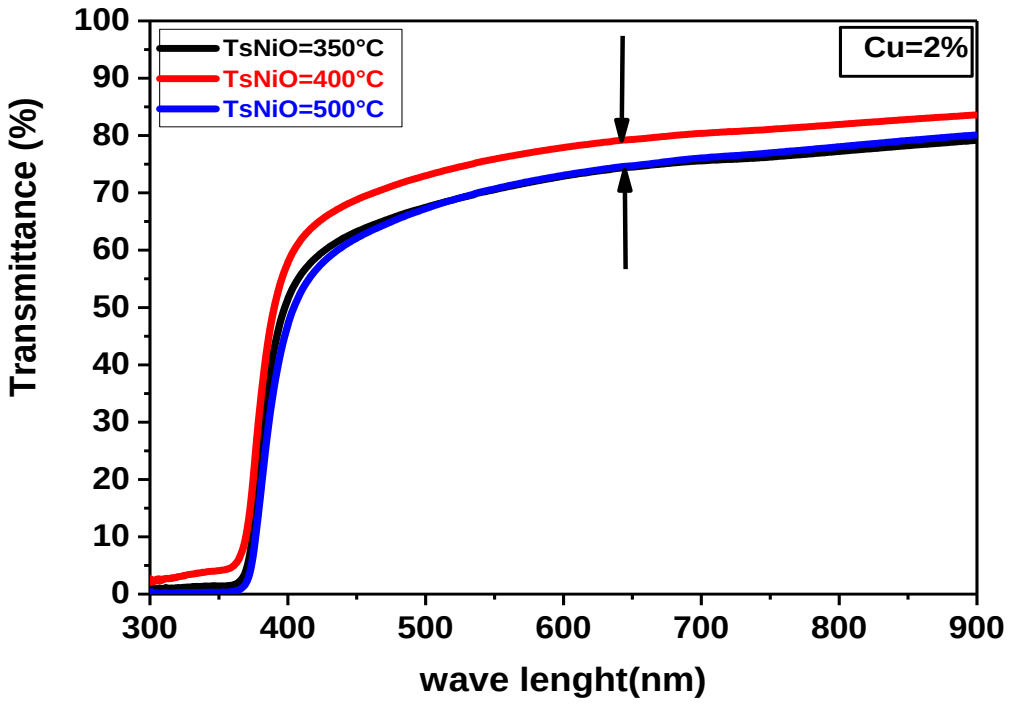

Figure V.9: Transmission specters of ZnO/$Ni_{1-x}Cu_xO$ (Cu=2%) at different deposition temperature of NiO

V.3.3 2 Results of Eg and Eu:

Fig V.10 shows the specters of gap energy of the Cu doped junctions. The transmittance and the optical band gap values Eg of the junctions, are listed in Table V.5. Fig 11 shows the variation of optical gap Eg values in ZnO/$Ni_{1-x}Cu_xO$ (Cu=2%) junctions at different deposition temperature of NiO.

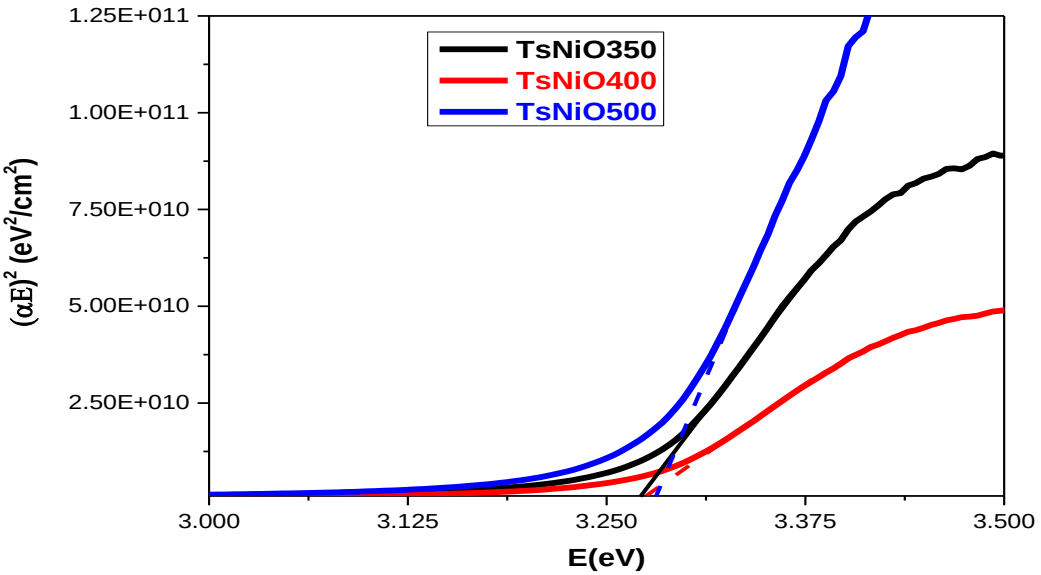

Figure V.10: Determination of Optical gap of ZnO/$Ni_{1-x}Cu_xO$ (Cu=2%) junctions at different deposition temperature of NiO

Table V.5: Values of transmittance and optical gap energy of ZnO/$Ni_{1-x}Cu_xO$ (Cu=2%) junctions

Ts $_{NiO}$°C	**T_{moy} (%)**	**Eg (eV)**
350	79	3.27
400	84	3.28
500	80	3.28

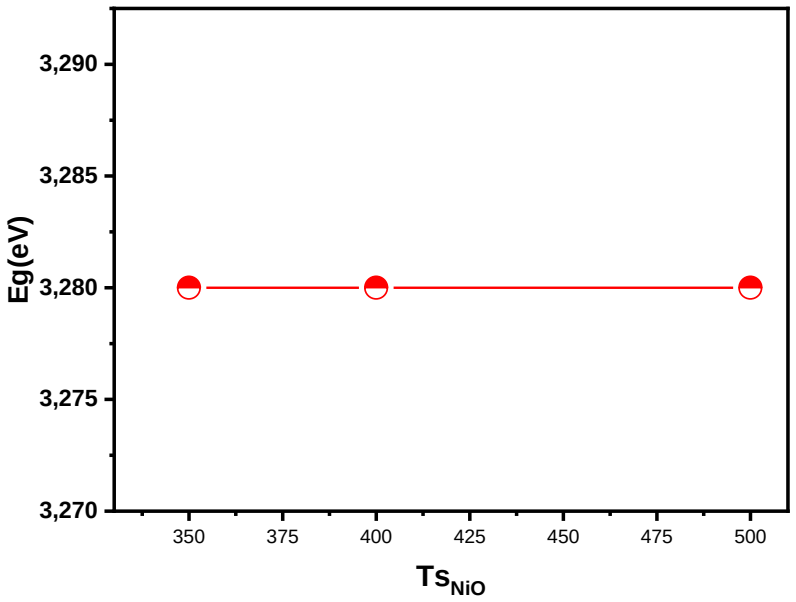

Figure V.11: Variation of Eg in ZnO/$Ni_{1-x}Cu_xO$ junctions with (Cu=2%)

V.4 Conclusion:

In the conclusion, we tried to make (n-p) heterojunctions by using ZnO and NiO oxides, for application in Photovoltaic. Based on the best crystallized sample of ZnO, which has prepared

at the concentration C=0.1 mol/l, and at substrate temperature Ts=380°C. A second layer of Cu doped NiO thin films was successfully deposited on the ZnO wafers to constitute ZnO/$Ni_{(1-x)}$ Cu_xO with Cu (0-4). We have studied the both effects of Cu concentration, and deposition temperature of NiO on the structural, morphological, and optical properties of these junctions.

Reference:

[1] Yang P, Song X, Jia C and Chen H S 2018 Metal-organic framework-derived hierarchical ZnO/NiO composites Morphology, microstructure and electrochemical performance J. Ind. Eng. Chem. 62 250–7

[2] Chen X, Wang X, Liu F, Song X and Cui H 2020 Fabrication of NiO–ZnO-modified g-C 3N 4 hierarchical composites for high-performance supercapacitors Vacuum 178 109453

[3] Mokoena T P, Swart H C, Hillie K T and Motaung D E 2021 Colour tuning from violet to blue emission stimulated by various nickel oxide nanostructures: influence of bias voltage towards volatile organic compounds vapours Appl. Surf. Sci. 542 148634

[4] Buldu-Akturk M, Toufani M, Tufani A and Erdem E 2022 ZnO and reduced graphene oxide electrodes for all-in-one supercapacitor devices Nanoscale 14 3269–78

[5] El-Kemary M, Nagy N and El-Mehasseb I 2013 Nickel oxide nanoparticles: synthesis and spectral studies of interactions with glucose Mater. Sci. Semicond. Process. 16 1747–52

[6] Kumar S, Saeed G, Zhu L, Hui K N, Kim N H and Lee J H 2021 0D to 3D carbon-based networks combined with pseudocapacitive electrode material for high energy density supercapacitor: a review Chem. Eng. J. 403 126352

[7] Chen, Z., Dedova, T., Spalatu, N., Maticiuc, N., Rusu, M., Katerski, A., ... & Krunks, M. (2022). ZnO/NiO heterostructures with enhanced photocatalytic activity obtained by ultrasonic spraying of a NiO shell onto ZnO nanorods. *Colloids and Surfaces A: Physicochemical and Engineering Aspects*, *648*, 129366.

[8] Ezhil Arasi S, Devendran P, Ranjithkumar R, Arunpandiyan S and Arivarasan A 2020 Electrochemical property analysis of zinc vanadate nanostructure for efficient supercapacitors Mater. Sci. Semicond. Process. 106 104785

[9] El-maghrabi H H et al 2021 Journal of colloid and interface science coaxial nanofibers of nickel/gadolinium oxide/ nickel oxide as highly effective electrocatalysts for hydrogen evolution reaction J. Colloid Interface Sci. 587 457–66

General Conclusion

The work presented in this thesis concerns the realization and characterized ZnO, NiO thin films and ZnO/$Ni_{(1-x)}$ Cu_xO (n-p) heterostructures by using spray pyrolysis technique on slide of glass substrates.

In order to obtain maximum information about our samples, several characterizations were carried out. Structurally, the films were analyzed using X-ray diffraction (XRD), scanning electron microscopy (SEM); and Fourier-transform infrared spectroscopy (FTIR). Additionally, optical and electrical characterization were performed using UV-visible spectroscopy and the four-point method.

The primary objective of this work was to investigate the effect of the molarity and the deposition temperature on ZnO thin films, the structural characterization confirmed the formation of ZnO films with polycrystalline and hexagonal wurtzite structure, with a preferential orientation along the (002) plane, which the sample was prepared at C=0.1 mol/l and Ts=380°C has the best crystallization. also, the analysis by FTIR has confirmed the existence of Zn-O bond. The study by UV-visibe spectroscopy shows that all the samples have high transparency in the visible range T≈83%, except the samples was prepared at low precursor concentration and low deposition temperature which may be relatively amorphous. The maximum band gap value was Eg=3.29 eV, however the minimum Urbach energy was Eu=0.08 eV for the sample prepared at Ts=380°C and C=0.125 mol/l.

The second objective of this work was to study the effect of Al concentration on optical, structural and electrical properties of NiO thin films. We focused on the fabrication and characterization of Na and Al codoped NiO thin films at different Al concentration Al (0-4%), by spray pyrolysis method. The structural characterization was confirmed that all the obtained films are nanocrystalline of cubic structure. Furthermore, the good crystallinity was achieved for Na 2% and Al 1% codoped NiO thin film. While the transmission spectra show that this film exhibited a transmission was detected between 45 and 65% in the visible region. However, the sample prepared at 2% Al and 3% Al has high transparency. The optical band gap was increased by increasing in Al concentration, where the maximum values is 3.926 eV, which was registered for 2% Na and 2% Al. However, the minimum value of Urbach energy is 0.319 eV, which was obtained for 2% Na and 3% Al. The four probes method was shown that the electrical resistivity decreases after codoping, the lowest value was registered for 2% Na and 1% Al. The figure of merit for p type is so lower than those obtained in the case of n type TCOs collectors and still needing more investigation.

In the third section of this thesis, we tried to make (n-p) heterojunctions by using ZnO and NiO oxides, for application in Photovoltaic. Based on the best crystallized sample of ZnO, which

has prepared at the concentration C=0.1 mol/l, and at substrate temperature Ts=380°C. A second layer of Cu doped NiO thin films was successfully deposited on the ZnO wafers to constitute ZnO/$Ni_{(1-x)}$ Cu_xO with Cu (0-4). We have studied the both effects of Cu concentration, and deposition temperature of NiO on the structural, morphological, and optical properties of this junctions. The XRD showed that a significant improvement in the crystallization of zinc oxide, in addition to the growth and stability of nickel oxide on the ZnO. SEM images revealed that the surface morphology was significantly affected by the increase in deposition temperature and copper concentration, the surfaces exhibit a lattice structure that becomes dense with higher copper concentrations and substrate temperatures. EDS specters showed that all the prepared junction are pure. While the UV-vis analysis showed an increasing in the transmittance of the junctions T = 90%.

As future perspectives we're looking forward to studying ZnO/$Ni_{(1-x)}$ Cu_xO electrically. Studying the effect of the increasing in nickel oxide film thickness on the junction. (by extending deposition time)

Synthesis and Characterization of ZnO Nanostructures and ZnO/$Ni_{1-x}Cu_xO$ Heterostructures Application to Photovoltaics

Abstract

In the present work, we prepared heterojunctions in the form of thin films based on ZnO and NiO, these thin films were deposited by pyrolysis spray technique on glass substrates. The adopted technique is simple, not expensive, it allows for deposition with a controllable property depending on the conditions of preparation. The first objective of this work is the preparation of thin films of ZnO; our interest is on the optimization of the parameters influence as a (molarity and substrate temperature on the physical and optical properties of ZnO thin films. On the other object is the preparation of thin films of NiO and the study of the doping level influence and substrate temperature on the structural, optical and electrical properties. One has used copper as source of dopants; the doping level was varied from 0 to 4% by weight. The structural study of films by XRD showed that all ZnO films obtained are polycrystalline with a hexagonal wurtzite structure and a preferred orientation along the direction (002) and for NiO films, the structure is cubic with a preferred orientation along the direction (111). While the transmission spectra show that this film exhibited a transmission was detected between 45 and 65% in the visible region. Whereas the electrical characterization I(V) was used to determine the electrical parameters of the realized Na and Al codoped NiO thin films, which revealed that the minimum values of Sheet Resistance was registered for Na (2%) and Al (1%). When studying the effect of the deposition temperature of nickel oxide and its doping ratio with copper on the ZnO/Ni1-xCuxO heterojunctions, we observed a significant improvement in the crystallization of zinc oxide, along with the growth and stability of nickel oxide. These changes led to a significant enhancement in the transparency of the junctions, thereby enhancing their optical properties.

Kay Words: ZnO, NiO, Cu, Heterojonction, Thin Layers, TCOs, Spray Pyrolysis method

تحضير ودراسة خواص الشرائح الرقيقة ل ZnO وللوصلات الغير متجانسة من الشكل $ZnO/Ni_{1-x}Cu_xO$ واستعمالها في تطبيقات الخلايا الكهروضوئية

الملخص:

في العمل الحالّي، قمنا بتحضير وصلات غير متجانسة على شكل أغشية رقيقة تعتمد على أكسيد الزنك وأكسيد النيكل، حيث تم ترسيب هذه الأغشية بتقنية الرش عن طريق الانحلال الحراري على ركائز زجاجية. التقنية المعتمدة بسيطة وغير مكلفة، فهِّي تسمح بالترسيب بخاصية يمكن التحكم فيها حسب ظروف التحضير. الهدف الأول من هذا العمل هو تحضير أغشية رقُّيقة من أكسيد الزنك؛ ينصب اهتمامنا على تحسين تأثير العوامل مثل: (المولارية ودرجة حرارة الركيزة على الخواص الفيزيائية والبصرية لأغشية أكسيد الزنك الرقُّيقة. وعلى الجانب الآخر هو تحضير الأغشية الرقيقة من أكسيد النيكل ودراسة تأثير مستوى التشويب وتأثير درجة حرارة الركيزة على الخواص التركيبية والضوئية والكهربائية حيث تم استخدام النحاس كمصدر لتشويب، وتراوح مستوى التشويب من 0 إلى 4 % بالوزن. أظهرت الدراسة التركيبية لهذه الأغشية باستخدام تقنية XRD أن جميع أفلام أكسيد الزنك التي تم الحصول عليها ةً متعددة البلورات ذات شكل سداسي ببنية الورتزايت واتجاه نمو مفضل على طول الاتجاه (002). أما بالنسبة للأفلام NiO فإن البنية تكون مكعبة مع اتجاه نمو مفضل على طول الاتجاه، (111) بينما تظهر أطياف الإرسال انتقالا تم اكتشافه بين 45 و65 % في المنطقة المرئية. في حين أنه تم استخدام التوصيف الكهربائي I (V) لتحديد المعلمات الكهربائية لأفلام NiO المشوبة مزدوجا ب Na وAl ، حيث أظهرت أن أقل قيمة للمقاومة السطحية تم تسجيلها عند نسبة تطعيم Na (2%) و Al (1%) . عند دراسة تأثير درجة حرارة ترسيب أكسيد النيكل و نسبة تطعيمه بالنحاس على الوصلات غير المتجانسة ZnO/Ni1-xCuxO ، لاحظنا تحسنا ملحوظا في تبلور أكسيد الزنك إلى جانب نمو و استقرار أكسيد النيكل. هذه التغيرات أدت إلى تحسين كبير في شفافية الوصلات، مما يعزز من خصائصها البصرية.

الكلمات المفتاحية: أكسيد الزنك, أكسيد النيكل, النحاس, الوصلات الغير متجانسة, الأغشية الرقيقة, الرش الكيميائي الحراري